WAFER SURFACE CLEANING FOR SILICON HOMOEPITAXY WITH AND WITHOUT ECR HYDROGEN PLASMA EXPOSURE

by

Hyoun-woo Kim

B.S., Seoul National University
(1986)

M.S., Seoul National University
(1988)

Submitted to the Department of
Materials Science and engineering
in Partial Fulfillment of the Requirements
For the Degree of

DOCTOR OF PHILOSOPHY

at the

MASSACHUSETTS INSTITUTE OF TECHNOLOGY

September 1994

Signature of Author _____

Department of Materials Science and Engineering
August 5, 1994

Certified by _____

Rafael Reif, Thesis Supervisor
Professor, Department of Electrical Engineering and Computer Science
Director, Microsystems Technology Laboratories

Accepted by _____

Carl V. Thompson
Professor of Electronic Materials
Chairman, Departmental Committee on Graduate Students

Science

WAFER SURFACE CLEANING FOR SILICON HOMOEPITAXY WITH AND WITHOUT ECR HYDROGEN PLASMA EXPOSURE

by

Hyoun-woo Kim

Submitted to the Department of
Materials Science and engineering
in Partial Fulfillment of the Requirements
For the Degree of

DOCTOR OF PHILOSOPHY

Abstract

The objective of this thesis is to investigate the low temperature *in-situ* cleaning process using the ECR (Electron Cyclotron Resonance) hydrogen plasma technique and the *ex-situ* cleaning process using the HF dipping method, for low temperature silicon homoepitaxial growth. A Load Lock Chamber was installed on the MS-CVD (Multi-chamber Chemical Vapor Deposition) reactor, to reduce the possibility of introducing contaminants into the system. The ECR plasma system was selected because it could deliver a higher density of low energy ions in a well-regulated manner, as compared to a conventional RF (Radio Frequency) system. Hydrogen gas was selected because of its light mass and its ability to react chemically with surface contaminants. Epitaxial layers were deposited on top of the *in-situ* cleaned wafers and the structural qualities of the epitaxial layers and the epilayer/substrate interface were investigated by XTEM (Cross-sectional Transmission Electron Microscopy) and RBS (Rutherford Backscattering Spectroscopy) techniques. SIMS (Secondary Ion Mass Spectroscopy) was used to detect the oxygen and carbon contaminants at the interface.

Process variables such as DC bias, cleaning time, microwave power, and gas pressure were set, and when the *in-situ* ECR hydrogen plasma process at 600°C was optimized, a defect-free epitaxial layer with an almost invisible interface was obtained. The effect of *in-situ* cleaning temperature on cleaning efficiency was then studied in the range of 25°C to 660°C and it was revealed that a defect-free epitaxial layer could be deposited with room temperature *in-*

situ cleaning. *Ex-situ* cleaning with HF dipping was performed and the effects of rinsing and drying techniques were investigated. Although rinsing encouraged the growth of natural surface oxide to grow, it improved the surface smoothness of the resulting epitaxial layer. The blow-drying technique was more efficient than the spin-drying technique. When *in-situ* cleaning was optimized at 600°C, it succeeded in removing natural surface oxide. When the *in-situ* cleaning was repeated at 660°C, it was even more efficient in removing the surface oxide from the wafer. Room temperature *in-situ* cleaning was efficient in removing carbon species from the wafer surface. The reaction mechanisms of oxygen and carbon removal were discussed.

Thesis Supervisor: Dr. Rafael. Reif
Title: Professor of Electrical Engineering and Computer Science
Director, Microsystems Technology Laboratories

Acknowledgments

I would like to thank my supervisor, Prof. Rafael Reif, for his patience and timely advises throughout my career at M.I.T. He provided me an opportunity for independent research. I would like to thank SRC/SEMATECH for partially funding this project. I thank Prof. Harry Tuller and Prof. Lionel Kimmerling for reviewing this thesis and providing helpful suggestions.

My gratitude goes to my colleagues, Julie Tsai, Ken Liao, Alex Cherkassky, Weize Chen, Andy Tang, Rajan Naik, Ben Tao and Dr. Takashi Noguchi for wonderful collaborations and friendships. I thank to Dr. Zhen-Hong Zhou in training me on the MS-CVD reactor and very helpful discussions, to Dr. Tri-Rung Yew, Dr. Euijoon Yoon, and Dr. Jaegab Lee for teaching me XTEM sample preparations, to Dr. Chang-Kyung Kim for helpful discussions on material characterizations. I thank to M. Frongillo for training me on TEM and ion milling, to J. Chervinski for training me on RBS. I am grateful to the staff in Microsystems Technology Laboratories: Octavio Hurtado, Paul Mcgrath, and Joe DiMaria for their helps with facilities. A special thanks goes to Carolyn Zaccaria for great helps.

I thank to Samsung company for providing me a scholarship and encouraged me throughout my PhD course. My father and mother have provided love and support throughout my life and I also appreciate encouragement from my wife' family. I specially thank my wife, Hye-gyu Lee, for her love, support and patience, without her this work was impossible. I also thank my lovely daughter, Juna for her happy smiles. Great thanks go to people, who have prayed for me throughout my life. Thank God and glorify Him with this small dissertation.

Contents

List of Figures

Chapter 1

Introduction and Background

1.1 Background and Motivation

As device dimensions are reduced into the sub-micron regime in pursuit of higher integration density and better circuit performance, low temperature epitaxy has been a major issue in microelectronics technology and will be more critical in the future. Low temperature processing, which includes the *in-situ* cleaning and epitaxial deposition, is not only important for future silicon ULSI (Ultra Large Scale Integration) technology but also for silicon-based heterostructures [1]. Thermal exposure at high temperatures needs to be minimized to reduce dopant diffusion and interface broadening [2] and to get an abrupt and well-controlled dopant transition profile. Additionally, in the heterostructures, heterolayers can be intermixed near the interfaces by thermal heating, and many defects such as misfit dislocations can be generated [3]. However, low temperature processing cannot volatilize or dissolve the surface contaminants just by heating the substrate, as it was done in the traditional high temperature epitaxial growth. Therefore, predeposition surface cleaning has become a crucial step for successful growth of the epitaxial layer.

Most cleaning techniques aim to reduce oxygen, carbon and metallic impurities, to deposit a device-quality epitaxial layer, because these impurities influence the crystallographic perfection of epitaxial films deposited on defect-free substrates [4]. Metal-containing precipitates are known to be correlated with the generation of stacking fault tetrahedra in epitaxial films. Oxygen is usually present as silicon dioxide on the substrate, and incomplete removal of oxide film from the substrate was found to generate stacking faults in the epitaxial overgrowth [5]. The growth of the silicon films around the patches of oxide occurs by the generation of stacking faults at the oxide-silicon boundary. Carbon degrades the perfect crystallinity of epitaxial films by forming SiC (silicon carbide) precipitates, which impede the sideways growth of silicon ledges, and structural defects are then nucleated. Carbon

causes the nucleation of dislocations and stacking faults by either forming silicon carbide precipitates or by the elastic distortion of the lattice by carbon which is in solid solution. Oxygen and carbon have major electrical effects in silicon. Oxygen atoms usually occupy the electrically inactive positions in the lattice [6]. In particular, an extrinsic stacking fault has no dangling bonds and should not be electrically active, but as a consequence of the presence of bounding dislocations and impurity-related effects, stacking faults cause detrimental electrical effects in the operation of device. The effects due to carbon are not sufficiently understood. However, with increasing carbon concentration, an abrupt decrease in the donor concentration was observed, which may be attributed to lattice strain caused by the presence of carbon [7]. Therefore, it has been crucial to remove oxygen and carbon from the substrate surface. In the ideal case, there is no accumulation at the epilayer/substrate interface or inside the film. Because it is important to reduce them, the origin of oxygen and carbon needs to be investigated.

There are several sources of gas impurities: the vacuum system, the process itself (*in-situ* cleaning process/ the process gases) and the substrate (maybe from *ex-situ* cleaning). The potential sources of gases and vapors in a vacuum system can be found in the literature [8]: real and internal leaks, vaporization, diffusion, desorption, permeation through the chamber materials, and backstreaming from the pumps.

Oxygen may be originated from the natural oxide on the silicon surface, which may grow during the exposure to air or water rinsing process. Water vapor may enter into the chamber when the wafer is loaded. Internal surfaces of the chamber are supposed to be evenly coated with layers of water molecules and will become a predominant residual gas [9]. Therefore, during heating, some water molecules desorb and may adsorb onto the wafer surface. Carbon can be originated from the organic contaminants on the oxide layer, from the HF solution, and from DI water [10]. Vacuum pumps can be a source of hydrocarbons. If the turbomolecular pump is operated in an improper manner, there is some danger of oil backstreaming into the process chamber. Hydrocarbons can also be originated from the mechanical pump, which is oil-sealed. The source of carbon and oxygen needs to be investigated in more detail.

The epitaxial process consists of the three steps: 1) wet cleaning to remove particles, metals, and organic species; 2) precleaning to remove the native oxide which was formed in the previous wet cleaning step; 3) and epitaxial growth. The most common type of wet cleaning is the RCA cleaning. In RCA cleaning, hydrogen peroxide solutions at high pH are effective for removing organic compounds by oxidation (Standard clean or SC-1 solution), and at low pH (SC-2 solution), they are effective for desorbing metal contaminants by complexing [11]. SC-1 solution is effective in removing particles as well [12]. No metallic impurities are present on the wafer surface after the RCA cleaning. Careful wafer handling after the RCA cleaning prevents recontamination.

The HF cleaning is a method used to achieve clean interfaces, and it is most efficient in getting rid of residual natural oxide. Dangling bonds of silicon surface are terminated by hydrogen atoms, and fluorine atoms remain as a minor species after HF treatment. This hydrogen passivation prevents the surface exposure to air and oxidation [13], but the effect of HF dipping on the carbon contamination on the substrate surface is still unclear. Etching is assumed to take place by the following reaction [14]:

$$SiO_2 + 6HF \rightarrow H_2SiF_6 + 2H_2O$$

and the etch rate of the oxide is a function of the concentration of HF [15]. The last steps in wafer cleaning are rinsing and drying; both are extremely critical steps because clean wafers become recontaminated easily if not processed properly [16]. Rinsing after wet cleaning is done with flowing high purity and ultrafiltered high-resistivity DI water, usually at room temperature [17]. Rinsing in deionized (DI) water is important at all stages of the preparation, as it removes species that are weakly bound to the surface (physisorbed or hydrogen bonded) and can even etch the silicon surface [18]. Not only is deionized water rinsing applied during RCA cleaning steps to remove the residual chemicals, but also employed especially after HF dipping, to remove fluorine-species, and to result in hydrogen passivation. However, extra rinsing not only generates microroughness [19] and stacking faults [20], but also increases chemical contamination such as carbon or oxygen [21]. The

effect of water rinsing on the level of contamination at the epilayer/substrate interface needs to be investigated.

A device-quality epitaxial film can be deposited without an *in-situ* wafer cleaning, immediately after the *ex-situ* cleaning process. Meyerson [22] deposited epitaxial film by pure thermal techniques at temperatures in the range 700 < T < 850°C. Furthermore, device-quality silicon-germanium alloys were deposited at temperatures in the range 400 < T < 500°C [23]. It could be achieved through the use of UHVCVD system (base pressure was 10^{-9} Torr), by exploitation of the $Si/O_2/SiO_2$ and the $Si/H_2O/SiO_2$ equilibrium system. In our system, the base pressure is about 1-2 X 10^{-8} Torr, higher temperature (700°) is needed to have an oxide-free silicon substrate, by thermodynamical equilibrium criterion [24]. The temperature ranges below 660°C were studied in our experiments and the structural qualities of the epitaxial film, with and without *in-situ* cleaning, were investigated.

Thermal heating is a method to achieve the surface cleanness without an *in-situ* plasma cleaning. With *in-situ* plasma cleaning, plasma energy can replace a considerable amount of thermal energy, it can be applied physically or chemically immediately before the deposition. *In-situ* Ar or He sputtering was applied in our system [25]. However, many defects were generated in the epilayer/substrate interfaces, where the substrates were submitted to ECR(Electron Cyclotron Resonance) argon plasma bombardment prior to growth. Defect-free epitaxial film could not be obtained once these stacking faults were generated, at low temperature. Even ECR helium (He; mass=4) plasma cleaning generated defects, and thus a lightest element (H; mass=1) was selected for our system. Current literature reports that a hydrogen plasma removed the native silicon oxide at high temperatures such as 800°C [26] and even at lower temperatures [27] without causing much damage. These techniques are supposed to replace the hydrogen prebake [28] which requires a high temperature to drive the reaction forward. Additionally, hydrogen plasma cleaning may be a chemical etching process in nature, rather than a physical sputtering, considering its light mass. Hydrogen plasma was reported to remove the native silicon dioxide and hydrocarbons effectively, resulting in a clean silicon surface that is thought to be terminated with hydrogen atoms [29]. Hydrocarbons are a tenacious species on the silicon surface and cannot be

removed easily by physical sputtering, it is hoped that the chemical reaction between those hydrocarbons and hydrogen can play a major role in removing those contaminants.

The ECR plasma system was selected because it has some advantages compared to conventional RF (radio frequency) plasma systems. The ECR plasma system, which operates at a microwave frequency of 2.45GHz, is able to deliver a higher density of low energy ions to the wafer because both ionization (about 10% of the gas is ionized) and the saturated ion current are much higher than in the RF plasma system [30]. In particular, the ECR can be operated with low energy (without sacrificing cleaning efficiency), and ion flux and ion energy can be controlled easily [31]. Possible substrate damage may be reduced by reduced plasma exposure time, and less contamination may be expected due to electrodeless discharge [32]. Additionally, because of the downstream-nature of this ECR plasma system, ions are made to impinge on the substrate with a controlled, low energy. Furthermore, a high electron collision rate is achieved through efficient coupling to propagating plasma waves and through a large aspect ratio (A=L/D=2.25). The ECR plasma system is compatible with UHV (Ultra-High Vacuum) CVD systems [33].

Delfino et al. found that an exposure to ECR hydrogen plasma for a few minutes, without applying heat or bias to the substrate, removed the hydrocarbons and the native silicon oxide. This observation was proved with x-ray photoelectron spectroscopy by measuring the O/Si ratio [29]. In our studies, epitaxial layers were deposited after the exposure to ECR hydrogen plasma. Depositions were done at low temperature (600°C), and the structural qualities were investigated. The *in-situ* cleaning process with ECR hydrogen plasma needs to be optimized by varying process variables such as DC bias, cleaning time, microwave power, cleaning gas pressure and cleaning temperature. Furthermore, the mechanism of surface cleaning by ECR hydrogen plasma has not been understood, it needs to be discovered. Delfino suggested the ion-induced etching mechanism, where low-energy hydrogen ion bombardment played a major role in the removal of native silicon oxide. Kishimoto et al. performed an *in-situ* RHEED monitoring of hydrogen plasma cleaning on the silicon substrate. They found that a low temperature cleaning was efficient. Zhou et al. found that an excessive hydrogen ion bombardment

damaged the silicon substrate at low temperatures (< 350°C). In our investigation, XTEM was employed to observe the structural qualities of epitaxial layers and the epilayer/substrate interface.

Even if the wafer surface is oxide-free after the *ex-situ* cleaning step, water vapor can be present on the wafer surface and will become a source of oxygen contamination at the epilayer/substrate interface. The load lock chamber was installed in our CVD system to minimize the entrance of water vapor or other contaminants into the CVD chamber. The impurity gases can be pumped from a vacuum chamber in a short time if they were located inside the volume of the chamber. However, internal surfaces of the chamber are evenly coated with layers of water molecules [9], because the inner wall of the chamber is frequently exposed to atmosphere. Therefore, during heating in the CVD chamber, water molecules from within the chamber may adsorb onto the wafer surface. In this case, *in-situ* plasma cleaning may not reduce contamination significantly, and recontamination occurs during the *in-situ* cleaning and deposition. It is crucial to investigate the origin of the contaminants in our system and to devise techniques to remove them.

1.2 Organization of Thesis

This thesis consists of 8 chapters. Chapter 1 introduced the whole contents of this thesis. Current applications of silicon epitaxial layers were discussed. The motives of this dissertation was stated, and the current problems associated with wafer surface cleaning was briefly reviewed. Fundamentals of ECR (Electron Cyclotron Resonance) plasma was reviewed for those who are not familiar with. Chapter 2 described the multi-chamber UHVCVD (Ultra-High Vacuum Chemical Vapor Deposition) reactor, which were used in this research. Chapter 3 explained the experimental procedure: *ex-situ* cleaning, *in-situ* cleaning with ECR hydrogen plasma, and materials characterization techniques, which were used in this research.

Chapters 4 through 7 were devoted to the explanation and discussion of the experimental results. *In-situ* ECR (Electron Cyclotron Resonance) hydrogen plasma cleaning at 600°C was studied and results are listed in Chapter 4, this

cleaning process was evaluated with varying the process variables. In Chapter 5, The structure of epitaxial film with the room temperature *in-situ* cleaning was demonstrated. The effect of temperature on the cleaning efficiency was studied. Chapter 6 was written on ex-situ cleaning by HF dipping technique. Epitaxial films, which did not receive the *in-situ* cleaning processes, were deposited and their structures were demonstrated. Effects of the water rinsing step was investigated in detail. Chapter 7 was written on the possible source of oxygen and carbon. Possible removal mechanisms of oxygen and carbon on the wafer surface were studied.

Chapter 8 concluded this dissertation. It stated the major conclusions made, and recommendations on the future work.

1.3 Literature Review

1.3.1 Applications of Silicon Epitaxial Layers

Epitaxial technology is essential to the fabrication of all vertical bipolar structures and is becoming increasingly important for an advanced metal-oxide-semiconductor (MOS) structures as well. Epitaxial layers have been used for the fabrication of integrated circuits and discrete devices. Increases in integration, the packing of a large number of smaller devices per unit area, are driven by pressure to reduce costs of manufacturing and to enhance device performance. Fabrication of smaller devices is challenging since it requires greater control of dopant profiles in both the horizontal and vertical dimensions. Low temperature processing, both during and after dopant incorporation, is essential to minimize redistribution by solid state diffusion.

Epitaxial technology can be applied to SOI (Silicon-On-Insulator) or SIMOX (Separation-by-IMplanted OXygen) technology, however, the silicon epitaxial layer on the silicon substrate will be a main focus in the following subsections.

1.3.1.1 Bipolar devices

Bipolar transistor fabrication technology was the first to utilize epitaxial deposition to enhance the performance of devices. Basically, lightly doped epitaxial layers are deposited to the heavily-doped regions to provide a rapid transition in carrier concentration along the vertical dimension. Afterwards, base and emitter regions are formed within the epitaxial layer by ion implantation. The epitaxial layers serve as an integral part of the bipolar device structure and requires precise control of thickness, resistivity, uniformity, transition width and structural quality. These factors determine device performance parameters such as speed, gain, breakdown voltage and yield. The digital technology is extremely sensitive to the penetration of the buried layer into the epitaxial layer, and the thinnest layers are needed for this application. It is crucial to grow the thick epitaxial layers for linear IC applications without significant diffusion of the buried layer into the epitaxial film [34].

n/n^+ and p/p^+ epitaxial layers were deposited in discrete devices to maintain proper collector-base breakdown voltages, while maintaining a low resistivity path for collector current through the heavily doped substrate [35]. The advent of the bipolar IC required the use of the epitaxial layer for device isolation as well. It can be achieved by depositing a high resistivity n-type layer on a high resistivity p-type substrate which had previously been patterned with degenerately doped n-type regions (buried layers) to serve as low resistivity subcollectors. Fig.1.1 shows a typical buried layer bipolar device employing an n-type epitaxial film on a p-type substrate.

The dopant profile determines the collector/base breakdown voltage, the depletion layer capacitance and the extent of base stretching. Increases in dopant concentration on the collector side of the junction will increase the capacitance associated with it and will reduce the switching speed of the device [36]. Base stretching occurs at high current densities and is defined as an effective movement of the collector/base junction toward the subcollector-side. This movement increases the base width and increases the base transit time of the device, resulting in reduced speed of the device. Tighter tolerances in the required epitaxial layer thickness will reduce the extent of base stretching and provide a performance benefit. This tight tolerance requires a low temperature processing.

The substrate/collector junction also has many associated capacitances which reduces the operational speed. Some of these capacitances are directly related to the dopant profiles obtained during epitaxial growth. Sharper junctions will reduce capacitances and increase operational speed. The sidewall capacitance is associated with the thickness of the subcollector region and this thickness is determined in part by the epitaxial deposition temperature. Lower-temperature epitaxial growth can reduce the sidewall dimensions and the capacitance.

Not only are there generic performance benefits to be achieved through a reduction in the deposition temperature of epitaxial layers, but also the capability of a low-temperature epitaxial process allows device designers to consider novel device structures, where the epitaxial deposition is performed after delineation of certain device regions.

1.3.1.2 MOS devices

Epitaxial layers are widely used in the fabrication of MOS device structures. The use of a lightly doped n-type epitaxial layers on heavily doped substrates provides an effective ground plane for NMOS circuits [37]. Also the use of lightly doped epitaxial layer on heavily doped substrates provides a barrier to minority carrier injection. In addition, it increases the uniformity in resistivity compared to bulk silicon wafers, which provides better control over threshold voltage variations and low noise conditions.

Although there are many performance benefits by fabricating MOS devices in the epitaxial layer, the major application of MOS devices is to enhance the reliability of the circuits rather than to provide a significant increase of device performance. In particular, the use of a high resistivity epitaxial layer (lightly doped) on a low resistivity substrate (heavily doped) of the same dopant type prevents the latch-up problem in complementary MOS (CMOS) technology. In this situation, a heavily doped substrate acts as a shunt for the lateral parasitic bipolar transistor which is one-half of the parasitic bipolar pair responsible for latch-up. A CMOS device configuration is shown in Fig. 1.2 [34].

Latch-up is a phenomenon which occurs due to the proximity of NPN and PNP transistors within a CMOS device architecture. The presence of parasitic junctions and transistor pairs, formed by the interaction of regions from two side-by-side devices, may lead to a condition in which the devices turn on and do not turn off. The presence of a conductive substrate encourages the electron-hole recombination and provides a ground plane for the collection of the stray currents, which are responsible for latch-up. The use of epitaxial technology to prevent the latch-up has the least detrimental effect on device processing and allow for high packing densities and high speed operation. The susceptibility to latch-up in CMOS is a function of the thickness of epitaxial layers, requiring a decrease in the epilayer thickness as device dimensions are reduced [38].

The use of n/n^+ and p/p^+ epitaxial structures provides improved radiation hardness in MOS memory cells. The alpha-particles [39] can be introduced primarily from packaging materials and when they penetrate the silicon substrate, large numbers of electron-hole pairs are produced. These carriers have long lifetimes and have may chances to penetrate into the active device regions. Charges can thus be collected on a memory cell and change the state of the memory bit. This phenomenon, which is called as soft error, can be reduced greatly by using a lightly doped epilayer on a heavily doped substrate, because electron-hole recombination in the bulk substrate will increase due to the higher doping level of it.

1.3.1.3 BiCMOS and other applications

Increasingly, semiconductor manufacturers are using epi-based BiCMOS for Mb-size memories and for other large chips. Many of the present BiCMOS wafers have at least two buried layers; usually arsenic and boron buried. The arsenic buried layer acts as the subcollector of the bipolar devices, whereas the boron buried layer acts as a host for the MOS devices. For successful high volume BiCMOS processing, extremely tight control over the thickness and resistivity is required. And, if thin and high-resistivity epitaxial layers are needed, autodoping from boron and arsenic-doped buried layers should be minimized. For small-geometry devices in the future, the epitaxial processing

temperature needs to be lowered to control the autodoping of the arsenic and boron buried layers and also to prevent damages to the device structure by thermal heating. Fig.1.3 shows the cross section of the 0.5μm BiCMOS technology [40].

BiCMOS applications, in the future, will demand a more strict particle and contamination control in epitaxial deposition. And, BiCMOS will drive the need for the epitaxial layers on large wafers. For successful BiCMOS processing with wafers as large as 200mm, wafer flatness becomes extremely important. Also, efforts to lower down the costs of the epitaxial film will be continued. Nowadays, an epitaxial wafer typically costs 2.5-2.75 times more than a polished silicon wafer. This number needs to be below 1.7 for DRAM applications [41].

Epitaxial layers are applicable to charged coupled devices (CCDs). CCD devices require totally a defect-free epitaxial layer which is 40-60 μm-thick. Any defect, either crystalline or particulate, are detrimental to the operation of the device. Also, striations in the image transmitted by a charged coupled device are strongly influenced by the uniform resistivity of the silicon, where the device is fabricated.

Silicon-germanium heterojunction bipolar (HBT) technology will soon emerge into the production of high speed ECL, analog-to-digital converters, high frequency output transistors. Using the epitaxial silicon-germanium (SiGe) layers in the base for heterostructure bipolar transistor results in the reduction of bandgap. This technology allows the use of silicon processing to produce transistors that rival the speeds of gallium arsenide. It is an advantage that development of high-density sophisticated ICs using SiGe HBT technology is a straightforward extension of present silicon wafer fabrication methods. The deposition of SiGe alloys for heterojunction bipolar applications requires extremely low oxygen content in addition to tight control of the growth rate and germanium composition. Lower temperature processing (less than 700°C) is required to avoid strain relaxation and to avoid the generation of misfit dislocation.

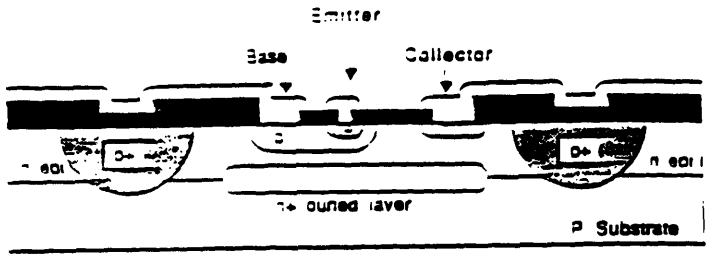

1.1 A typical buried-layer bipolar device configuration[34]

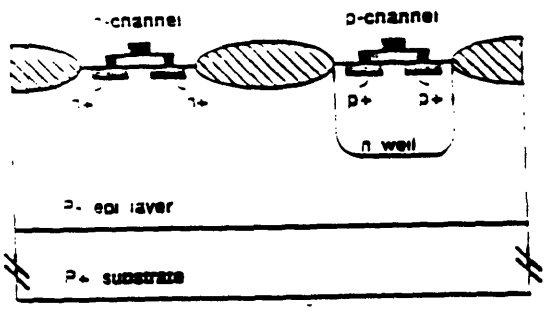

1.2 A typical CMOS device configuration [34]

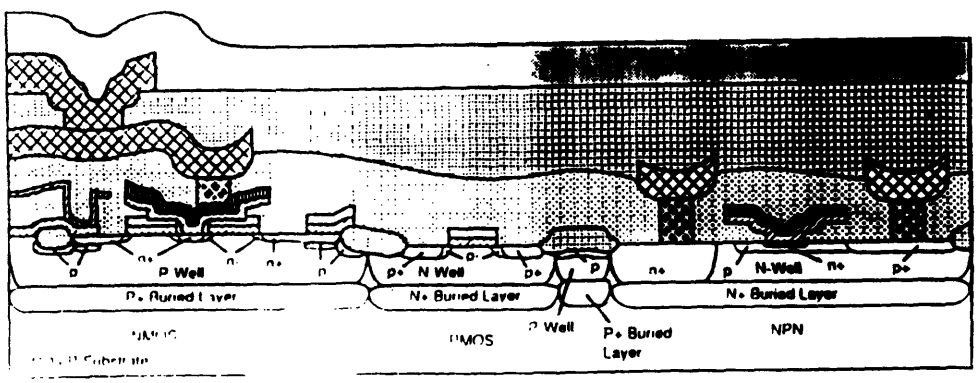

1.3 0.5μm BiCMOS device configuration [40]

1.3.2 Fundamentals of ECR Plasma

1.3.2.1 Introduction

The ECR (Electron Cyclotron Resonance) plasma system delivers a high density of low energy ions to the wafer, so that plasma damage can be reduced without sacrificing etch rates. Ionization ratios by this technique can be three orders of magnitude greater than possible with the conventional RF techniques. In ECR system, ionization occurs by transmitting microwave energy directly to the electrons, because relatively heavy ions cannot be accelerated by the extremely high frequency microwave electric fields: Ion cyclotron resonance may occur, but it does not affect the discharge significantly. So in ECR system, the ionization ratios will be greater than the conventional plasma system. Also, ions have a much lower energy and cause less damage. However, in case of RF plasma system, a large portion of the energy is imparted to ions as well as electrons. The plasma density can be increased further by tightly confining the electrons with magnetic fields in a mirror-like configuration. The mirror confinement refers to a plasma bounded by two high field strength region.

In real discharge processes, the electron resonance condition can be met in a volume or surface layer, where the static magnetic field strength is adjusted to the resonance and a component of the electric field is perpendicular to the static magnetic field. The electrons are accelerated in the ECR volume and ionize and excite the neutral gas. This results in a low-pressure, almost collisionless plasma that can be varied from a weakly to highly ionized state by changing the gas pressure, gas flow rate, and input microwave power. This technique, borrowed from fusion [42] and electric propulsion [43] plasma and modified for the requirements of plasma processing [44] [45], can create low pressure (< 0.5 Torr) discharges.

An ECR source can be operated at lower pressures, and higher anisotropy etching with small geometry (< 0.5μm) can be attained. If plasma process is performed at a lower gas pressure (lower than 0.1Pa), the mean free path of the ions becomes longer than the width of the sheath, and the accelerated ions can impinge on the substrate perpendicularly without being scattered by

other particles. In this case, surface damage and contamination can be minimized, since ions are accelerated by low (about 20eV) floating potential energy. Chemical reactions occur between low kinetic energy ions or radicals and the etched surface, and the reaction by-products are volatile. These further facilitate the removal of the possible residues, particles, and contamination. The main problem with the conventional radio frequency (RF) plasma source is that they cannot operate at low pressures. The difficulty lies in the fact that there is a rapid drop in ion density as pressure decreases, and this means lower etch rate and lower throughput. Ion energies raised by applying the power of the wafer bias will increase the etch rate and throughput but may cause damage and contamination.

Microwave should be penetrated into the plasma to transfer the microwave power from the wave to the electrons. The degree of penetration is determined by electron density and the strength of the magnetic field. In ECR system, which provides a high wave frequency (2.45GHz), the penetration occurs for less electron densities, because the wave easily penetrates the plasma from any direction, with its higher wave frequencies. In addition, in ECR system, plasma can be produced without high RF (Radio Frequency) voltages, and low temperature plasma can be obtained, and sheath drop is reduced. Microwave plasma etching is compatible with reactive gases such as oxygen and chlorine, since no electrodes or filaments are needed in the discharge. Lawrence Bourget, who is a research scientist at ASTeX (a manufacturer of ECR systems) commented on the main advantages of ECR as follows:

1. low energy, high current ion source
2. controllable ion flux and energy by tailoring magnetic field
3. independent control of ion flux and ion energy when RF bias is used
4. efficient coupling of power to the plasma
5. operate and starts over a wide pressure range
6. compatible with reactive gases
7. UHV compatible
8. automatic tuning
9. mature technology

ECR is increasingly needed in production environment, and especially in Japan, ECR is reported to be used to fabricate 64Mb DRAMs. Even U.S.critics point out that although ECR systems are complicated and expensive, ECR will give less damage to the substrate and devices. Also, ECR has been the longest investigated and the best characterized technique. Table.1.1 compares the ECR and RF plasma.

Table 1.1 Comparison between ECR and RF plasma [46]

parameters	ECR plasma	RF plasma
frequency	2.45GHz	13.56MHz
gas pressure(Torr)	$4X10^{-4}$	$7X10^{-2}$
electron temperature	3.8eV	8eV
plasma density(cm^{-3})	$3X10^{11}$	$1X10^{10}$
saturated ion current	7.5 mA/cm^2	0.3mA/cm^2
ion energy (eV)	controllable	200-1000
ionization efficiency	$2x10^{-2}$	$4x10^{-6}$
mean free path(mm)	110	0.7

1.3.2.2 ECR Glow Discharges

An applied magnetic field causes electrons to move in a counterclockwise fashion on a plane normal to the field (and vise versa for holes or positively charged ions) by the Lorentz force:

$$\mathbf{F} = q(\mathbf{v} \times \mathbf{B}) \qquad (1.1)$$

To make it simple, we assume that the electric fields are negligible. A constant electric field applied to a plasma is not so interesting because the plasma adjusts itself by forming a thin sheath of space charge, which shields the main body of plasma from the field. A constant magnetic field causes the particles to gyrate about the field lines without altering the space-charge distribution.

The frequency of this cyclotron motion, known as the cyclotron frequency, is given by

$$\omega_{ce} = \frac{eB}{m_e} \quad , \tag{1.2}$$

in case of electrons. (where e = charge on an electron, B = strength of a static magnetic field and m_e = mass of an electron.) If we substitute the value of the free-electron mass, we find that

$$\nu_c = \frac{\omega_c}{2\pi} = 2.8B \text{ GHz, where B is in kilogauss.}$$

Thus for B = 875 Gauss, the cyclotron frequency, ν_c, is 2.45 GHz, which is in the microwave range. In the electron cyclotron resonance (ECR) discharge, microwave energy is coupled to the natural resonant frequency of the electron gas in the presence of a static magnetic field. The rate of absorption is greatest when the frequency of the signal is exactly equal to the frequency of the electron. At this moment, each electron moves synchronously with the wave throughout the cycle, and therefore the absorption continues all through the cycle. On the other hand, if it is not the case, the electron is in phase with the wave through only a part of the cycle and absorbs energy from the signal, but for the remainder of the cycle the electron is out of phase and returns energy to the signal wave [47].

1.3.2.3 Process Variables

a) Pressure, Flow rate and Molecular flux

The flux (i.e. number per unit area per unit time) of atoms (or particles) bombarding the walls of a chamber exerts a pressure. The formula for the mean speed of a particle in a gas is given by

$$c = \left(\frac{8kT}{\pi m}\right)^{1/2}, \tag{1.3}$$

and the impingement flux per unit area is represented by nc/4, which yields

$$\text{Flux/area} = \frac{n}{4}\left(\frac{8kT}{\pi m}\right)^{1/2}, \tag{1.4}$$

where k is Boltzmann's constant, T is the gas temperature, m is the weight of the gas atom or molecule, and n is the number density of the gas. The mean free path is the average distance traveled by a particle between collisions with other particles and increases at lower pressures. At lower pressures, the mean free paths of the ions are long compared to the width of the sheath, in which the ions are accelerated along the electric fields, and the probabilities of collisions with other particles are lower. And the impinging ions may not lose their kinetic energy. However, at low pressure, the number density of the gas is low and thus the molecular flux should decrease (1.4). In most plasma processes, especially in *in-situ* wafer cleaning, the gas flow is in the molecular flow regime, i.e. $\lambda >> d$, in the sense that the mean free path is much larger than the characteristic dimension of a vacuum chamber. There is virtually no interaction between particles. The pumping speed measures the volume of gas passing per second, but the more useful term is the flow rate, Q, pressure times the pumping speed, which is thus proportional to the flux of passing molecules. It means the inlet rate of a reaction gas and the convenient unit is the standard cubic centimeter per minute (sccm), standard referring to standard temperature (0°C) and standard pressure (1 atm). So 1 sccm = $6.023 \times 10^{23} / 22414 = 2.69 \times 10^{19}$ molecules per minute. In the relation of the gas pressure and flow rate, pressure can be varied without changing the gas flow rate by adjusting the conductance which is the ability to transmit a gas flow [48]. The ECR plasma is reported to vary from a weakly to a highly ionized state by changing gas flow rates, discharge gas pressures [49].

b) Plasma Potential and Sheath Region

Suppose a small electrically isolated substrate is put into the plasma. In the beginning, it will be struck by electrons and ions. Kinetic theory shows that random thermal motion of a gas results in a flux of particles to the substrate, and the flux of electrons is far greater than that of ions or neutrals because $T_e >> T_g$, T_i and $m_e << m_g, m_i$. Then the substrate builds up negative charges and hence negative potential with respect to the plasma. The negative charges build up until the repulsive electric sheath field becomes intense enough to reduce electron current to the level of the ion current flux (Fig.1.4) [50].

Plasma is actually electric-field-free and equipotential. We call this potential the *plasma potential*, V_p, and we associate a *floating potential*, V_f with the isolated substrate. Since electrons are repelled by the difference, V_p-V_f, we have a net positive charge around it, and it is known as a space charge and forms a sheath. Most of the potential drop appears across the sheath, and voltage across the sheath ranges from a few to thousands of volts. If we start from Poisson's equation and keep in mind the concept of barrier to electrons, V_p-V_f, then from the Maxwell-Boltzmann distribution function and from the charge balance consideration, we get [51] :

$$V_p - V_f = \frac{kT_e}{2e} \ln(m_i T_e / m_e T_i). \qquad (1.5)$$

Here m_i and m_e are the masses of ions and electrons, and T_i and T_e are the ion and electron temperatures, respectively. The voltage across the sheath accelerates the ions, which entered with very low energy, and in the absence of collisions in the sheath, will strike the substrate with a kinetic energy equivalent to the sheath voltage. The sheath thickness is on the order of a Debye length, which is given by:

$$\lambda_D = (kT_e\varepsilon_0 / n_e e^2)^{1/2}, \qquad (1.6)$$

where n_e is the electron density and ε_0 is the permittivity of free space.

c) Substrate Bias (DC) and Ion Energy

The substrate can be floated, grounded, dc biased, or RF biased. The sheath potential for an insulator is equal to V_p-V_f and for the grounded substrate, V_p-V_g, where V_g is the ground potential. Since the ECR plasma system is classified as a reactor of the external-electrode type, the V_f is close to the V_g, and V_g is usually set to zero. When a voltage is applied to the bias electrode(V_b), from Langmuir's probe theory, the bias I_b-V_b characteristic will be given as [52]:

$$I_b = A_1(j_{es} \exp\{ - [e(V_p-V_b)/kT_e] \} - j_{is}) \ , \qquad (1.7)$$

where A_1 is the area of the bias electrode, while j_{es} and j_{is} are the saturation current densities of the electron and the ion, respectively. By inserting a small wire or plane surface into the plasma glow, the current-voltage characteristic curve can be obtained, which was first used as a diagnostic by I.Langmuir [53]. When the probe has a high negative charge (left-hand side of the Fig. 1.5 [54]), it collects all positive ions entering the plasma sheath while the electrons are repelled. As the probe is made more positive, the highest energy electrons overcome the applied bias and reach the probe, so the net value of current increases toward zero. At V_f ,the electron current is just equal to the ion current. As the probe is made more positive, electrons with still lower energies can reach the probe surface, and the current increases further. At the point of V_p, the probe is at plasma potential, without relative bias, and the ion and electron fluxes correspond to the random thermal motion given by kinetic theory. When the probe is made more positive than the plasma potential, ions are repelled, so that the net current increases by an amount equal to the ion saturation current. The imposition of a bias more positive than the floating potential is reported to result in significant electron losses from the plasma [55]. On the contrary, the electron density increased with the application of a negative dc bias [56].

d) Microwave power and Ionization efficiency

Microwaves are a convenient source of excitation for several applications. The electric fields associated with a microwave discharge system are very complicated, so that they are used mainly as free radical generators or as a source of ions in conjunction with an acceleration system. The usual frequency is 2.45GHz, identical to that used in microwave ovens. When the

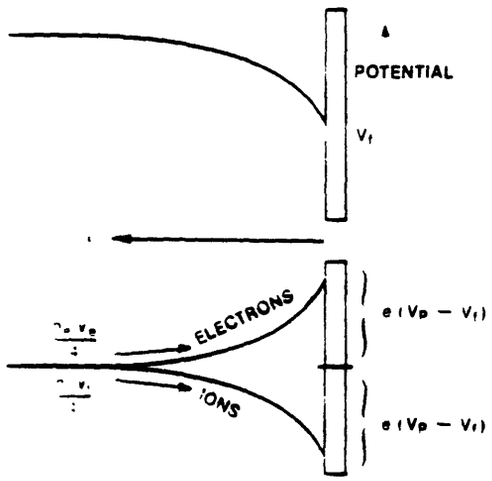

1.4 Variation of the electrical potential and the potential energies of electrons

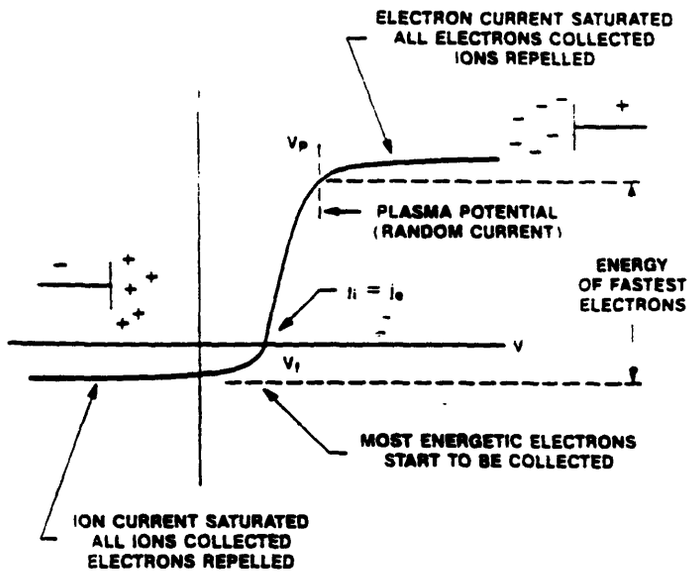

1.5 I-V characteristics of a probe inserted into a plasma glow [54]

magnetic field was lower than 875G, no detectable microwave propagation through the overdense plasma was observed. The increase of microwave power (0-1000W range) causes the increase of the plasma density, and ion saturation current, but electron temperature T_e does not change significantly [57] [58]. However, Outten et al. [59] reported that T_e decreases with the increase of microwave power, and this phenomenon may be explained by the mean free path consideration.(As density increases, the mean free path decreases and in turn causes electron energy loss.) Delfino et al [60] verified that in his ECR hydrogen plasma cleaning experiments, the oxygen removal rate is approximately linear, with considerably more efficient oxygen removal occurring at higher microwave power regime, and the hydrogen atom density is almost proportional to the net microwave power.

e) Magnetic field and Its profile

A magnetic field by solenoid coils is applied to the chamber. The reflection of an electron from a high field strength region leads to the magnetic mirror and by the mirror confinement, plasma is bounded by two high field strength region. In our configuration, the window magnet is centered on the top flange of the ECR chamber and the bottom magnet is centered on the lower flange. Flux density can be computed as a function of Z which is a linear distance along the axis of the ECR chamber, starting at the face of the top flange [61]. As an example, the flux density along the axis for an experimental condition is calculated by using the superposition principles; by adding the field strengths contributed by each individual magnet (Chapter 3).

Under the resonance condition the ionization by microwave power is most efficient. So the plasma density (N_e) peaks up near B = 875G, as expected [62]. It is surmised that the electron temperature is dependent on the magnetic field, furthermore, the average ion energy and the ion energy distributions are reported to be controlled by changing the magnetic field [63].

1.3.2.4 Process Mechanisms

Glow discharge process may proceed by physical sputtering or chemical reaction (etching) or ion-assisted mechanisms. In physical sputtering,

positive ions are accelerated across the sheath and strike the substrate, mechanically eject substrate material. In chemical etching, the role of plasma is only to supply the etching species (and this may be accomplished by the reactive gases without plasma). Chemical etching occurs when active species from the gas phase reach the surface and react to form a volatile product. In ion-assisted etching, neutral species cause little or no etching without ion bombardment, because ion damages the substrate material and make it more reactive toward incident neutral radicals. It should be considered that, however, a variety of elementary mechanisms may come into play depending on the etchant, surface being etched and even on other process variables.

In physical sputtering, the sputter rate can be expressed as [64]:

$$R = -Y_E J/d \tag{1.8}$$

(where R = sputter rate, Y_E = effective yield = f(bias), J = ion flux = f(power, bias, pressure), and d = target density)

In sputtering of SiO_2 in an ECR argon plasma [65], the sputter rate depended on the density and energy of the Ar^+ ions striking the substrate surface. The density of Ar^+ is primarily controlled by the ECR microwave power, and the ion energy can be varied by changing the DC bias.

$$\begin{aligned} \text{Average ion energy} &= V_p - V_{dc} \\ &= (V_p - V_f) + (V_f - V_{dc}) \\ &= V_p + |V_{dc}| \end{aligned} \tag{1.9}$$

where V_p is the plasma potential, V_f = floating potential, V_{dc} = applied substrate bias (negative value).

The chemical etching processes can be divided into a series of steps and an example can be found in case of etching of undoped silicon by chlorine [66]:

1. ion and electron formation:
2. etchant formation:
3. adsorption of etchant on the substrate:

4. reaction to form the products:
5. product desorption:

In ion-assisted etching processes, ion bombardment is required in step 4. In some cases, product desorption is a rate limiting step. The evaporation rates of a material (A) of molecular weight M_a is proportional to its vapor pressure p_A, which also depends on temperature (T), according to the Clausius-Clapeyron equation [67] [68]. Efficient factor α is between 0.1 and 1.0 and the material removal rate (evaporation rate) is given as:

$$\mu_A = \alpha C_a \left(\frac{M_a}{2\pi RT} \right)^{-1/2} e^{-\Delta H/RT} \tag{1.10}$$

The exponential term dominates the temperature dependence. ΔH is the latent heat of evaporation and C_a is a constant for the Clausius Clapeyron equation [69].

Chapter 2

Reactor Description

2-1. Introduction

A multichamber single wafer chemical vapor deposition reactor was built and located in a class 100 cleanroom in TRL (Technology Research Laboratory). Compared to the conventional reactor, which has only one chamber for a particular process, this system integrates multiple but independently controlled vacuum chambers or modules, with a device that can move the wafer from one place to another in the system.

This reactor is a system capable of performing cluster tool processing. With cluster-tool processing, the exposure of the substrate to air, moisture and other contamination can be reduced and the yield and reliability of the process can be increased. In addition to that, however, the adoption of a multichamber system rather than a conventional single chamber system, reduces unnecessary cleaning between successive steps. Because the system can be upgraded module by module, its lifetime can be increased. And the cluster-tool system occupies less cleanroom floor space. Therefore, this cluster tool can reduce the manufacturing costs significantly [70] [71].

To overcome the limitations of a conventional reactor and meet the requirements of device fabrication in the future, the reactor needs to have a maximum flexibility. The present reactor allows us to explore and demonstrate the *in-situ* monitoring of the CVD process. *In-situ* monitors can provide the necessary information on critical parameters, such as film thickness in real time and the information from these monitors can provide feedback and helps control the process parameters.

In addition to having a flexible cluster tool with an *in-situ* monitor and capability of controlling feedback, the new reactor has a capability to control

the condition of wafer surface, which is very important to get a defect-free silicon epitaxial layer. The ECR plasma system has a downstream-nature and needs a separate chamber, where the plasma is generated through the interaction of magnetic field and the microwave. The ECR hydrogen plasma was effective in removing the surface contaminants.

2.2 Chambers

Our reactor design is based on the cluster tool concept, which was designed with a total of five chambers (Fig.2.1 [72]). Four chambers have already been installed, but the fifth one does not yet exist, but have been left for future expansion. The four chambers are Load Lock, Analysis, CVD, and ECR Chamber, respectively. All chambers except for the Load Lock Chamber have been designed to achieve UHV (Ultra High Vacuum). The chambers are made of chemically polished 304 stainless steel.

The Load Lock Chamber has a 100 l/s Alcatel CFF100 turbomolecular pump and additional mechanical pump (3.2 CFM, model UM2004ASL). This chamber has an ionization gauge and a thermocouple for pressure measurement. When a wafer is introduced into the Load Lock Chamber, a chamber pressure of 10^{-7} torr can be obtained in approximately ten minutes.

The Analysis Chamber has cylindrical shape with an inner diameter of 14 inches and also a height of 14 inches. This chamber is an analysis station, which has many ports for future implementation of *in-situ* analysis or inspection tools. At present, LEED (Low Energy Electron Diffraction) and AES (Auger Electron Spectroscopy) have been installed. The top plate of the chamber is removable so that possible modifications can be easily made in the future by the installation of a new top plate. The pumping unit consists of a chemical-resistive, 1500 l/s turbomolecular pump (Leybold Turbovac 1500) backed by a mechanical pump (Leybold Trivac 65 BCS). This is the main pumping unit of this reactor, because the CVD Chamber does not have its own pumping system. There is no gate valve between the Analysis Chamber and CVD Chamber.

A MKS 390 HA capacitor manometer was used to measure pressure throughout the process. The gas pressure was regulated by a control gate valve, which was located between the chamber and the turbomolecular pump. This control gate valve has a 10-inch inner diameter at its maximum and was operated by a Series 64 model 64048-UE52 step motor. When the gas pressure and gas flow rate were set at specific values, the gate valve changed its diameter correspondingly.

A Varian ion gauge was used to measure the base pressure of the chamber, which is 8×10^{-9} Torr. At present, this pressure can be attained by means of an over-night pump-down without bake-out. In the future, it is hoped that a base pressure of 1×10^{-10} Torr may be attained by replacing a KBR window in this reactor with a UHV-grade window. The KBR window is required for FTIR measurement. The analysis chamber is also used as a central facility for wafer transfer, and this chamber will be described in a later section (Section 3.6).

The CVD Chamber is a double-wall, water-cooled chamber with an inner diameter of 14 inches and a height of 12 inches. Water cooling reduces unnecessary deposition on the chamber wall (i.e. when silane is decomposed at high temperature, silicon atoms can be deposited on the hot chamber surface) and as a result a source of particulate contamination is also reduced. Process gases (silane and hydrogen) were delivered through the Nanochem purifiers before entering the CVD chamber, to minimize the level of contaminants within the introduced gas.

An *in-situ* monitor has been installed in the CVD Chamber to monitor the growth of epitaxial film. Currently an E-FTIR (Emission Fourier Transform Infra-Red Spectrometer) is used for the *real-time* monitoring of epitaxial film thickness. In addition to that, a QMS (Quadrupole Mass Spectrometer) was used for an *in-situ* monitoring of gas species. And a Langmuir probe was installed and used for plasma diagnostics study. There are over a dozen ports available for future addition of other *in-situ* monitors and pumping ports. There are some spaces under the chamber for future installation of an independent pumping unit to reduce cross contamination.

The ECR (Electron Cyclotron Resonance) chamber is attached to the side of the CVD chamber and it will be explained in detail in the following section (Section 3.3). The uninstalled fifth chamber can be used for the investigation of other new technologies or innovations.

2.3 Plasma System

The ECR chamber was placed at the side of the CVD chamber (Fig. 2.2 [72]). The magnetic field was generated by the electro-magnets around the ECR chamber. The field causes circular motion of the electrons with the cyclotron frequency, and resonance occurs when the frequency of an incident electromagnetic wave is equal to the cyclotron frequency. When resonance occurs, free electrons and ions are generated and the energy can be transferred very efficiently to other ions and neutrals through series of collisions. The generated plasma can be extracted by magnetic fields or an electrostatic potential applied to substrate in the CVD chamber.

The microwave power source was designed by Applied Science and Technology, Inc. The S-1000 series delivers up to 1.5 kW CW of 2.45 GHz microwave power, precisely regulated to 0.5% of output power with less than 1% ripple. The power source includes advanced automatic protective features and it allows the output power to be clamped so that a preset value of reflected power is not exceeded. The magnetron filament power was controlled automatically within the S-1000 series for optimum operation at every power level. ECR operates at the S-band (2.45 GHz) microwave frequency, so that moderate size magnets could be used. Commercial ASTEX mirror magnets provided the ECR plasma. They consisted of a tube, which was 6 inches in inner diameter and 13 inches in length, with two surrounding coil magnets. The generated plasma was guided in a rectangular copper wave-guide. The plasma passed through a dummy load, directional coupler, a three-stub tuner, a circulator, and entered the ECR Chamber through a UHV grade alumina window.

A circulator directed the reflected microwave power into the dummy load to protect the magnetron and the dummy load absorbed the reflected microwave power. The dummy load was water cooled. A directional coupler coupled the

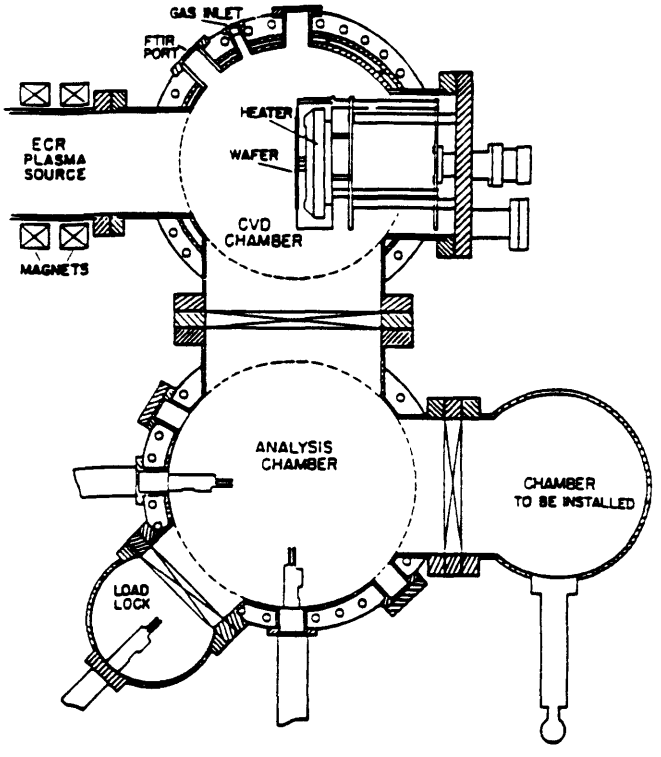

2.1 Schematic of the horizontal cross section of the UHVCVD system [72]

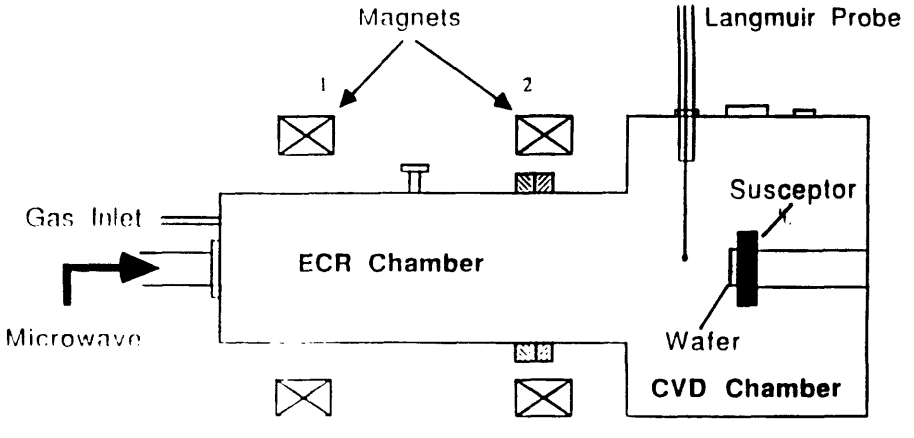

2.2 Schematic of the ECR Chamber [72]

forward and reflected components of the microwave power to the forward and reflected power detectors and monitors. Three-stub tuners matched the impedance of the transmission line to the source. Plasma glow could be seen through the alumina window during the process. A separate gas inlet was located at the side of the alumina window in the ECR plasma. The microwave power varied from 0 to 1000 Watts.

The ECR plasma was characterized by a Langmuir probe; this is one of widely used simple diagnostic technique [73] [62]. The probe measured the plasma potential (or space potential), electron temperature, plasma density and its uniformity. A spherical tip (1.73 mm in diameter) tungsten wire, which extended 2 mm from a ceramic insulator, was embedded in the center of a cylindrical rod and was inserted into the CVD chamber through a double viton o-ring seal. The probe was perpendicular to the magnetic field so that the disturbances of the magnetic field could be minimized.

Water cooling was required for the turbomolecular pump to prevent its over-heating. An interlock was installed on the cooling water line and when the water flow fell below a specified level, the interlock sent a signal to the control box, which then turned off the pump and other equipment. A pressure sensor was installed to prevent the high-pressure operation of the ECR plasma source. The above features contributed to the safe operation of the system.

2.4 Heating System

Resistive/radiant heating was used, because other alternatives (RF induction heating, lamp heating, etc.) were not suitable for this reactor. In the case of lamp heating, a quartz window needed to be installed in the chamber to transfer the energy from the lamp outside the chamber, to the wafer, inside the chamber. To maintain a UHV condition, the seal between the quartz window and the stainless steel chamber needs to be UHV (Ultra High Vacuum) grade and needs to be cooled effectively. But such a seal arrangement was not found. There was an outgasing from the stainless steel chamber wall under strong radiation by lamp and it increased the level of contamination during the CVD process. RF induction heating was not suitable, because the RF energy would have interfered the CVD process, especially where the ECR plasma is

involved. Resistive/radiant heating was compatible with the UHVCVD system, and commonly used in MBE (Molecular Beam Epitaxy) system.

A heater stage was installed in the side of the CVD chamber. The heating element has a pancake shape and its diameter is 5 inches. The heating element is made of silicon-carbide (SiC)-coated graphite filament and the resistance of the filament is 3.5Ω. The heater stage was built by Superior Technology of Edina and has a four-inch wafer holder vertically facing the ECR chamber. Heat shields surrounds the filament to reduce heat losses to the sides, thereby promoting heating efficiency and reducing the heating of the chamber wall. They are made of 5 layers of Tantalum sheets. The heater and its shield are mounted on a 10-inch ConFlat™ flange which is attached to the chamber.

A thermocouple tip was attached behind the first layer of the heat shields to measure the wafer temperature. It was not in contact with the wafer directly, because it was difficult to maintain a repeatable and consistent contact. In addition, a pyrometer was installed to assist the temperature calibration. A DC power supply was used to heat the wafer and the thermocouple signal provided feedback to control the heater power supply, so that a preset wafer temperature can be maintained. Either RF (Radio Frequency) or DC can be applied to bias the wafer substrate through an electrical feedthrough within the entirely isolated heater stage. To hold the wafer and provide its movement and bias connection, there were three fingers outside the heater and its shield. Each fingers had slots, in which the wafer could fit. During the process the wafer was held against the heater.

2.5 Wafer Delivery System

A wafer was hand-loaded into a wafer holder in the Load Lock Chamber. The wafer holder was attached to a rod with two viton o-rings and intermediate pumping in-between. The rod was moved linearly and rotationally. Once the door to the Load Lock Chamber was closed, the pumpdown was started. As soon as the Load Lock Chamber attained the suitable vacuum ($< 10^{-6}$ Torr), the gate valve between the Load Lock Chamber and the Analysis Chamber was opened and the wafer was transferred into the Analysis Chamber. Hydrogen gas was flowed through the Analysis and CVD Chamber to avoid the contamination of

the Analysis Chamber and thus the CVD Chamber. The wafer was transferred to a magnetically coupled rod with a pincher and this pincher was activated by the rotational motion of the magnetic rod (Fig 2.3 [72]). After the wafer was transferred to the pincher, the wafer holder was returned to the Load Lock Chamber by pulling back the rod manually. In this way, contamination from the transfer devices was avoided. After the gate valve was closed, the Analysis chamber/ CVD chamber came back to UHV condition. The wafer was transferred linearly to the CVD chamber by the magnetic rod and then transferred to the heater stage.

Three fingers with slots outside the heater hold the wafer steady. During deposition, the wafer was held against the heater. During transfer, the fingers were moved to the center line of the CVD Chamber to receive and deliver the wafer. After the process was finished, the wafer was taken by the magnetic rod and linearly transferred to the Analysis Chamber. Then it was moved into the wafer holder and transferred to the Load Lock Chamber. The pincher was pulled back outside the CVD chamber to reduce contamination. The wafer was handled vertically throughout the system to reduce particle contamination.

2.6 Gas Handling System

The gas handling system consisted of a gas cabinet which had four gas cylinders inside, house gas points, tubes for gas lines, and a gas distributor. Each gas line had an eight-foot-long tubing, which extended from the cabinet to the chambers. Fast switching and versatility were the goals in building this gas handling system. Dead space was avoided when the distributor was installed. It was placed underneath (and very close to) the chambers so that the gas lines between the distributor and the inlets could be short, and thus fast switching is guaranteed.

As shown in Fig 2.4 [72], the main process valves and the main bypass valves are placed few inches apart from the inlet so that fast and clean gas switching were guaranteed. In the design of the gas inlet to the CVD chamber, there were two independent process lines and two independent bypass lines so that one set of gas mixtures could be prepared (by flowing them through bypass lines), when the other set of gas mixtures were flowing through the

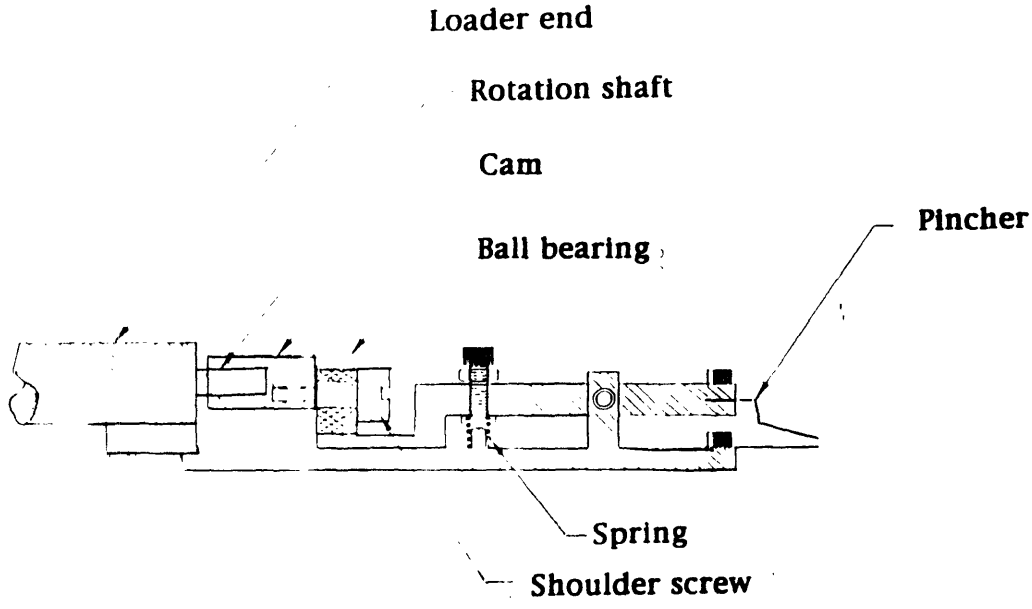

2.3 Schematic of the wafer transfer device [72]

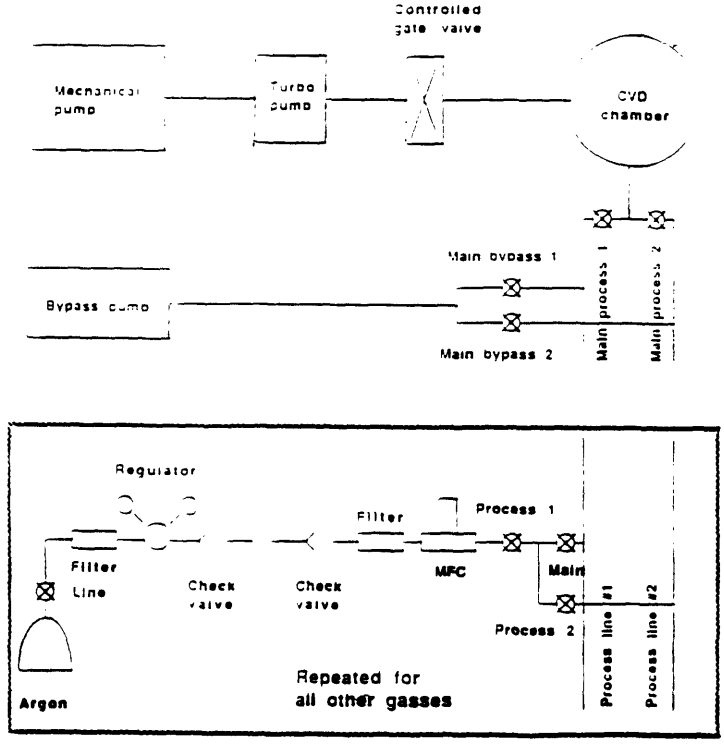

2.4 Schematic of the gas delivery system [72]

process lines. In this system, the first set of gas mixtures could be shut off rapidly, immediately after the second set of gas mixtures were introduced, because of the short distance between the valves and the inlet. This characteristic is useful in growing multilayers or superlattices, which requires sharp interfaces. Currently, a total of six different gases can be introduced into the CVD chamber, and two more can be added if necessary in the future. Dopant concentration in the gas phase can be varied over many orders of magnitude. The ECR Chamber can accept two sets of gas or gas mixtures at the same time. Also argon gas purging can be provided for all chambers.

MKS type 1159 mass flow controllers were used for regulating gas flows. House hydrogen and pure silane passed through the Nanochem purifiers, which proved to be effective in reducing trace impurities, water and oxygen molecules in particular [74]. Nanochem purifiers were installed very close to the inlets just before the mass flow controllers to provide the most purified gases. The long tubing between the gas cabinet and the inlets was not desirable but was unavoidable because there was space nearby for the cylinders in the cleanroom in TRL. Long tubing is not desirable, because it takes much longer to purge all the gas lines and because the chances of contamination are increased.

A high pressure pneumatic valve was installed on the outlet of each gas cylinder. These valves could be closed from the control box inside the cleanroom and shut themselves off in case of fire. Three MDA toxic gas monitors were installed in the gas cabinet, above the Load Lock Chamber and inside the ventilation enclosure. If any of these units were to detect traces of toxic gases, the control box would have automatically shut down the cylinder and all the valves, and the flow of gas would have been terminated.

2.7 Pumping System

There were 4 pumping units (each pumping unit was comprised of a turbomolecular pump backed by a mechanical pump) and one stand-alone mechanical pump. The main pumping system was hooked up to the Analysis Chamber. It consisted of a Leybold Model TMP 1500 l/s turbomolecular pump

and a Leybold Model DCS65 65, cubic feet per minute (CFM) mechanical backing pump. They both were corrosion-resistant, for possible use of dichlorosilane in the future.

The CVD and the Analysis Chamber were not isolated and to get a UHV condition, a large pumping throughput was necessary. A cryogenic pump would be more effective in attaining a lower base pressure, but it is not a "throughput" pump in that it condenses gases instead of pumping them out to exhaust, so it is not suitable for the CVD deposition process, particularly in our reactor. The ideal method would be to use a cryogenic pump to achieve a base pressure and then to use a turbomolecular pump for throughput deposition. Cryopumps are more effective to pump water vapor, but turbomolecular pumps have a very high compression ratio for hydrocarbons. This characteristic is essential to maintain a carbon free environment. The Load Lock Chamber had a small turbomolecular pump (80 l/s, model 5080) and a backing mechanical pump (3.2 cubic feet per minute model UM2004ASL).

The QMS also had a turbomolecular (160 l/s, model 5010) and a backing mechanical pump (3.2 l/s, model UM2004SL) for differential pumping. They all were from Alcatel company. They were not chemical resistant because the chance of exposure to such a corrosive environment would have been unusual. Turbomolecular pumps were used to eliminate carbon contamination. An Alcatel model UM2012 11.2 l/s chemically resistant mechanical pump was used for bypass pumping. Molecular sieve traps were installed in the forelines to prevent the backstreaming of pumping oil. These characteristics helped to maintain a carbon-free environment. To prevent excessive reduction of pumping speed, all the forelines had large diameters. The foreline for the main turbomolecular pump was 4 inches in diameter.

2.8 Quadrupole Mass Spectrometer (QMS)

A Quadrupole Mass Spectrometer (Vacuum Generator 200) with a closed ion source was installed to analyze gas species and this QMS was mounted on the CVD chamber [72]. The inlet path was used either as a residual gas analyzer (RGA) when the system was at base pressure or as an *in-situ* gas monitor when the system was at process pressure (around 1 mTorr). A quartz capillary (its

inner diameter was about 3mm) was extended near the wafer surface. In *in-situ* mode, the capillary was also used as a flow restrictor, so that the vacuum level of 10^{-5} Torr could be obtained. When the QMS was operating in its *in-situ* mode, the high conductance valve was closed and the low conductance valve was opened. Gases were extracted from the wafer edge near the reaction zone and transported through the capillary to the analyzer and then analyzed so that real-time information on gas concentration could be gathered. The analyzer housing was pumped with an independent pumping system consisting of a 450 l/s turbomolecular pump (Alcatel CFF450) backed by a mechanical pump.

A QMS was used as an *in-situ* monitor for gas species. It monitored the pump-down process in real-time in our reactor [75]. The turbomolecular pump was turned on 12 minutes after the mechanical pump was turned on. The level of residual gases in the reactor dropped rapidly after the turbomolecular pump was turned on. Water vapor required the longest time to pump out. Also, changes in residual gas concentration were observed as a result of disturbances due to mass flow controller fluctuation, external magnetic field effect, and a gas line pressure surge. This capability allowed disturbances to be monitored in real-time and permitted the exploration of the source of these disturbances in the future.

Chapter 3

Experimental Procedures

3.1 Surface Cleaning and Deposition

In-situ ECR plasma surface cleaning and the following deposition was performed in a multichamber single-wafer UHV (Ultra-High Vacuum) chemical vapor deposition reactor. The reactor has been located in a class 100 cleanroom in the Technology Research Laboratory (TRL). In our system, the *in-situ* cleaning and deposition cycle was short and efficient, compared to the conventional VLPCVD reactor in TRL: Bake-out was not necessary because the CVD Chamber was not exposed to atmosphere. Also by replacing the RF plasma system with the ECR plasma system, the *in-situ* cleaning time was greatly reduced.

3.1.1 *Ex-situ* Cleaning

Substrates were 4-inch, czochralski-grown, p-type <100> Silicon with the resistivity of 0.5-20 Ω-cm. The wafers were RCA cleaned. The RCA cleaning process consists of the following 7 steps:

1) Dipping in SC-1 solution at 75°C for 10 minutes
2) rinsing
3) HF dipping in 50:1 aqueous solution for 15 seconds
4) rinsing
5) Dipping in SC-2 solution at 75°C for 15 minutes
6) rinsing
7) spin and drying.

The RCA cleaned wafer was HF dipped for 20 seconds in 10:1 aqueous solutions and rinsed in DI (deionized) water. The wafer was then dried by blowing nitrogen with the nitrogen gun inside the station. If the wafers was to be spin-dried, it was transferred to the near-by RCA station. In the spin-

drier, the rinsing time was set at 160 minutes and the drying time was set at 240 minutes. In some cases, HF cleaning process was varied; as an example, the rinsing step could be omitted to observe the effect of water rinsing the cleaning efficiency. All the above processes were done inside the class 100 cleanroom.

It took about only 10 seconds to load the wafer into the Load Lock Chamber of our CVD reactor, after the wafer was blow-dried or spin-dried. A 4-inch wafer was loaded into the Load Lock Chamber by opening the door of the chamber. The wafer was inserted into the wafer holder. After the Load Lock Chamber was pumped down to about $1x\ 10^{-7}$ Torr with the door closed, the wafer could be transferred to the Analysis Chamber by opening the gate valve between the two chambers. Before the gate valve was opened, hydrogen gas was introduced and kept flowing through the CVD Chamber and Analysis Chamber, to avoid cross contamination. A magnetically coupled rod with a pincher held a wafer and it was transferred linearly to the CVD Chamber, where it was unloaded to the heater stage. After the wafer was loaded onto the heater stage, the CVD Chamber was pumped down and ultimately $8\text{-}10 \times 10^{-9}$ Torr could be attained. In our experiments the base pressure was kept at $1\text{-}2x10^{-8}$ Torr.

3.1.2 *In-situ* Plasma Cleaning

In situ predeposition cleaning was done by using ECR hydrogen plasma. The ECR Chamber was at the side of the CVD Chamber (Fig.2.2). The ECR source is a commercial ASTEX mirror magnet and the magnetic field was generated by electromagnets around the ECR Chamber. ECR was operated at the 2.45 GHz S-band microwave frequency and the moderate size magnets were used. The microwave was generated from the magnetron under the control of the model S-1000 microwave power supply. The generated wave was guided in a rectangular copper wave-guide and entered the ECR Chamber through the alumina plasma window. In the region where the magnetic field was 875 gauss, resonance occurred and a very high density of electrons and hydrogen ions was produced efficiently. These electrons and hydrogen ions diffused outward from the source onto the wafer surface in its downstream mode.

The window (top) magnet was centered on the top flange of the ECR Chamber and the bottom magnet was centered on the lower flange. The magnitude of magnetic flux density can be calculated at any point inside the chamber by the superposition principle. Fig.3.1 shows the values of the magnetic field (Gauss) when the window magnet was operated at 150 A and the bottom magnet was operated at 120 A. It is notable that there are three points (actually faces), where the magnetic field is 875 gauss.

3.1.3 Deposition Procedures

Depositions were done by flowing 10 sccm SiH_4 without carrier gases, immediately after the plasma was extinguished, for *in-situ* cleaning at 600°C. For *in-situ* cleaning at room temperature, the wafer was heated up to deposition temperature (600°C) in hydrogen atmosphere, after the plasma was extinguished. A heater stage was installed to the side of the CVD Chamber. A DC power supply was used to heat the wafer and the thermocouple signal provided feedback to the power supply to control the supply of heat to the wafer, so that a preset wafer temperature could be maintained throughout the deposition process. Pure silane and house hydrogen were used for our experiments and these gases passed through the Nanochem purifiers, which were known to be effective in reducing trace impurities [74].

3.2 Materials Characterization Techniques

3.2.1 Haze inspection and Nomarski Optical Microscopy

Haze inspection was performed by using a Model B-100-Y UV inspection lamp (Spectronics Corp.) with a yellow filter to observe the surface of deposited film. The existence of the specific haze pattern or the presence of particulate could be determined [64]. The advantage of haze inspection technique was that the quality of the deposited epitaxial layer could be estimated readily, immediately after the deposition was performed. The ideal epitaxial film may exhibit no visually observable variations in reflected intensities and may appear featureless. However, the surface variation under the UV lamp could not be explained. And the observation (degree of haziness)

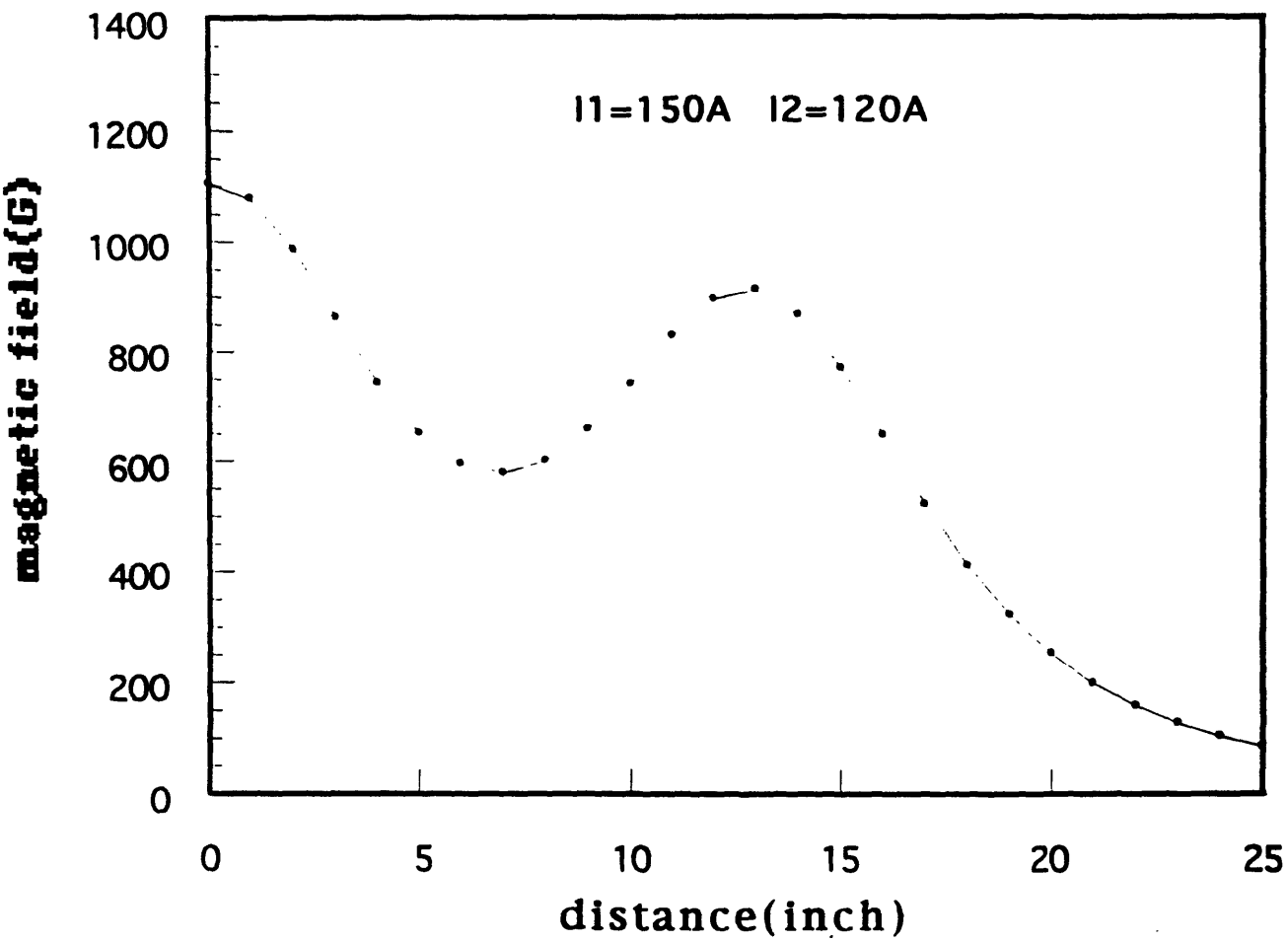

3.1 Magnetic field profile in our two-magnet system (The currents were set at 150 ampere for the top magnet and 120 ampere for the bottom magnet)

under the UV lamp did not correlate well with the structural quality determined by RBS and XTEM. The degree of haziness seemed to be dependent on the thickness of the epitaxial layer.

Differential interference contrast of Nomarski microscopy is a simple and versatile tool for observation of the surface morphological variations. 400x objectives were used with a Nikon optical microscope and a Polaroid camera stage was installed for taking a picture of images. The sensitivity of the technique depends on the specific light source and optics employed, theoretically the periodic undulations or sharp features can be in the 10Å range. The surface quality of the epitaxial layer could be roughly estimated. Fig.3.2(a) shows the surface micrograph of the defect-free epitaxial film, where the surface was perfectly smooth. Fig.3.2(b) shows the surface of the epitaxial film, where the film had stacking faults and the surface was not smooth. It could be confirmed by XTEM analysis.

3.2.2 Plain-view Transmission Electron Microscopy

Plain-view transmission electron microscopy (PTEM) was used to observe the surface of the epitaxial layer, and certify the structural orientation of the epitaxial film with respect to the silicon substrate. This could be done by observing the electron diffraction pattern of film. The procedures for preparing PTEM samples were similar to a portion of the procedures for XTEM. A small part of the wafer was taken off and dimpled on the backside. Ion milling was performed to make a hole and to obtain a very thin region, to be examined by the transmission electron microscope.

3.2.3 Cross-sectional Transmission Electron Microscopy

Cross-sectional transmission electron microscopy (XTEM) was used to observe the epitaxial layer and the epilayer/substrate interface. The TEM used was a model of JEOL 200CX with LaB_6 filament and a line-to-line resolution of about 2.7Å. The procedures for preparing XTEM samples are listed in Appendix B. XTEM could be used to observe the polycrystalline structure and to observe the stacking faults or threading dislocations in the epitaxial layer. It could also be used to determine the degree of surface smoothness in the epitaxial layer by

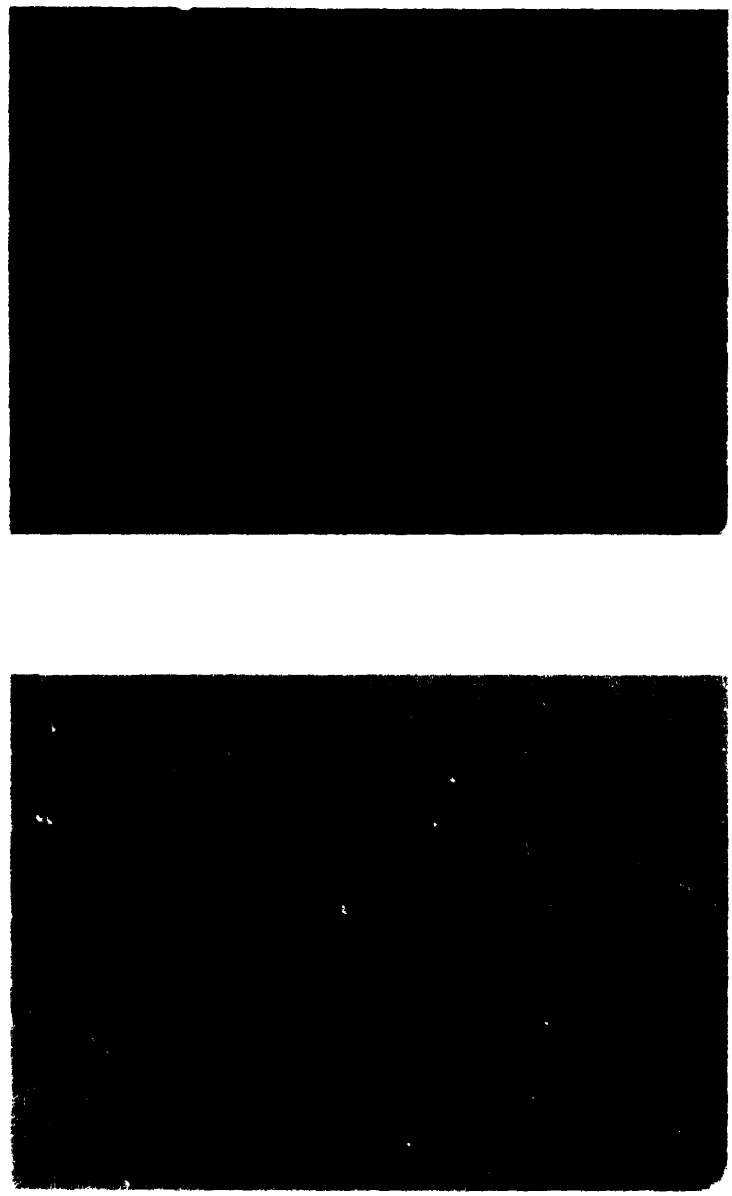

3.2 (a),(b) Optical micrographs of epitaxial films (x400 magnification)

directly observing the deposited film. Dark/bright-contrasted regions were observed and interpreted as areas stressed by hydrogen ion bombardment. By using (110) zone axis technique, the epilayer/substrate interface was observed and the thickness of the interface was determined. It was possible to observe the interface more closely by HR (High Resolution) XTEM technique.

3.2.4 Secondary Ion Mass Spectroscopy

SIMS is an analytical technique that can be used to characterize the surface and near surface (~30μm) region of solids. This technique uses a beam of energetic (0.5 - 20keV) primary ions to sputter the sample materials in the surface layer, producing ionized secondary particles that can be detected by a mass spectrometer. The measurements were made in Evans East, which utilized Perkin Elmer/PHI Model 6300 and Model 6600 Quadrupole SIMS systems. In this analysis, Cs^+ with the energy of 5keV was used and the beam current was about 50na. SIMS had sub-ppm sensitivity for most elements and had a depth resolution of less than 50Å even at depths greater than 1μm and its spatial resolution was less than 5μm. Carbon, oxygen and nitrogen were detected in our research.

Raw data (counts/sec vs. number of sputter cycles) were plotted at the first stage. These raw data were transformed to the processed data (concentration (atoms/cc) vs. depth(microns)) by using RSF (Relative sensitivity factor) as a conversion factor. ^{30} Si isotopes were used in this analysis. The overall accuracy of the profiles were expected to be in the 15-20% range. Areal densities of carbon and oxygen were measured by integrating their areas under the interfacial peaks in SIMS depth profiles.

3.2.5 Ion Channeling / Rutherford Backscattering Spectroscopy

Rutherford backscattering spectroscopy is a non-destructive method to measure the structural quality of the epitaxial layers. This method uses a beam of monoenergetic and collimated alpha particles (mostly ^{4}He particles). These particles impinge on the surfaces of the sample and the energy of the backscattered alpha particle can be measured.

Crystalline materials can be analyzed by energetic ions. The influence of the crystal lattice on the trajectories of such ions is referred as channeling. $^4He^+$ ions with 2 MeV of energy penetrated deeply into the crystal lattice without substantially perturbing the atomic structure. Channeling effects were observed when the crystal axes were aligned to within 1% of the beam direction. The energy spectrum of the particles scattered back from the crystal was observed. In the aligned spectrum, the scattering yield from the bulk of the solid was reduced by almost two orders of magnitude and a peak occurred at a position corresponding to the scattering from the surface atoms (Fig.3.3). This ratio of the channeling yield of the film to the random yield is called χ_{min} and it represents the deviation from perfect crystallinity. The χ_{min} value of the perfect crystal ranges 3-4%. Fig.3.3 (a) shows the result of RBS channeling experiment, which was performed with the defect-free epitaxial film. The χ_{min} value of this film was in 3-4% range. Fig.3.3(b) shows the result of channeling experiments comparing the substrate (perfect crystal) and the defect-free epitaxial layer. Glancing angle was set at 75°.

3.2.6 FTIR Measurements - *In-situ* Monitoring Technique

Epitaxial film thickness was measured *in situ* by E/FTIR (Emission Fourier Transform Infrared spectroscopy) technique. A simple drawing of the E-FTIR set-up is in Fig.3.4 [72]. A Bio-Rad FTIR (model FTS-40) spectrometer, which had a room temperature deuterated triglycine sulfate (DTGS) detector was used to collect the emission FTIR spectra. The E/FTIR technique used the heated wafer as the source of IR radiation, because an external IR source could be used only for *ex-situ* measurement. IR radiation was emitted by the heavily doped substrate (0.001-0.002 Ω cm resistivity) and traveled through the film to the surface. An epitaxial layer was deposited on a wafer, which already had a 7μm-thick epitaxial layer (about 0.5 Ω cm resistivity). The thickness of the growing film was the measured film thickness minus the original film thickness (7μm). The E-FTIR measurement is a non-contact, non-destructive, real-time, and *in-situ* epi-film thickness monitoring technique which was demonstrated to be useful for observing real time growth rates and an incubation time. This technique allowed a fast (2 seconds/scan) and accurate measurement (0.01μm resolution).

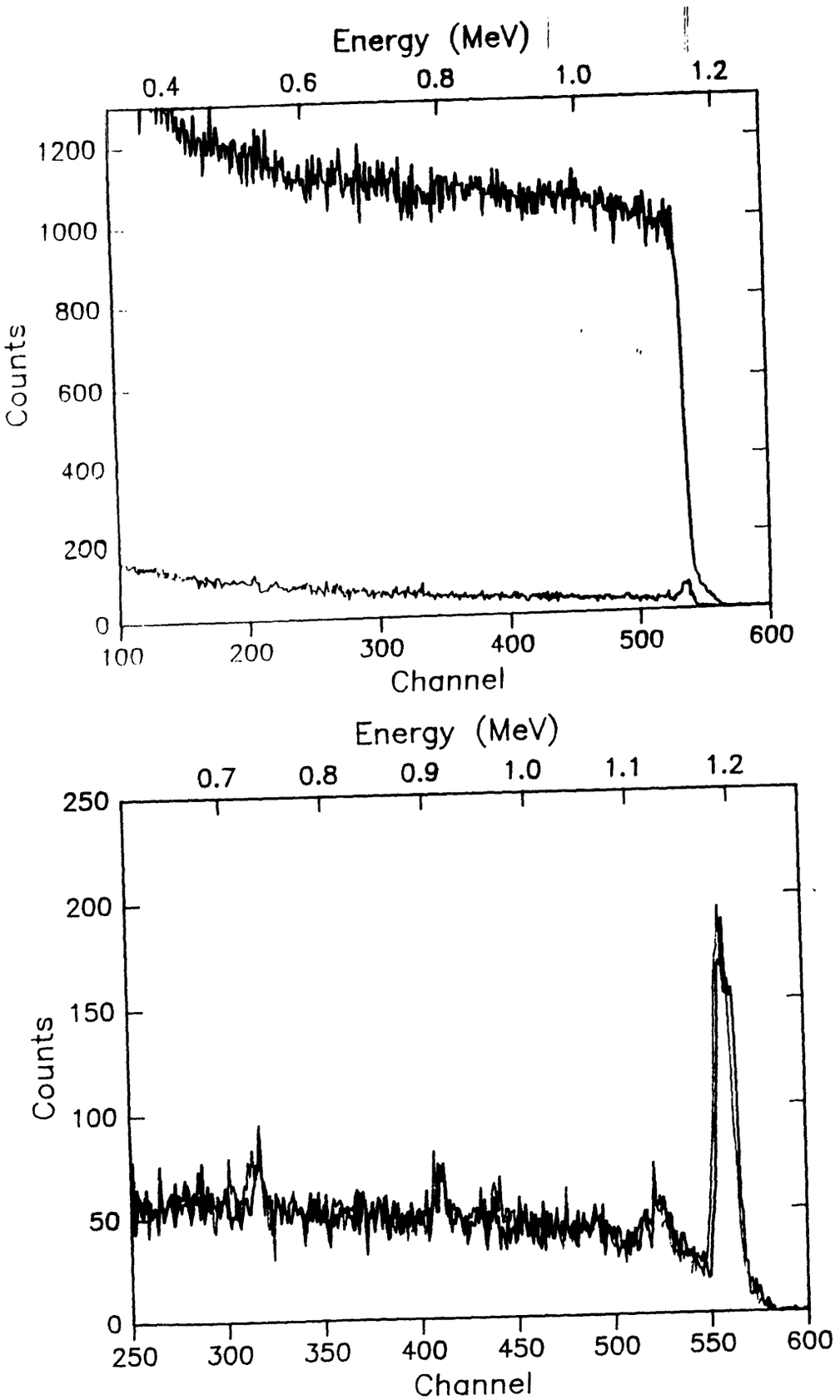

3.3 (a),(b)RBS data for a defect-free epitaxial film

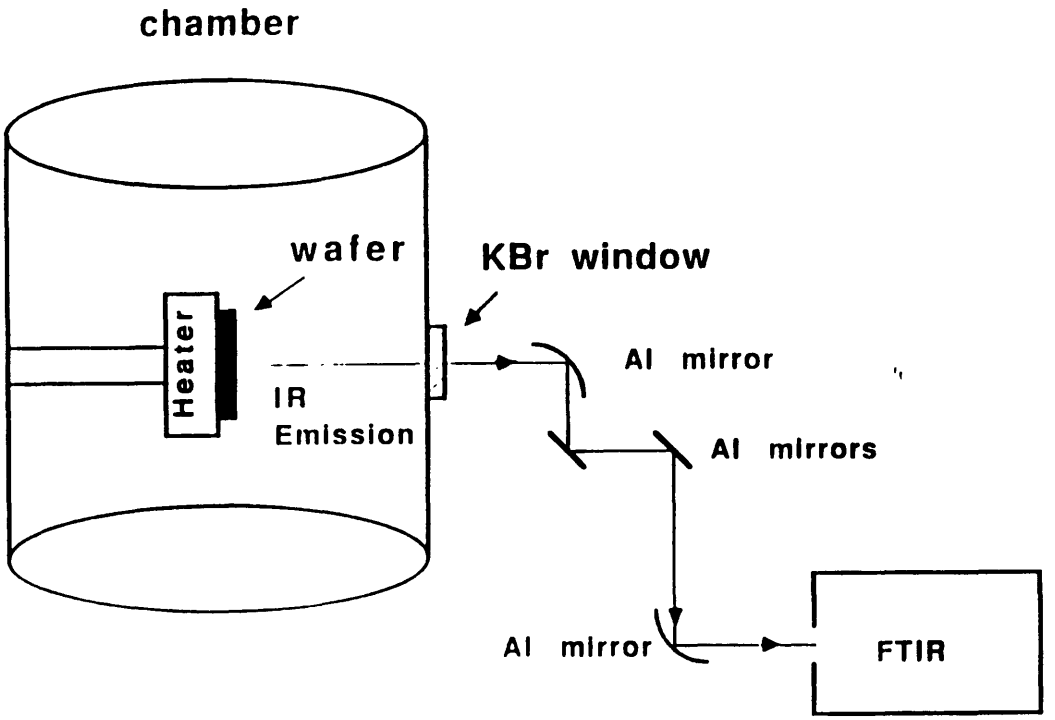

3.4 Schematic of the E-FTIR (Emission-Fourier Transform Infrared Spectroscopy) set-up [72]

Chapter 4

In-situ cleaning : part 1

ECR (Electron Cyclotron Resonance) hydrogen plasma was applied at 600°C to *in-situ* clean the silicon surface of contaminants, such as oxygen and carbon species for subsequent low temperature epitaxial growth. The standard condition with *in-situ* hydrogen plasma cleaning at 600°C has been optimized and process variables such as DC bias, cleaning time, microwave power, and cleaning gas pressure were varied with respect to the standard condition. The epitaxial films, which were deposited in our CVD systems, immediately after these *in-situ* cleaning processes were characterized by XTEM (Cross-sectional Transmission Electron Microscopy), etc. The role of a hydrogen ion in *in-situ* cleaning was clarified by investigating cleaning efficiencies for a variety of conditions. The hydrogen ion, which was produced by ECR plasma excitement, played a crucial role in removing surface contaminants in low temperature (600°C) *in-situ* ECR plasma cleaning processes.

4.1 Introduction

Low temperature processing, which includes low temperature cleaning and low temperature epitaxial growth, is not only important for future silicon ULSI (Ultra Large Scale Integration) technology, but also for silicon-based heterostructures [1] [3]. Thermal exposure at high temperatures needs to be minimized to reduce the dopant diffusion and interface broadening [2] to get an abrupt, well-controlled dopant transition profile. Thermal heating can achieve the surface cleanness, especially at high temperature. With *in-situ* plasma cleaning, plasma energy can replace a considerable amount of thermal energy; it can be applied physically or chemically immediately before the deposition. *In-situ* Ar or He ECR plasma sputtering was applied in our system [25]. However, many defects were generated in the epilayer/substrate interfaces, where the substrates were submitted to ECR argon plasma bombardment prior to growth. A hydrogen plasma is reported to remove the

native silicon oxide at high temperatures such as 800°C [26] and even at lower temperatures [27] without causing much damage, due to its light mass and because hydrogen reacts chemically and removes the surface oxide and hydrocarbons [29]. This issue is particularly important for our low temperature epitaxial growth, because once the stacking faults were generated, defect-free epitaxial film could not be obtained.

The ECR plasma system was selected because it has some advantages compared to conventional RF (radio frequency) plasma systems. The ECR (Electron Cyclotron Resonance) plasma system, which operates at a microwave frequency of 2.45GHz, is able to deliver a higher density of low energy ions to the wafer, because both ionization (about 10% of the gas is ionized) and the saturated ion current are much higher than in the RF plasma system [30]. Particularly, the ECR plasma can be operated with low energy (without sacrificing cleaning efficiency) and ion flux and ion energy can be controlled easily [31]. Possible substrate damage may be reduced because of reduced plasma exposure time and less contamination may be expected due to electrodeless discharge [32]. Additionally, because of the downstream-nature of this ECR plasma system, ions are made to impinge on the substrate with a controlled, low energy. Furthermore, a high electron collision rate was achieved through efficient coupling to propagating plasma waves and a large aspect ratio. ECR is a mature technology and is compatible with UHV (Ultra-High Vacuum) CVD systems [33].

Exposure to ECR hydrogen plasma for a few minutes without applying heat or bias to the substrate completely removed the hydrocarbons and the native silicon oxide. Additionally, it was analyzed and proved by x-ray photoelectron spectroscopy by measuring the O/Si ratio [29]. It is thought that this resulted in a hydrogen terminated surface that was resistant to reoxidation. In our studies, epitaxial layers were deposited at the cleaning temperatures (mostly 600°C) and their structural qualities were investigated to evaluate the efficiency of the ECR hydrogen plasma cleaning processes.

4.2 Experimental

Substrates were 4 inch, czochralski-grown, p-type <100> silicon with 0.5-20 Ω-cm resistivity. The wafer was RCA cleaned and HF dipped for 20 to 30 seconds in 10:1 aqueous solutions. It was then rinsed in DI (deionized) water and dried by blowing nitrogen with the nitrogen gun inside the station. It took approximately 10 seconds to load the wafer into the Load Lock Chamber, after the wafer was blow-dried. After the Load Lock Chamber was pumped down to about 1x 10^{-7} Torr, the wafer could be transferred to the Analysis Chamber by opening the gate valve between the chambers. Before the gate valve was opened, hydrogen gas was introduced and kept flowing through the CVD chamber, to avoid cross-contamination. A magnetically coupled rod with a pincher held a wafer and it was transferred linearly to the CVD Chamber, where it was unloaded to the heater stage. After the wafers were loaded onto the heater stage, the CVD Chamber was pumped down and ultimately 1-2 x 10^{-8} Torr could be attained. It took about 7 minutes to heat the wafer to 600°C, with the flow of the hydrogen gas.

In-situ predeposition cleaning was performed by using ECR hydrogen plasma at 600°C. The ECR Chamber was at the side of the CVD Chamber. The ECR source was commercial ASTEX mirror magnets and the magnetic field was generated by the electromagnets around the ECR Chamber. The microwave was generated from the magnetron under the control of the model S-1000 microwave power supply, was guided into a rectangular copper wave-guide and entered the ECR chamber through an alumina plasma window. The ECR system was operated at the 2.45 GHz S-band microwave frequency and resonance occurred in the region of 875 gauss, where a high density of electrons and hydrogen ions could be produced. These electrons and hydrogen ions diffused outward from the source onto the wafer surface in its downstream mode. In our configuration, the window magnet was centered on the top flange of the ECR chamber and the bottom magnet was centered on the lower flange. Flux density was computed as a function of Z, which is a linear distance along the axis of the ECR chamber, starting at the face of the top flange (Fig.3.1). Resonance absorption occurs when B = 875G and the ionization by microwave power is most efficient under this condition. It seems reasonable to assume that as long as resonance absorption occurs the value of

magnetic flux density is not a critical factor in evaluating the cleaning efficiency. However, plasma density can be affected by confining the electrons with magnetic fields in a mirror-like configuration [61]. Also the average ion energy and the ion energy distribution are reported to be controlled by changing magnetic field [63]. Depositions were done by flowing 10 sccm SiH_4 without carrier gases, immediately after the plasma was extinguished.

4.3 Results

In this study, there were some crucial variables in the ECR plasma cleaning process. The *in-situ* cleaning condition was optimized by the structural characterization of the deposited films. The XTEM micrographs were used to observe the images of the substrate and epitaxial layer and their interfaces. Among the process variables, the effects of microwave power, DC bias voltage, cleaning time, gas pressure and cleaning temperature were the main points to be investigated. Table 4.1 shows the summary of *in-situ* cleaning conditions in our experiments.

4.3.1. Standard Condition

The *in-situ* cleaning process was optimized and the process was evaluated. Samples 4.A and $4.A^+$ were RCA cleaned and dipped for 20-30 seconds into 10:1 DI (Deionized) water : HF solutions, to remove the surface natural oxide. The wafers were rinsed in DI water for about 3 minutes, and were dried by blowing nitrogen. Sample 4.A received the standard (optimized) *in-situ* cleaning, Sample $4.A^+$ did not. The standard condition corresponded to the microwave power of 300W, magnet currents of 150A and 120A for the top and bottom magnets, respectively. A positive 10V DC bias was applied: the positive ions were repelled rather than accelerated across the sheath region, which means that the hydrogen ion energy was reduced. The cleaning was performed by flowing 20 sccm of H_2 at 1 mTorr, at 600°C for 5 minutes. Deposition was done by introducing 10 sccm of SiH_4 at 1mTorr and at 600°C, immediately after the plasma was extinguished. Fig.4.1(a) shows the XTEM micrograph of sample 4.A. A defect-free epitaxial layer and almost invisible epilayer/substrate interface were observed. The epitaxial layer has a perfectly smooth surface. HRXTEM

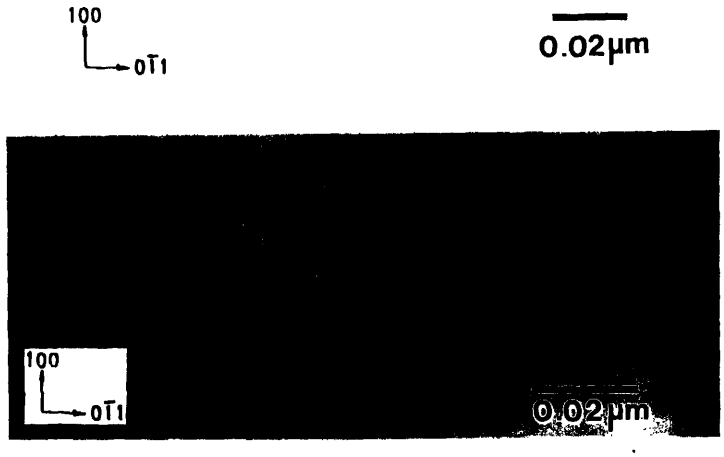

4.1 (a) XTEM micrograph of epitaxial film, cleaned *in-situ* with standard condition at 600°C.

(High Resolution Cross-sectional Transmission Electron Microscopy) micrographs were shown in Fig.4.1(b). Lattice images could be observed in the substrate and in the epitaxial layer. The interface was discrete.

Fig.4.1(c) shows the micrographs of Sample 4.A$^+$. Stacking faults were initiated in the epilayer/substrate interface. The thickness of the epilayer/substrate interface was about 150Å. The interfacial oxygen concentration of Sample 4.A$^+$ was much higher than that of Sample 4.A (Table 4.2). Therefore, the standard *in-situ* cleaning was effective in removing surface natural oxide, which was present on the wafer surface after *ex-situ* cleaning. Since Sample 4.A$^+$ did not receive an *in-situ* cleaning, the surface contaminants, surface oxygen, should have caused the stacking faults.

In RBS channeling experiments, the χ_{min} of Sample 4.A and Sample 4.A$^+$ was about 3% and 7%, respectively. Therefore, the structural quality of the epitaxial layer in Sample 4.A was comparable to that of the substrate. Also in RBS channeling experiments, a detector with a high glancing angle (about 75 degrees) was used to maximize the sensitivity in detecting heavy metal elements. For sample 4.A, no trace of such elements were found by this technique. This result is compared to an ECR Ar (argon) plasma cleaned sample [72] in our system, in which a considerable amount of heavy elements (Ar, Mo, Ta) were found in the epilayer/substrate interfaces.

4.3.2. Effect of DC Bias

The substrate was either floated or DC biased in our experiments. V_p- V_f is the difference between the plasma potential and the floating potential, and $e(V_p-V_f)$ - $e(V_{dc})$ thus represents the ion energy in the presence of the substrate DC bias. V_{dc} is a negative value and thus - $e(V_{dc})$ is positive.

Fig.4.1(a), Fig.4.2(a) and Fig.4.2(b) are XTEM micrographs of Samples 4.A, 4.B and 4.C and in these cases +10V, 0V(floated) and -50V of DC bias was applied, respectively. The other process variables were the same. When increasing the hydrogen ion energy by the amount of 10eV from the standard condition, the substrate was floated and the interface became clear and thick (about 30Å) enough to be observed, while the defect-free epitaxial layer was deposited

4.1 (b) HRXTEM micrograph of epitaxial film, cleaned *in-situ* with standard condition at 600°C

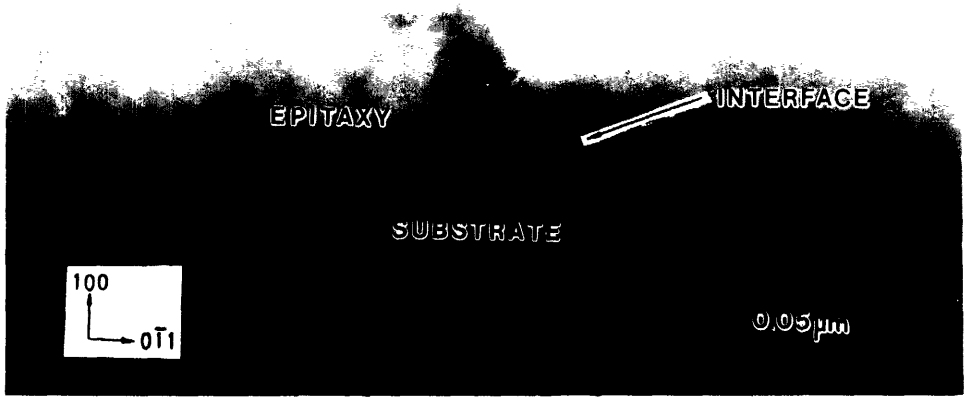

4.1 (c) XTEM micrograph of epitaxial film, without *in-situ* cleaning (Rinsed and blow dried)

(Fig.4.2(a)). It is interesting to observe that the surface of the 0V-cleaned epitaxial layer is a little bit curved compared to the +10V-cleaned one, in which case, the surface of the epitaxial film is quite smooth. It is not clear what causes this difference. SIMS data tell us that Sample 4.B has a higher oxygen concentration than Sample 4.A in the epilayer/substrate interface (Table 4.2). Oxygen species may be present at the epilayer/substrate interface of Sample 4.B. As the epitaxial layer grows to some thickness, the silicon around the second phase coalesces and forms some surface structures. This may happen without generating dislocations or stacking faults if the sizes and quantities of the second phases are small. Possible damage to the substrate by hydrogen ion bombardment is not clear. Hydrogen ion energy is transferred to the silicon substrate, rather than used in removing oxygen. It is surmised that plasma in this sample had some non-uniformity.

In Sample 4.C, where - 50V of DC bias was applied to the substrate, the ion energy was increased by the amount of 60eV with respect to the standard condition (Sample 4.A). About 300Å-thick layer of substrate was highly damaged and the substrate below this region was observed to be highly stressed (Fig.4.2(b)). Dark/bright contrasted regions were observed in the substrate, and high densities of stacking faults and dislocations were present in the film. This observation can be related to the hydrogen ion bombardment, which was energized by applying a negative substrate DC bias.

Fig.4.2(c) is a XTEM micrograph of Sample 4.D and in this case, + 30V of DC bias was applied in its *in-situ* plasma cleaning and the other process variables were the same as the standard condition. The film was an epitaxial layer with a smooth surface, but it had a considerable amount of stacking faults which were initiated from the interface. Threading dislocations were generated in the epilayer/substrate interface and they existed throughout the film. It was surmised that oxygen or other contaminants could not be removed easily from the surface, because ion bombardment energy was reduced by supplying a positive 30V of DC bias. The substrate DC bias played a significant role in obtaining a damage-free, chemically clean interface [76].

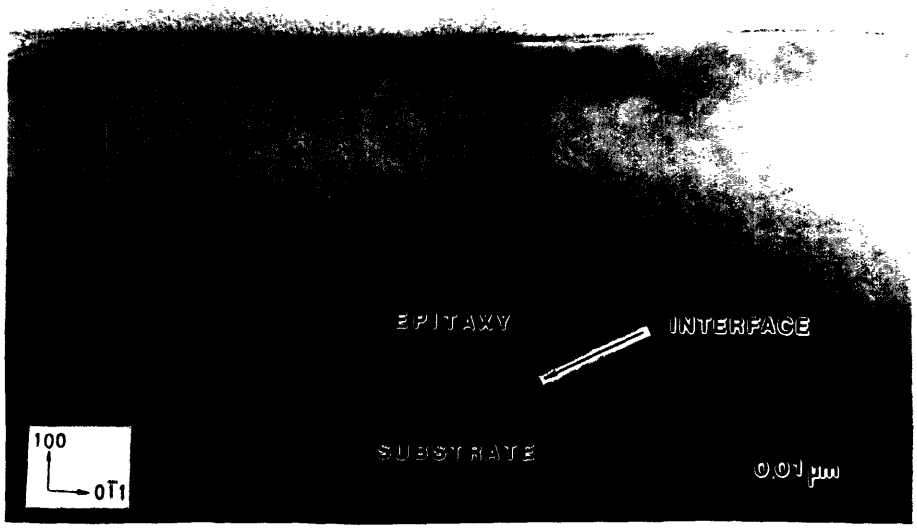

4.2 (a) XTEM micrograph of epitaxial film, cleaned *in-situ* at 600°C with DC bias set at 0V

4.2 (b) XTEM micrograph of epitaxial film, cleaned *in-situ* at 600°C with DC bias set at -50V

4.2 (c) XTEM micrograph of epitaxial film, cleaned *in-situ* at 600°C with DC bias set at 30V

4.3.3. Effect of Cleaning Time

Fig.4.3(a) and Figs.4.3(b),(c) show the XTEM micrographs of Sample 4.E and Sample 4.F, which were cleaned for 2 minutes and for 20 minutes, respectively and the other process variables were the same as the standard condition. Fig. 4.3(a) showed broad (about 200Å) interfaces, but a well-grown epitaxial layer. In some positions (not shown here), however, defects were present near the epilayer/substrate interface, which were regarded as oxygen-induced stacking faults or dislocations. Fig.4.3(b) shows the XTEM micrographs of Sample 4.F, which represent the well-grown epitaxial layer. Fig.4.3(c) shows the HRXTEM micrographs of Sample 4.F and the lattice images of the epitaxial layer; the substrate and the epilayer/substrate interface were observed. This sample had a higher interfacial oxygen concentration than Sample 4.A (Table 4.2). The interface looked discrete at some points but compared to Fig.4.1(b), the interface was thicker (20-30Å) and more distinct.

Cleaning for 20 minutes, did not improve the quality of the epilayer/interface that much. Clearly, the oxygen species accumulated in the epilayer/substrate interface, during the long-time cleaning for some reason; this could be proved by SIMS oxygen analysis (Table 4.2). Small quantities of process-generated oxygen containing species may have chemisorbed on the surface during exposure to the hydrogen plasma [28], and the bare silicon surface may have been reoxidized during exposure to the plasma. However, longer cleaning at the standard condition did not induce significant damage to the substrate. During the *in-situ* cleaning process, there should be a competition between the silicon dioxide etching and the reoxidation of the silicon surface. The source of reoxidation is not clear but the internal surfaces of the stainless steel chamber were probably covered with layers of water molecules. These could be excited and desorbed by ECR plasma energy during the *in-situ* cleaning process and may have adsorbed on the silicon surface.

4.3.4. Effect of Microwave Power

Current literature reports that in an ECR (electron cyclotron resonance)-type plasma system, an increase of microwave power does not cause an elevation in the electron temperature but causes the growth of the level of

4.3 (a) XTEM micrograph of epitaxial film, cleaned *in-situ* at 600°C for 2 minutes.

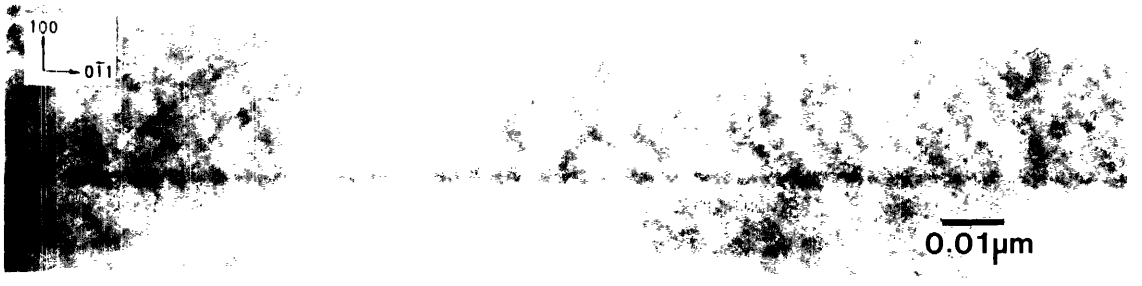

4.3 (b) XTEM micrograph of epitaxial film, cleaned *in-situ* at 600°C for 20 minutes.

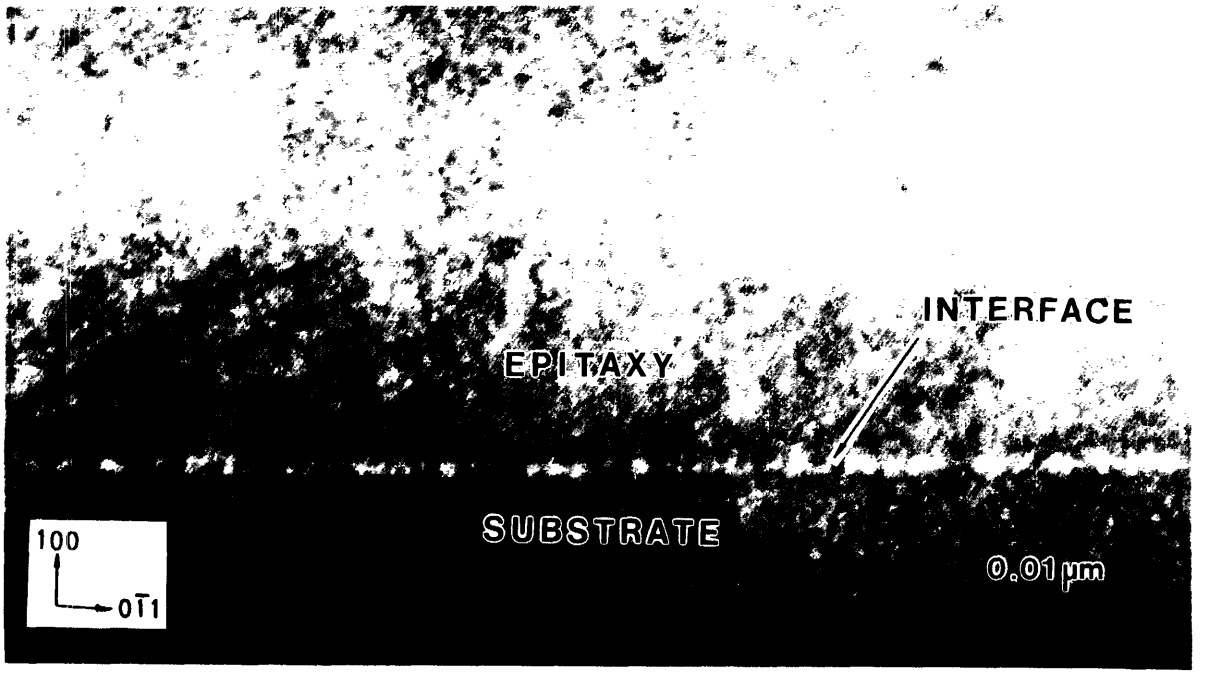

4.3 (c) HRXTEM micrograph of epitaxial film, cleaned *in-situ* at 600°C for 20 minutes.

.icrowave power absorption, which results in further ionization and an increase of plasma density and ion saturation current [57]. In electron cyclotron resonance hydrogen plasma, an increase of net microwave power (0-1000W range) causes an increase in the plasma density and ion saturation current. Delfino et al. [31] verified that in his ECR hydrogen plasma cleaning experiments, the oxygen removal rate turned out to be proportional to the microwave power, because the XPS measured O/Si ratio was inversely proportional to the net microwave power. The hydrogen atom density was proportional to the net microwave power (i.e. applied microwave power - reflected microwave power).

In our studies, the net microwave powers varied from the standard condition; XTEM micrographs are shown in Figs.4.4(a) and 4.4(b). Fig.4.4(a) shows the micrograph of Sample 4.G, where the net microwave power was 150W. The micrograph shows a highly defective epitaxial layer. Stacking faults was formed in the epilayer/substrate interface, probably due to surface oxygen species. It seems that there is a threshold power between 150 and 300W and beneath this threshold power, plasma density is not big enough to clean up the oxygen species form the wafer surface. Sample 4.H, where the net microwave power was about 540W, shows a continuous interface and a defect-free epitaxial layer. Although high-microwave-powered *in-situ* cleaning proved to be effective in cleaning substrate, it did not generate many defects in spite of its higher plasma density. Instead, cleaning efficiency became saturated as the net microwave power increased to 300W and above. Delfino's cleaning experiments were done at 2.5 mTorr and at room temperature, for 60 seconds. Two distinct regimes of oxygen removal were observed and there was a discontinuous transition at around 600W. Our experiments were done at 1mTorr and at 600°C, for 300 seconds. This condition is favored in efficient cleaning compared to the Delfino's *in-situ* cleaning conditions. In our case, a threshold power to get a defect-free epitaxial layer seems to have moved to a lower value.

4.3.5. Effect of Cleaning Gas (H_2) Pressure

The mean free path of an ion, defined by collisions with neutral particles, is inversely proportional to the gas pressure [77]. Microwave plasma etching

4.4 (a) XTEM micrograph of epitaxial film, cleaned *in-situ* at 600°C with microwave power set at 150W.

4.4 (b) XTEM micrograph of epitaxial film, cleaned *in-situ* at 600°C with microwave power set at 540W.

tends to be performed at lower gas pressure, because the mean free path of an ion becomes longer than the width of the sheath and the accelerated ions along electric fields can impinge on the substrate perpendicularly, without being scattered by other particles. This argument can be applied to our microwave plasma *in-situ* cleaning processes. In the RF plasma system, at a lower pressure of 10-100 mTorr, the energy-driven damage mechanism tends to be more important than the chemical etching and finally, at a very low pressure, below 10 mTorr, physical sputtering dominates [78]. The ECR plasma system has an advantage over the conventional RF plasma system, because ions are accelerated by low potential energy and both surface damage and contamination can be reduced. Therefore, in the ECR plasma system, the regime of chemical etching will expand compared to RF plasma systems, lower pressure is needed to turn the *in-situ* cleaning process into the physical sputtering regime. Delfino [31] et al. observed the decrease of the O/Si ratio with the decrease of hydrogen pressure over 0-25 mTorr range in his ECR plasma cleaning system. However, the oxygen removal rate was relatively insensitive to pressure up to 14 mTorr.

In our experiments, standard *in-situ* cleaning was done at the hydrogen pressure of 1 mTorr. Fig.4.5(a) shows the XTEM micrograph of Sample 4.I. In this experiment, *in-situ* cleaning was done at 8 mTorr instead of 1 mTorr. Stacking faults were shown to be initiated in the epilayer/substrate interface and the thickness of the interface is around 100Å. Table 4.2 shows the SIMS data of Sample 4.I. High concentrations of oxygen were observed in the epilayer/substrate interfaces. Probably oxygen contaminants could not be removed easily in this case. Fig.4.5(b) shows the XTEM micrographs of Sample 4.J. *In-situ* cleaning at lower pressure (0.5 mTorr) was proved to be effective as well and its XTEM micrograph shows the continuous but relatively thin interface (around 20Å) and defect-free epitaxial layer. It is reasonable to assume that the ECR hydrogen plasma cleaning in our experiments is not purely chemical in nature, because mainly ions, not neutrals were involved in the cleaning processes.

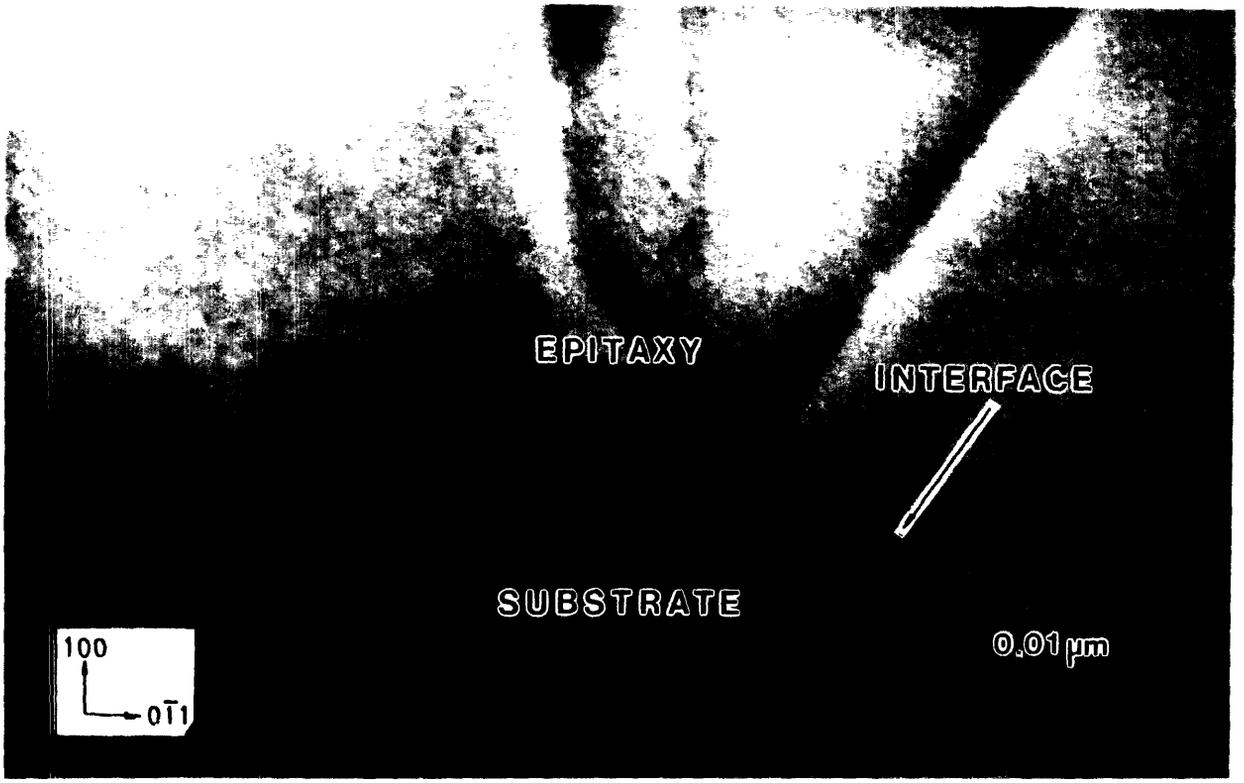

4.5 (a) XTEM micrograph of epitaxial film, cleaned *in-situ* at 600°C with pressure set at 8mTorr

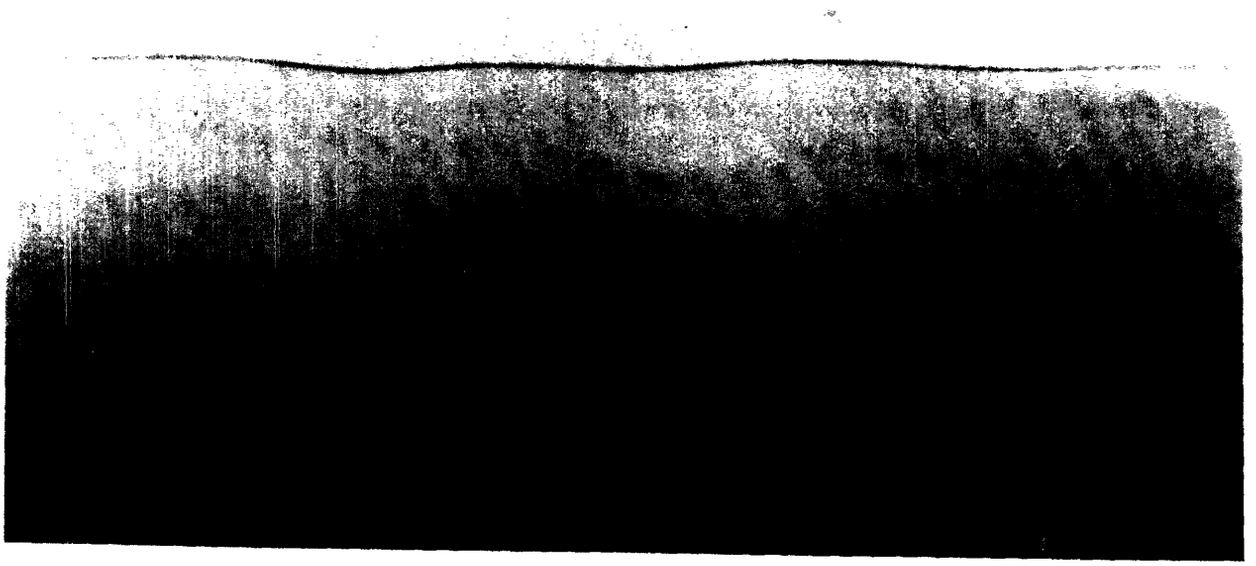

4.5 (b) XTEM micrograph of epitaxial film, cleaned *in-situ* at 600°C with pressure set at 0.5mTorr

Table 4.1 Summary of *in-situ* cleaning conditions

	Power	DC bias	Temp.	Time	Pressure
Sample 4.A	300W	10V	600°C	5min	1mTorr
Sample 4.B	300W	0V	600°C	5min	1mTorr
Sample 4.C	300W	- 50V	600°C	5min	1mTorr
Sample 4.D	300W	30V	600°C	5min	1mTorr
Sample 4.E	300W	10V	600°C	2min	1mTorr
Sample 4.F	300W	10V	600°C	20min	1mTorr
Sample 4.G	150W	10V	600°C	5min	1mTorr
Sample 4.H	540W	10V	600°C	5min	1mTorr
Sample 4.I	300W	10V	600°C	5min	8mTorr
Sample 4.J	300W	10V	600°C	5min	0.5mTorr

Table 4.2 Summary of SIMS data

	oxygen(cm^{-2})	oxygen(cm^{-3})	carbon(cm^{-2})	carbon(cm^{-3})
Sample 4.A+	$1.0x10^{15}$	$7x10^{20}$	$1.1x10^{14}$	$1x10^{20}$
Sample 4.A	$4.8x10^{13}$	$9x10^{19}$	$4.5x10^{14}$	$6x10^{20}$
Sample 4.B	$8.1x10^{14}$	$3x10^{20}$	$3.8x10^{13}$	$3x10^{19}$
Sample 4.F	$5.9x10^{14}$	$7x10^{20}$	$2.1x10^{13}$	$2x10^{19}$
Sample 4.I	$1.0x10^{15}$	$8x10^{20}$	$6.3x10^{14}$	$6x10^{19}$

4.4 Discussions

In-situ ECR plasma cleaning may proceed by physical sputtering or chemical reaction (etching) or ion-assisted mechanisms. Excessive hydrogen ion bombardment produced a highly damaged silicon surface [79] and in our experiments, applying - 50V of DC bias during *in-situ* cleaning damaged the substrate. A positive bias was needed to reduce the hydrogen ion energy [80]. Also in our experiments, reducing the hydrogen ion energy by supplying a positive DC bias resulted in growing a defect-free silicon epitaxial layer. It was observed that *in-situ* cleaning at higher hydrogen pressure generated many

defects in the epitaxial layer and a defect-free epitaxial film was deposited with the *in-situ* cleaning at pressures less than 1mTorr. Therefore the ECR hydrogen plasma cleaning is more like an ion-assisted or physical sputtering process, rather than a pure chemical etching process. The effect of microwave power on the *in-situ* cleaning efficiency was not clear but ion density is reported to scale with microwave power [81]. Delfino et al. reported that more efficient oxygen removal occurred at a higher microwave power regime [29] and this trend has been proven in our experiments by real epitaxial depositions and structural analysis of the epitaxial films. At any rate, the ECR (Electron Cyclotron Resonance) hydrogen plasma cleaning process is closely related to the behavior of a hydrogen ion, whether that hydrogen ion leads to reactions with some Si-O bonding configuration or whether it directly strikes the bonding configurations and breaks them by ion bombardment.

The kinetic energy of the ions can be obtained by summing the plasma potential : $e(V_p - V_f)$ and a negative of DC bias energy : $e(-V_{dc})$. If the collision-cascade theory of physical sputtering holds, the threshold energy for physical sputtering is proportional to surface binding energy. Relative threshold energy (threshold energy/surface bonding energy) is a function of the mass ratio : the mass of incident ion to that of target atom. Stuart and Wehner found in their experiments that the threshold energy is proportional to the surface binding energy independent of the ion-target combination. In case of SiO_2 physical sputtering with hydrogen ion, the relative threshold energy is approximately 4 [82]. The surface binding energy of SiO_2 can be derived from the sublimation energy (8.4 eV), it is 33.6 eV and in good agreement with the measured value (34 eV) in our system [83]. Therefore, the threshold energy for physical sputtering is calculated to be about 134 eV (magnitude) in our case and if it is assumed that $e(V_p - V_f)$ is about 30± 5 eV for ECR hydrogen plasma [84], it is surmised that at least - 100 V of DC bias is needed for physical sputtering to be effective in our ECR hydrogen plasma cleaning system.

In our experiments, ion energy was reduced by supplying a positive DC bias in optimizing the *in-situ* cleaning processes. So the physical sputtering cannot be a dominant process and since the hydrogen ion is doing a crucial role in surface cleaning, ion-assisted etching will be a dominant process. In this case an impinging ion damages the surface and increases its reactivity.

Hydrogen neutrals or ions react with some Si-O bonding configuration and volatile species can be desorbed from the surface. The mechanisms of these reactions will be discussed in more detail in Chapter 7.

Reoxidation of a silicon surface may occur because the plasma may transform a portion of the residual water vapor into OH radicals which could adsorb on the silicon bare surface. In our experiments, longer (20 minutes) exposure to plasma did not improve the interface quality that much and oxygen clusters could be shown in HRXTEM micrographs (Fig.4.3(b)). This observation may be explained by the reoxidation of a silicon surface during over-exposure to plasma. Water vapor, the most abundant source of oxygen, may exist in the form of residual gas inside the chamber and also may be present on the inner surfaces of the chamber wall.

Chapter 5

In-situ cleaning : part 2

A defect-free silicon epitaxial layer was deposited by *in-situ* ECR (Electron Cyclotron Resonance) hydrogen plasma cleaning at room temperature (25°C) in a MS-CVD (Multi-Chamber Chemical Vapor Deposition) system with a Load Lock Chamber. ECR (Electron Cyclotron Resonance) hydrogen plasma was used and films were deposited thermally at low temperature (600°C). Plain-view TEM, XTEM, RBS, SIMS and *in-situ* E-FTIR (Emission-Fourier Transform Infrared Spectroscopy) results were presented to demonstrate the efficiency of room temperature *in-situ* wafer cleaning processes. Process variables such as microwave power (and gas pressure), cleaning temperature and DC bias were investigated, and a DC bias turned out to play a crucial role in room temperature *in-situ* cleaning processes. The effect of *in-situ* cleaning temperature on cleaning efficiency was investigated and discussed.

5.1 Introduction

Lower temperature processing for the semiconductor device fabrication process has been a major issue in solid state microelectronics and is becoming more important in modern ultra large scale integration technologies. The reduction in temperature may suppress the dopant diffusion so that abrupt transition regions can be obtained. It is crucial to minimize the thermal heating during *in-situ* cleaning to reduce autodoping and broadening of dopant profile. A low temperature cleaning technique not only reduces thermal heating during the cleaning process, but it also may be able to lower the subsequent deposition temperature by effectively cleaning the silicon wafer surface before depositing the epitaxial layer.

For low temperature *in-situ* cleaning, numerous methods such as Ar ion sputtering [85], Ar/hydrogen ion sputtering [86], and hydrogen plasma

cleaning [87] have been tried and investigated. Ar or Ar/H_2 plasma sputtering is an effective cleaning technique but high temperatures were required to anneal out substrate damage which was generated during plasma exposure. The substrate damage is reported to be generated mostly by heavy ion (Ar) bombardment. Compared to conventional RF plasma systems, the ECR (Electron Cyclotron Resonance) plasma system can deliver a higher density of low energy ions to the substrate without sacrificing cleaning efficiency. This system is easily and more accurately controlled and substrate damage can be reduced [28]. *In-situ* wafer cleaning was performed with Ar ECR hydrogen plasma at 600°C in our system. Epitaxial layers could not be deposited due to the excessive damage on the substrate surface. Therefore it is surmised that the ECR technique may reduce the ion energy. However, once damage was introduced to the substrate, it could not be annealed at temperatures of 600°C or below.

Hydrogen is the lightest element and is reported to react chemically with carbon or oxygen, so severe substrate damage during ion bombardment may be reduced, while keeping the substrate surface clean. Hydrogen plasma exposure may be based on the ion etching effect [88] [89] and the hydrogen passivation effect at low temperatures [90]. Internal reflection measurements showed the presence of Si-H bonds on the HF-treated silicon surface at about a monolayer density [91] [92]. H_2 prebake is a simple and reliable method for removing contaminants like carbon and oxygen from the silicon surface [2] but a very high temperature, more than 1000°C, is required. In an attempt to lower down the prebake temperature, hydrogen plasma exposure has been tried [28].

Although it is required to lower the *in-situ* cleaning temperature for thermal budget and for future application, the effect of temperature on the *in-situ* cleaning efficiency has been unclear. Kishimoto et al. [93] studied the temperature dependence of the hydrogen plasma cleaning process by *in-situ* RHEED monitoring of the cleaned surface. They concluded that the cleaning efficiency was inversely proportional to the cleaning temperature. In our experiments, the temperature dependence of cleaning efficiency was studied by depositing epitaxial layers on the *in-situ* cleaned surfaces and by observing the structural qualities of those films. Kishimoto et al. suggested a

silicon etching mechanism for the *in-situ* ECR hydrogen plasma cleaning in a temperature range of 300-500°C. Zhou et al. investigated the mechanisms of room temperature *in-situ* cleaning with hybrid microwave-RF plasma hydrogen plasma by the ATR-FTIR (Attenuated Total Reflection Fourier Transform Infrared spectroscopy) method [79]. Possible mechanisms need to be investigated and discussed.

Without thermal heating at a high temperature, it would be best to minimize the sources of possible contamination. For a conventional CVD system, the inner wall of the main chamber was frequently exposed to atmosphere when loading/unloading the wafers and bake-out treatment was needed before *in-situ* cleaning and deposition. However, even after the bakeout, considerable amounts of contaminants stayed inside the chamber and were adsorbed onto the wafer surface during the processes. A Load Lock Chamber was installed in our system to minimize the possible exposure of the inner wall of the main chamber and thus minimize the introduction of contaminants such as water vapor.

5.2 Experimental

Substrates were 4 inch, czochralski-grown, <100> oriented, p-type silicon with 0.5-20 Ω-cm resistivity. In some cases, a heavily doped wafer was used for E-FTIR (Emission-Fourier Transform Infrared Spectroscopy) and its resistivity was 0.001-0.002 Ω-cm. The wafers were RCA cleaned in an RCA station. A wafer was dipped in 10:1 DI (Deionized) water: HF solution for 20 to 30 seconds and then rinsed in deionized water and dried by blowing nitrogen, which was done in an acid-hood in the TRL (Technology Research Laboratory) class 100 cleanroom. After these *ex-situ* cleaning processes, the wafer was loaded into the Load Lock Chamber of our CVD system.

After a wafer was loaded into the Load Lock Chamber (Fig.2.1) [72], the Load Lock Chamber was pumped down to about 1×10^{-7} Torr and the wafer was transferred to the Analysis Chamber by opening the gate valve between the Analysis and the Load Lock Chamber. It was then transferred linearly to the CVD Chamber, where it was unloaded to the heater stage. After the wafers were

loaded onto the heater stage, the base pressure was measured to be around 1-2 x 10^{-8} Torr.

In-situ predeposition wafer cleaning was done by using ECR hydrogen plasma at room temperature. The hydrogen pressure was kept at 1mTorr and the flow rate was kept at 20 sccm (standard cubic centimeters per minute) and the *in-situ* cleaning was done for 5 minutes. ECR was operated at the 2.45 GHz S-band microwave frequency. The window magnet was centered on the top flange of the ECR chamber and the bottom magnet was centered on the lower flange. Their currents were set to 150A and 120A, respectively. The wafer was then heated up to 600°C in hydrogen flow with a pressure of 1mTorr (or 8mTorr) and a flow rate of 20 sccm. It took about 7 minutes to heat up from 25°C to 600°C, which was a well-characterized deposition temperature in our system. When the *in-situ* cleaning was done at 250°C, it took about 4 and-a-half minutes to heat it up. A heater stage was installed to the side of the CVD chamber and the wafer was seated vertically in front of a resistive/radiant heater, which was made of SiC (silicon carbide)-coated graphite.

Rutherford backscattering spectroscopy (RBS) was used to measure the crystalline quality of the epitaxial films. The crystalline quality of the epitaxial film was determined by the ratio of the channeling yield of the film to the random yield (χ_{min}). Cross-sectional transmission electron microscopy (XTEM) was used to observe the epitaxial layer and the epilayer/substrate interface. Plain-view transmission electron microscopy (PTEM) was used to check the epitaxial quality and crystal direction of the deposited films. The SIMS measurement was done in Evans East, New Jersey and Cs^+ ion was used as the ion source for sputtering.

Epitaxial film thickness was measured *in situ* by the E/FTIR (Emission Fourier Transform Infrared spectroscopy) technique. A Bio-Rad FTIR (model FTS-40) spectrometer equipped with a room temperature deuterated triglycine sulfate (DTGS) detector, was used to collect the emission FTIR spectra. The E/FTIR technique took advantage of the heated wafer as the source of IR radiation. The principles of operation for the E/FTIR were reported elsewhere in detail [72]. A non-contact, non-destructive, real-time, and *in-situ* epi-film

thickness monitoring tool was demonstrated to be useful for observing real time growth rates and an incubation time.

5.3 Results and Discussion

Figs. 5.1(a), (b), (c), and (d) show the XTEM micrographs of Samples 5.A, 5.B, 5.C, and 5.D. All these samples were cleaned *in-situ* at room temperature. *In-situ* cleaning conditions for Samples 5.A, 5.B, 5.C, and 5.D are listed in Table 5.1. In Samples 5.A and 5.B, in addition to having high densities of dislocations and stacking faults, polycrystalline structures were observed (Fig.5.1(a) and (b)). The bright/dark contrast area just beneath the epilayer/substrate interface in both XTEM micrographs and was interpreted to be damaged regions of a substrate. Their χ_{min} values, which were based on RBS ion channeling experiments, were 27% and 10%, respectively. Samples 5.C and 5.D (Fig.5.1(c) and (d)) showed defect-free epitaxial layers and continuous interfaces. Their χ_{min} values were measured in the 3-5% range, which confirmed that a good epitaxial film had been deposited. The interface thickness of Sample 5.C was measured to be 20-30Å and that of Sample 5.D, 30-50Å.

Fig.5.2(a) is the plain-view TEM micrograph, and Fig.5.2(b) is the electron diffraction pattern of Sample 5.D. Fig.5.2(a) shows a successfully grown epitaxial layer. Fig.5.2(b) corresponds to the electron diffraction pattern of a typical {100} diamond cubic (silicon) structure, which is the same as the diffraction pattern of a {100} substrate. Some extra spots in Fig.5.2(b) may represent some contaminants that exist on the outer surface. These contaminants may have come from the atmosphere or they may have been generated during sample preparation. Fig.5.3(a) and (b) is the real-time *in situ* monitoring results of Sample 5.C and Sample 5.A, respectively. Fig.5.3(a) does not show an incubation time and shows a well-grown epitaxial layer. Fig.5.3(b) shows an incubation time of about 30 minutes, probably resulting from a deposition on a native oxide which exists on the silicon surface. This E-FTIR technique is suitable for real-time process monitoring and allows an accurate measurement (50Å resolution) of film thickness. This technique was proven to be useful for studies of incubation time.

Samples 5.C and 5.D received an *in-situ* cleaning at room temperature with a positive 10 V of DC bias. Samples 5.A and 5.B received a room temperature *in-situ* cleaning with 0V of DC bias. During the application of a 0V of DC bias, a hydrogen ion, accelerated in the sheath region, damaged the substrate and a polycrystalline film was deposited. In other experiments, when hydrogen ion energy was reduced by application of a positive 10V of DC bias, no damage was observed in the epitaxial layer. Probably at low temperatures, the surface damage induced by the hydrogen ion bombardment did not anneal easily. The damage was observed by XTEM analysis. Also from the SIMS and FTIR analysis, oxygen contamination was reduced by application of a positive 10V of DC bias. This may be another reason why defect-free epitaxial layers were deposited.

Fig.5.1(e) shows the XTEM micrograph of Sample 5.K. In this experiment, the microwave power was set at 300W and the DC bias was set at a positive 20V during the *in-situ* cleaning. Considerable amounts of stacking faults were generated in the epilayer/substrate interface, and the interface looked broad and contaminated. The thickness was measured to be about 50Å. This matches our observation: When the *in-situ* cleaning occurred at 600°C [88] with a DC bias set to a positive 30V, XTEM analysis revealed that considerable amounts of dislocations and stacking faults were at the epilayer/substrate interface. A large positive DC bias reduced the hydrogen ion energy significantly, and surface contaminants, mainly oxygen species, seemed less likely to be removed from the wafer surface under those conditions. From the above experiments, we observed that DC bias played a major role in obtaining a defect-free epitaxial layer in the *in-situ* cleaning process at room temperature. Sample $5.A^+$ received the same *ex-situ* cleaning but no *in-situ* cleaning was performed before the epitaxial deposition. Stacking faults were initiated in the epilayer/substrate interface. By SIMS analysis (Table 5.2), the interfacial oxygen concentration (areal density) was 1.0×10^{15} atoms/cm^2 and the oxygen species in the interface may have been on the initial silicon surface before loading into the chamber. Native oxides may have grown during the water rinsing process. By comparing Samples 5.D or 5.C with Sample $5.A^+$ in their XTEM micrographs, the room temperature cleaning with an appropriate positive DC bias was effective in removing contaminants which came from the *ex-situ* wafer cleaning.

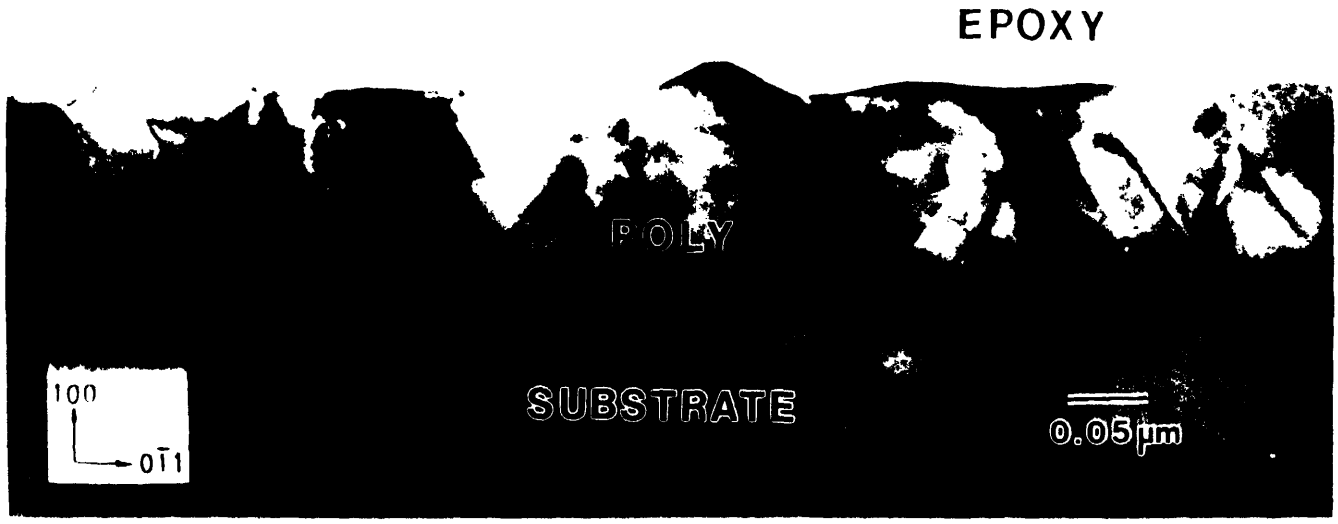

5.1 (a) XTEM micrograph of polycrystalline film, cleaned *in-situ* at room temperature, with microwave power set at 750W and DC bias set at 0V.

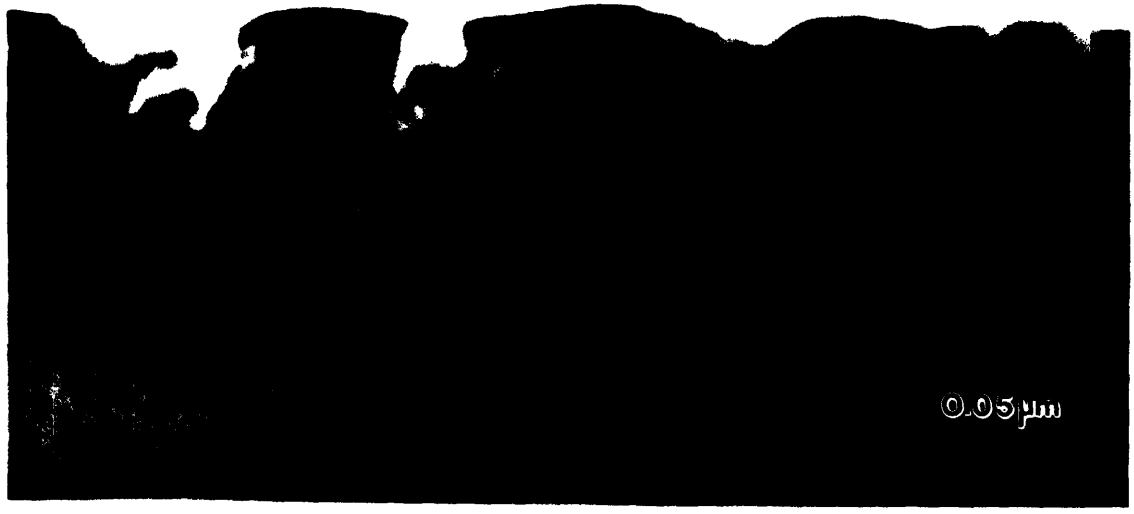

5.1 (b) XTEM micrograph of polycrystalline film, cleaned *in-situ* at room temperature, with microwave power set at 300W and DC bias set at 0V.

5.1 (c) XTEM micrograph of epitaxial film, cleaned *in-situ* at room temperature, with microwave power set at 750W and DC bias set at 10V.

5.1 (d) XTEM micrograph of epitaxial film, cleaned *in-situ* at room temperature, with microwave power set at 300W and DC bias set at 10V.

5.1 (e) XTEM micrograph of epitaxial film, cleaned *in-situ* at room temperature, with microwave power set at 300W and DC bias set at 20V.

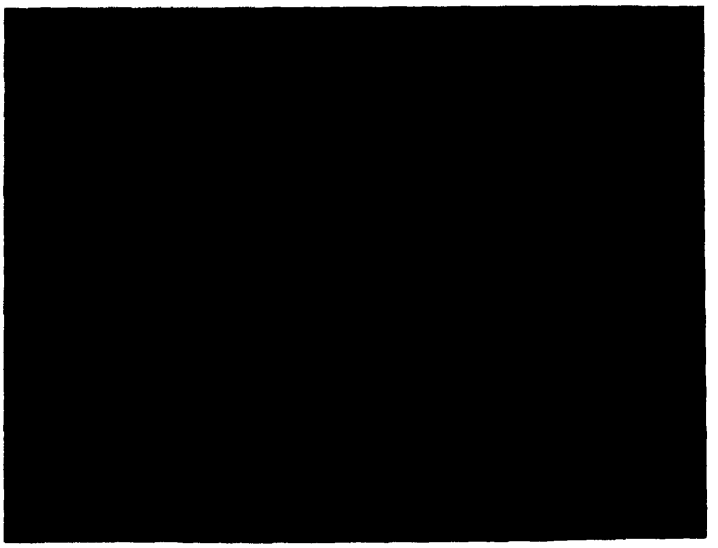

5.2 (a) Plain-view TEM micrograph of epitaxial film, cleaned *in-situ* at room temperature, with microwave power set at 300W and DC bias set at 10V.

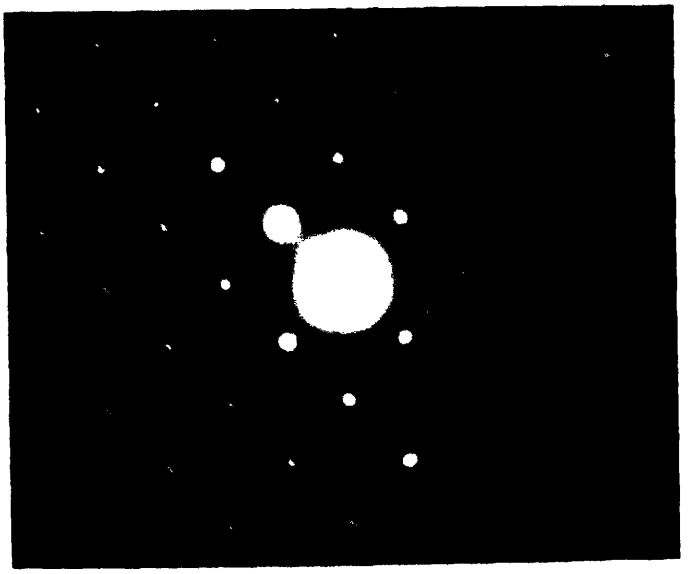

5.2 (b) Electron diffraction pattern of epitaxial film, cleaned *in-situ* at room temperature, with microwave power set at 300W and DC bias set at 10V.

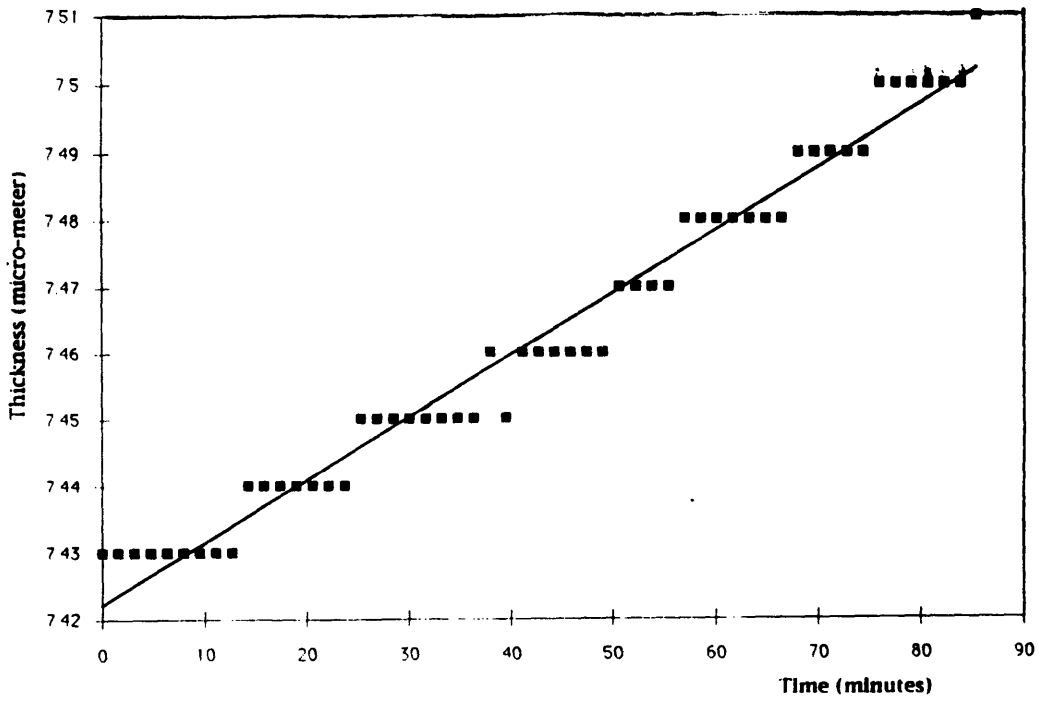

5.3 (a) Real time *in-situ* monitoring of film thickness for defect free epitaxial film

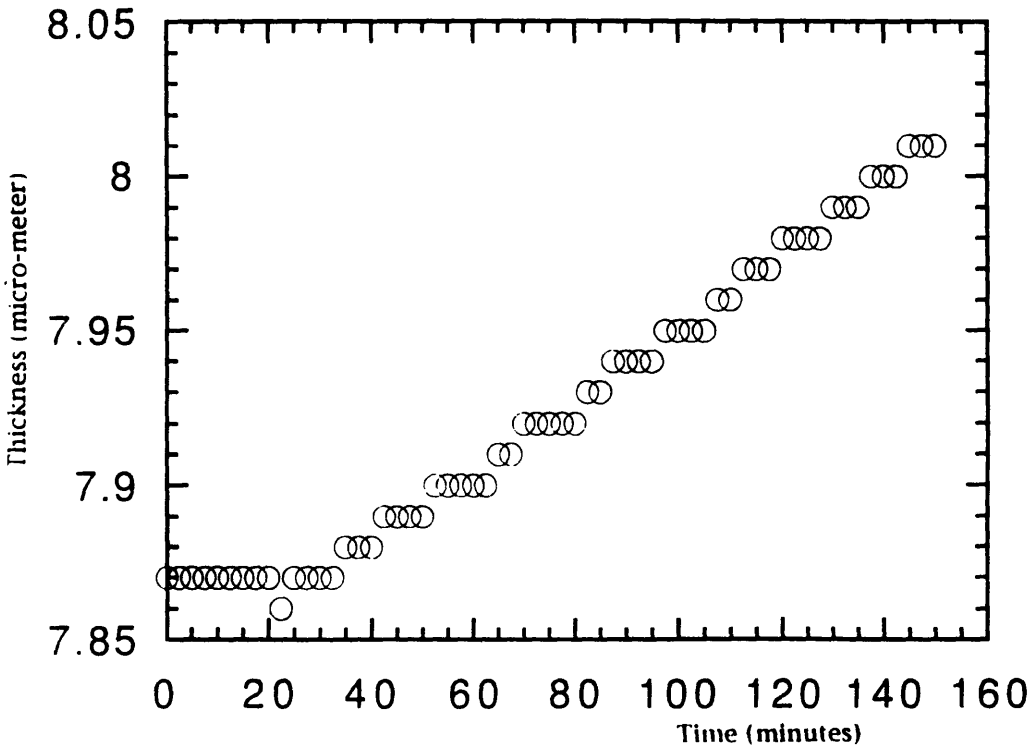

5.3 (b) Real time *in-situ* monitoring of film thickness for polycrystalline film.

Four pairs of samples (Samples 5.A and 5.E, Samples 5.B and 5.F, Samples 5.D and 5.H, and Samples 5.C and 5.G) were compared : the room temperature *in-situ* cleaning vs. the high temperature (600°C) *in-situ* cleaning. Table 5.1 shows the *in-situ* cleaning conditions (microwave power (gas pressure), DC bias, cleaning temperature) of each sample. Microwave power (gas pressure) was set at 750W (8mTorr) and 300W (1mTorr) , DC bias was set at 0V and 10V. Cleaning temperature was set at room temperature and at 600°C.

Fig.5.4(a) and Fig.4.2(a) are the XTEM micrographs of Samples 5.E and 5.F, respectively. Samples 5.E and 5.F received a high temperature (600°C) *in-situ* cleaning. Samples 5.A and 5.E were compared. In Fig.5.4 Sample 5.E showed an epitaxial layer although there were some defects near the interface. Samples 5.B and 5.F were compared. Fig.4.2(a) shows that Sample 5.F had an almost defect-free epitaxial layer with a continuous epilayer/substrate interface. Sample 5.H was compared with Sample 5.D: both samples show defect-free epitaxial layers, although Sample 5.H has an almost invisible interface, as was shown in the HRXTEM (High Resolution Cross-sectional Transmission Electron Microscopy) micrograph [94]. Samples 5.G and 5.C were compared. The XTEM micrograph of Sample 5.G is shown in Fig.5.4(b). It shows an epitaxial layer, however, its interface has some stacking faults and other defects. In both samples, their χ_{min}'s were in the 3-5% range. In our structural analysis, room temperature *in-situ* cleaning was found to be an efficient cleaning process and comparable to the higher temperature cleaning processes at 600°C. Efficient cleaning could be achieved by choosing an appropriate DC bias.

In addition, experiments (using Samples 5.I, 5.J) were performed to investigate the effect of cleaning temperatures between 25°C and 550°C, on cleaning efficiency in terms of structural analysis. *In-situ* cleaning was performed with a microwave power of 300W and a DC bias of +10V, for both samples. In Sample 5.I, *in-situ* cleaning was done at 280°C and the wafer was heated up during hydrogen flowing for about 4 and-a-half minutes. Deposition was performed at 600°C. The XTEM micrograph of Sample 5.I shows that an almost defect-free epitaxial layer was deposited. The thickness of epilayer/substrate interface was about 20Å. The purpose of this experiment was to reduce the hydrogen exposure time and at the same time to lower the cleaning temperature as much as possible.

5.4 (a) XTEM micrograph of epitaxial film, cleaned *in-situ* at 600°C, with microwave power set at 750W and DC bias set at 0V.

5.4 (b) XTEM micrograph of epitaxial film, cleaned *in-situ* at 600°C, with microwave power set at 750W and DC bias set at 10V.

Fig.5.5 is the XTEM micrograph of Sample 5.J. *In-situ* cleaning was done at 480°C. The plasma was turned off after 5 minutes and silane was introduced immediately at the same temperature. Deposition temperature was adjusted to 600°C afterwards. Although hydrogen passivation may have begun to be lost at low temperatures at about 400°C [95], if we accept the report that the hydrogen desorption temperature is between 510 to 520°C [96], some hydrogen species may stay at 480°C so that they prevent oxygen species from being adsorbed on the silicon surface. From the micrograph, a defect-free epitaxial layer was grown and the epilayer/substrate interface was thin (less than 20Å). However, the interface clearly existed and was not invisible. There should be some remaining oxide or surface contaminants, probably due to low initial deposition temperature. Samples 5.D, 5.I, 5.J, and 5.H were compared, to see the effect of the cleaning temperature to the cleaning efficiency. The thickness of epilayer/substrate interface was plotted as a function of cleaning temperature (Fig.5.6). Averaged values were used for the interface thicknesses and possible measurement error was considered. The interface thicknesses for Samples 5.D, 5.I, 5.J, and 5.H were in range of between 10 to 50Å. It showed a slight decrease as cleaning temperature increased from 25°C to 600°C. It is shown that the structural qualities of epitaxial layers are not affected by the *in-situ* cleaning temperature significantly, as long as standard condition holds.

By using column bar graphs, a more systematic analysis on the 8 Samples (Samples 5.A, 5.B, 5.C, 5.D, 5.E, 5.F, 5.G, and 5.H) will help verify the above findings and help understand the room temperature *in-situ* cleaning process. The χ_{min} values of epitaxial layers were measured by RBS analysis. Interfacial oxygen and carbon concentrations were measured by SIMS. Interfacial impurity concentration was represented by its areal density, instead of volumic concentration at a particular interface.

Fig.5.7(a) shows the effect of cleaning temperature on the interfacial carbon concentration. For every pair of samples, the sample which received the room temperature *in-situ* cleaning had a lower carbon concentration in its epilayer/substrate interfaces than did the sample which received the *in-situ* cleaning at 600°C. Interfacial carbon concentrations of the samples which received the room-temperature *in-situ* cleaning were even lower than those

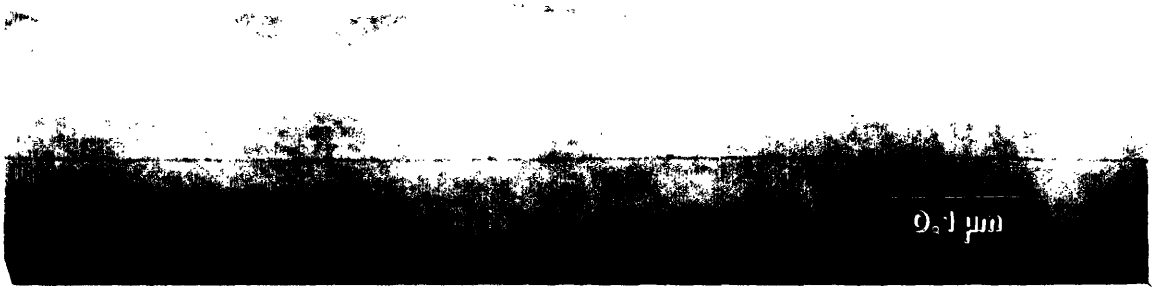

5.5 XTEM micrograph of epitaxial film, cleaned *in-situ* with standard condition at 480°C.

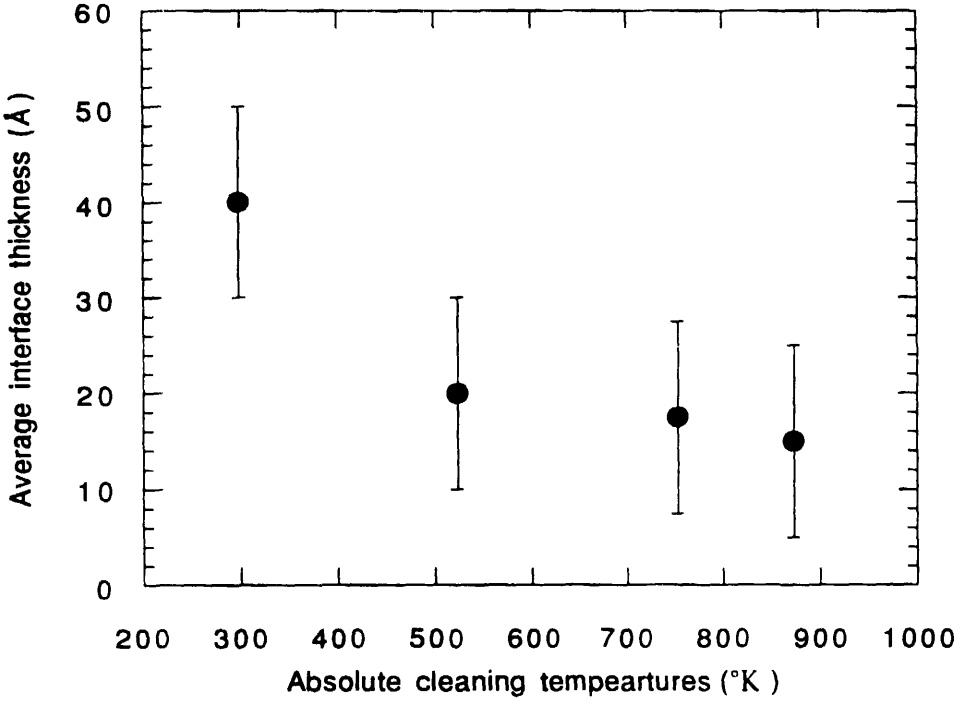

5.6 Average thickness of epilayer/substrate interface as a function of cleaning temperature.

of Sample 5.A$^+$. Sample 5.A$^+$ did not receive an *in-situ* wafer cleaning after *ex-situ* wafer cleaning and its interfacial carbon concentration was 1.1 x10^{14} atoms/cm^2. Fig. 5.7(b) shows the effect of substrate DC bias on the interfacial carbon concentration. A DC bias was not an important process variable affecting the interfacial carbon concentration. Therefore, a hydrogen ion does not play a major role in removing carbon from the silicon surface and the carbon removal process will be a hydrogen chemical etching process which corresponds to the interaction of atomic hydrogen with carbon species, such as the methyl group, as an example [97].

It is unclear why the room temperature *in situ* cleaning was so efficient in removing hydrocarbons from the surface. There are reports that the low temperature process was more effective in removing hydrocarbons from the surface [98] [99]. A more likely form of the carbon species at the initial surface would be a hydrocarbon, which is physisorbed or partially chemisorbed on the silicon surface [28]. At low temperature (room temperature) *in-situ* cleaning, hydrocarbons on the surface are susceptible to attack by hydrogen before they are thermally decomposed. Therefore, the carbon removal in room temperature *in-situ* cleaning is thought to occur by volatilization through hydrogenation. Therefore, it is surmised that the carbon removal in our room temperature *in-situ* cleaning process would be a chemical etching process.

The interfacial carbon concentration does not seem to affect the quality of the epitaxial layer and K.Kim et al.'s studies also support our observation [100]. If β-SiC formed at the interface during epitaxial growth, the presence of the β-SiC does not affect the crystalline quality of the epitaxial layer. β-SiC precipitate has the zinc-blende structure and the crystallographic relationship between β-SiC and the silicon substrate is quite common, so it does not generate many defects during initial growth. β-SiC precipitate was not easily removable once it has been formed. The solubility of carbon in solid silicon is known to be 3.5 x 10^{17} atoms/cc or slightly less at the melting point (about 1400°C) and the solidus line below the melting temperature is almost vertical [101]. In our samples, carbon concentration is above 1 x10^{18} atoms/cc at or near the interface, most interface carbons are supposed to precipitate as β-SiC from thermodynamic considerations. However, in order for carbons to precipitate, many carbon atoms must condense and the probability of their

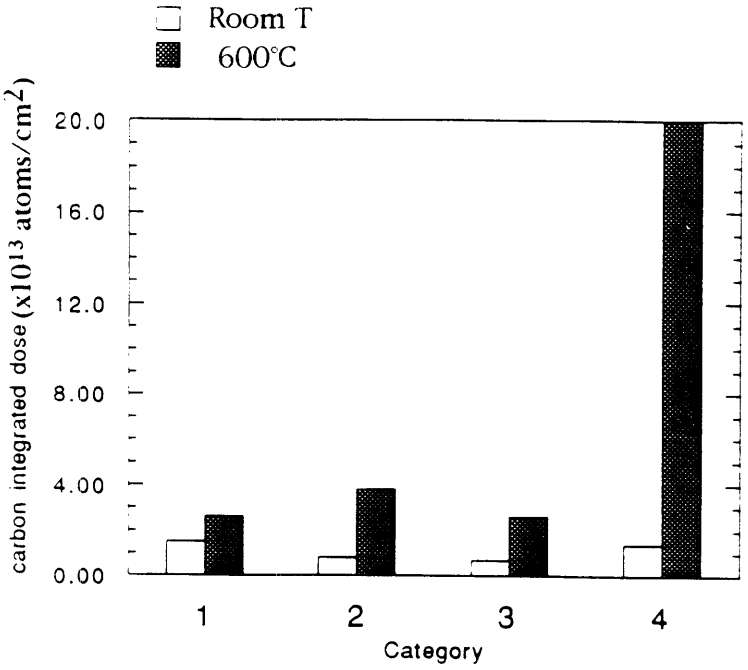

5.7 (a) Column bar graph showing the effect of cleaning temperature on interfacial carbon concentration.

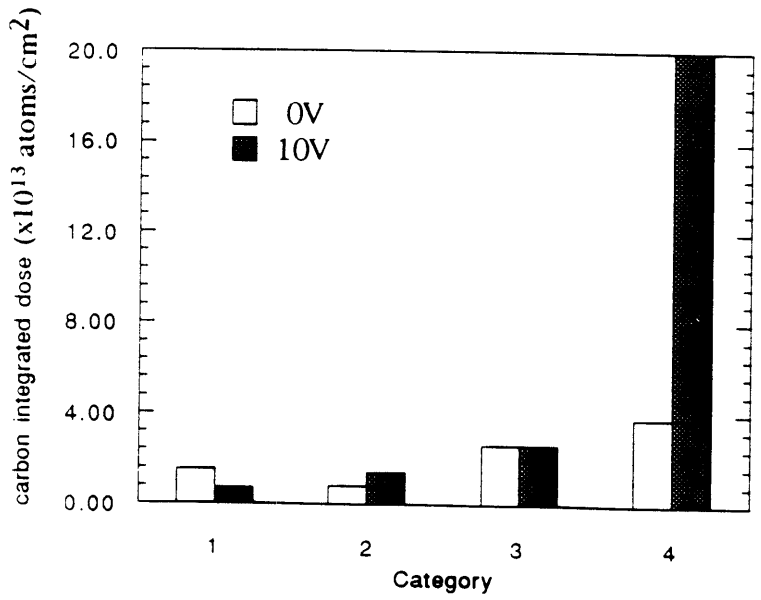

5.7 (b) Column bar graph showing the effect of substrate DC bias on interfacial carbon concentration.

encounter is quite small due to their low concentrations. β-SiC formed when chemically prepared silicon surfaces are heated to 800°C [102] and the carbide was not formed below 700°C [28] [103]. In our case, carbide is less likely to be formed because of low temperature processing (≤ 660°C). Carbon may be present as another form (as an example, elemental carbon inside the silicon lattice) in its metastable state.

Fig.5.7(c) shows the effect of a DC bias on the interfacial oxygen concentration. The interfacial oxygen concentration of the sample was affected by a substrate DC bias. The samples which received an *in-situ* cleaning with 10 V of DC bias had a particularly reduced oxygen concentration when compared to the samples which received an *in-situ* cleaning with 0V of DC bias. The removal of oxygen species is an ion etching process [88] [89], with an impinging hydrogen ion which damages the surface and increases its reactivity. Hydrogen neutrals or ions react with some Si-O bonding configuration and volatile species are desorbed from the surface. In our analysis, the surface oxygen concentration was reduced by adjusting the hydrogen ion energy with a substrate DC bias. In room temperature *in-situ* cleaned samples (first and second categories) oxygen concentrations were not as much affected by a DC bias as the 600°C-cleaned samples (third and fourth categories) were. So it may be inferred that 0V-biased *in-situ* cleaning, which provides higher ion energy than +10V-biased cleaning, degraded the epitaxial quality during room temperature *in-situ* cleaning. In this case, hydrogen ions damaged the substrates, not only to activate it but also generated the unwanted defects. This finding matches with the observation made by XTEM analysis.

For most pairs of samples, the sample which received the room temperature cleaning had the higher χ_{min} value. In other words, its structural quality, was inferior to the sample that received the *in-situ* cleaning at 600°C. This tendency was more evident in the case of the first two categories, where the DC bias was set at 0V. Fig.5.7(d) shows the effect of a DC bias on the χ_{min} value of the film. Samples which received an *in-situ* cleaning with a 0V of DC bias had an inferior structural quality compared to samples which received a cleaning with 10V of DC bias. This tendency was more evident in the first two categories, which are room temperature *in-situ* cleaned samples. Fig 5.7(c) and Fig.5.7(d) can be compared, interfacial oxygen concentrations are closely related to the

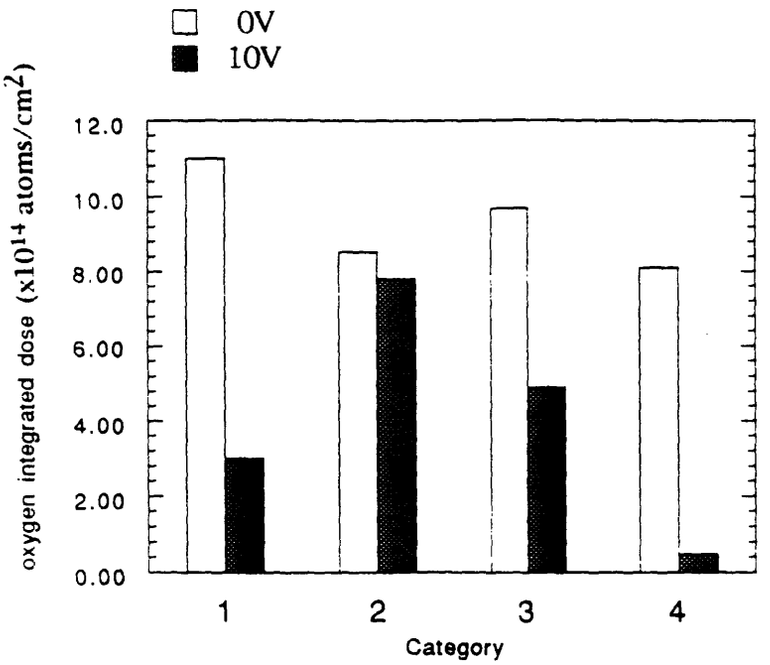

5.7 (c) Column bar graph showing the effect of substrate DC bias on interfacial oxygen concentration.

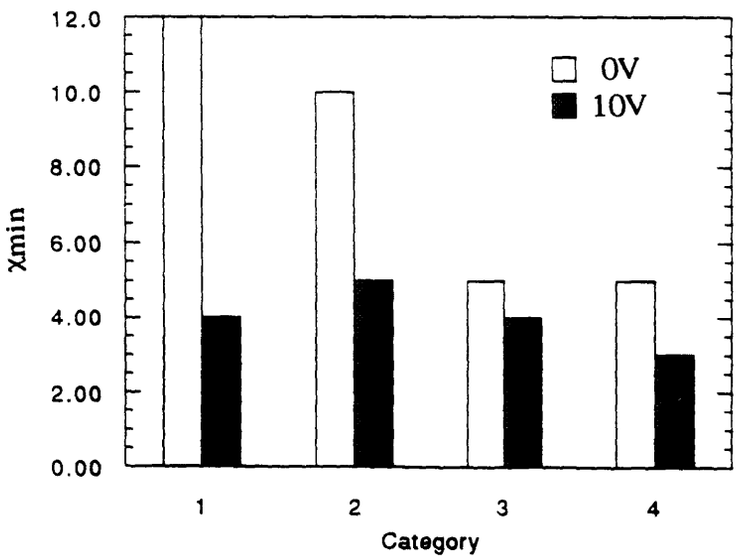

5.7 (d) Column bar graph showing the effect of substrate DC bias on the χ_{min} value of the film.

crystalline qualities of epitaxial layers. In our analysis, hydrogen gas density (represented by microwave power and gas pressure) did not affect the film quality significantly, in the range from 300W (1mTorr) to 750W(8mTorr), compared to DC bias and cleaning temperature. This is another evidence that the impurity (oxygen) removal is not a purely chemical process. In this case, high pressure reduce the amounts of ions which strike the wafer surface by high collision in the sheath region, although more ions were produced by applying high microwave power (Chapter 4).

Current literature reports that lower temperature *in-situ* cleaning might be more efficient than higher temperature cleaning in removing oxygen contaminants because at higher temperatures, the sticking coefficient of hydrogen to the silicon surface decreases and hydrogen atoms are easily desorbed and hydrogen passivation will be lost [93]. Oxygen removal is affected by hydrogen passivation. In this case, the sticking coefficient of the hydrogen radicals decreases at higher temperatures and may take longer to clean the surface at the higher temperature.

But this observation does not necessarily apply to our system because although *in-situ* wafer cleaning can be performed at room temperature, the temperature should be raised to at least 600°C in our depositions for actual epitaxial growth to be initiated. It took at least 7 minutes to heat the wafer from room temperature to 600°C in our system and hydrogen passivation may be lost during this process. It was shown by SIMS that some oxygen and carbon may have stuck onto the silicon surface, when hydrogen was kept flowing at 600°C. But this oxygen contamination may be reduced at higher temperatures because of oxygen desorption phenomena. It can be assumed that oxygen desorbs at high temperatures. Also, Oxygen removal is feasible only for weakly adsorbed oxygen [99], since the surface reaction between reactive species and passivation oxide films proceeds very slowly at temperatures less than 800°C [104]. Even for submonolayer coverage of oxygen on silicon, the desorption temperature of the oxide, such as SiO, was reported to be about 700°C [105]. If the oxide layer is sufficiently thick from the beginning, or the cleaning temperature is so low that the desorption process becomes a rate determining step, the rate of oxygen removal and thus the cleaning efficiency will increase with increasing temperature.

Table 5.1 *In-situ* cleaning conditions (Microwave power, DC bias, Cleaning temperature)

	Microwave power (W)	DC bias(V)	Cleaning temperature (°C)
Sample 5.A	750W(8mTorr)	0V	room T
Sample 5.B	300W(1mTorr)	0V	room T
Sample 5.C	750W(8mTorr)	10V	room T
Sample 5.D	300W(1mTorr)	10V	room T
Sample 5.E	750W(8mTorr)	0V	600°C
Sample 5.F	300W(1mTorr)	0V	600°C
Sample 5.G	750W(8mTorr)	10V	600°C
Sample 5.H	300W(1mTorr)	10V	600°C
Sample 5.I	300W(1mTorr)	10V	280°C
Sample 5.J	300W(1mTorr)	10V	480°C
Sample 5.K	300W(1mTorr)	20V	room T

Table 5.2 SIMS and RBS data

	oxygen(cm^{-2})	oxygen(cm^{-3})	carbon(cm^{-2})	carbon(cm^{-3})	χ_{min}
Sample 5.A+	$1.0x10^{15}$	$7x10^{20}$	$1.1x10^{14}$	$1x10^{20}$	7%
Sample 5.A	$1.1x10^{15}$	$3x10^{20}$	$1.5x10^{13}$	$9x10^{18}$	27%
Sample 5.B	$8.5x10^{14}$	$1x10^{21}$	$8.0x10^{12}$	$7x10^{18}$	10%
Sample 5.C	$3.0x10^{14}$	$3x10^{20}$	$6.9x10^{12}$	$6x10^{18}$	3-5%
Sample 5.D	$7.8x10^{14}$	$7x10^{20}$	$1.4x10^{13}$	$1x10^{19}$	5%
Sample 5.E	$9.7x10^{14}$	$9x10^{20}$	$2.6x10^{13}$	$2x10^{19}$	5%
Sample 5.F	$8.1x10^{14}$	$3x10^{20}$	$3.8x10^{13}$	$3x10^{19}$	5%
Sample 5.G	$4.9x10^{14}$	$3x10^{20}$	$2.6x10^{13}$	$2x10^{19}$	3-5%
Sample 5.H	$4.8x10^{13}$	$8x10^{19}$	$4.5x10^{14}$	$5x10^{20}$	3%

5.4 Conclusion and Summary

Defect-free epitaxial layers were deposited by applying the room temperature *in-situ* wafer cleaning processes with a positive 10V of DC bias.

Polycrystalline films were deposited by the application of a 0V of DC bias. The cleaning process with a 20V of DC bias was not effective.

In general, the samples which received the room temperature *in-situ* cleaning had a lower interfacial carbon concentration than those of the samples which received the *in-situ* cleaning at 600°C and the samples which did not receive the *in-situ* wafer cleaning. In room temperature *in-situ* ECR hydrogen plasma cleaning, the carbon removal process was a hydrogen chemical etching process, while the removal of oxygen species was an ion-etching process. The interfacial carbon concentration was not affected by substrate DC bias, while the interfacial oxygen concentration was reduced by adjusting the hydrogen ion energy with a substrate DC bias. Carbon removal mechanisms will be discussed in detail in Chapter 7.

The interfacial carbon concentration did not affect the structural qualities of the epitaxial layer and the epilayer/substrate interface, while the interfacial oxygen concentration did. K.Kim et al. observed that β-SiC did not affect the epitaxial quality at 1000°C. In phase diagram of Si-C system, carbon at the epilayer/substrate interface at 600°C is supposed to precipitate as silicon carbide.

Defect-free epitaxial layers were deposited by applying the *in-situ* wafer cleaning at 250°C and 480°C. The epitaxial layers were deposited at 600°C. The thickness of the epilayer/substrate interface ranged from 10 to 50Å, by changing the temperature of *in-situ* cleaning. The thickness tended to decrease as the *in-situ* cleaning temperature increased from 25°C to 600°C. The thickness is thought to be closely related to the interfacial oxygen concentration, the result is an indirect evidence that *in-situ* cleaning is more efficient at higher temperature, in removing oxygen contaminants.

The E-FTIR technique was suitable for real-time process monitoring and allowed an accurate measurement of the film thickness and the incubation time. Incubation time could be related to the presence of surface native oxide.

Chapter 6

Ex-situ cleaning with HF dipping

Ex-situ silicon wafer cleaning by HF dipping has been studied in terms of cleaning efficiency. Silicon epitaxial layers were deposited in the MS-CVD (Multi-Chamber Chemical Vapor Deposition) reactor, which had a Load Lock Chamber. *In-situ* cleaning was performed with an ECR (Electron Cyclotron Resonance) hydrogen plasma exposure. The XTEM (Cross-sectional Transmission Electron Microscopy) was performed to investigate the structural qualities of the epitaxial layer and the epilayer/substrate interface. The SIMS (Secondary Ion mass Spectroscopy) was performed to investigate their interfacial carbon and oxygen concentrations. HF dipping without water rinsing, followed by thermal heating up to 660°C provided the best results in terms of contamination. Rinsing seemed to help the surface natural oxide grow, but it improved the surface smoothness of the epitaxial layer. Blow-drying by nitrogen was important in reducing the interfacial oxygen concentration of the deposited epitaxial layer. The *ex-situ* cleaning played a major role in reducing the amounts of surface contaminants.

6.1 Introduction

In the new ULSI (Ultra Large Scale Integration) era, the ultra-clean wafer surfaces represent particle free, metallic and organic contaminant free, and native oxide free surfaces. In addition, wafer surfaces need to be smooth and hydrogen-terminated [106]. The silicon bare surface is highly reactive and susceptible to impurity adsorption. Furthermore, at low temperatures (less than 650°C), oxygen or carbon cannot be desorbed easily.

The epitaxial process consists of three processes: 1) wet cleaning to remove particles, metals, organic species; 2) precleaning to remove the native oxide which was formed in the previous wet cleaning step; 3) epitaxial growth. The most common type of wet cleaning is the RCA cleaning, a two step process typically performed in automated wet benches. In the RCA cleaning process,

organic compounds, metal contaminants and particles can be removed [11] [12].

Before silicon epitaxial growth, two precleaning strategies were widely used. The first one used an oxidizing chemical clean to form a thin hydrophilic carbon-free oxide [11] [107] which should then be removed *in-situ* to exposure the crystalline silicon surface for epitaxy. In the second strategy, a final HF dipping or exposure was used to create a hydrophobic hydrogen-terminated surface [108] [109]. In our experiments, the second approach was chosen because the CVD Chamber in our system was not exposed to the atmosphere, and thus the protecting oxide was not needed, and because the protecting oxide could contaminate the CVD chamber. Thermal desorption could not be attained in this low temperature cleaning process; it was more important to get a contamination-free, damage-free substrate with undestroyed hydrogen passivation.

HF cleaning is a method used to achieve clean interfaces, and it is most efficient in getting rid of residual natural oxide. Dangling bonds of silicon surface are terminated by hydrogen atoms, and fluorine atoms remain as a minor species after HF treatment. This hydrogen passivation prevents the surface from being exposed to air and to oxidation [13], but the effect of HF dipping on the carbon contamination on the substrate surface is not clear.

The last steps in wafer cleaning are rinsing and drying; both are extremely critical steps because clean surfaces become recontaminated easily if not processed properly [16]. Rinsing after wet cleaning is done with flowing high purity and ultrafiltered high-resistivity deionized (DI) water, usually at room temperature [17]. Rinsing in DI water is important at all stages of the preparation; it removes species that are weakly bound to the surface (physisorbed or hydrogen bonded) and can even etch the surface [18]. Not only is deionized water rinsing applied during RCA cleaning steps to remove the residual chemicals, but it is also employed especially after HF dipping, to remove fluorine-species, and to bring about hydrogen passivation. However, extra rinsing not only generates microroughness [19] and stacking faults [20], but it also increases chemical contamination such as carbon or oxygen [21].

Chabal et al. [110] concluded that the HF treated silicon surface is inhomogeneous and atomically rough, and they observed surface silicon hydride structures such as -SiH, $-SiH_2$, $-SiH_3$. Watanabe et al [18] found that water reacted with di- and tri- hydrides and removed them, resulting in the monohydride termination. Immersion in water was an essential step in obtaining a homogeneous surface. The existence of large amounts of $Si-CH_2$ and Si-N in addition to Si-G, on the HF-treated silicon surface, was reported [13]. $Si-CH_2$ may be formed by the reaction of the substrate with organic contaminants which were on the oxide layer, or from within HF solution, or from water used in the process. The effect of water rinsing and N_2 blow drying on the structural and chemical qualities of the epitaxial film needs to be investigated.

A dilute HF dip followed by rapid introduction into the CVD reactor and rapid heat-up to growth temperature were sufficient to grow device quality epitaxial films [111]. Meyerson et al. accomplished this in their UHVCVD system. Although the vacuum level of our system ($1\text{-}2\times10^{-8}$ Torr) was higher than theirs (1×10^{-9} Torr), we needed to deposit epitaxial layers without the *in-situ* cleaning processes. Those films needed to be compare with the films which received an *in-situ* cleaning.

6.2 Experimental

Substrates were 4 inch, CZ-grown, p-type <100> Silicon with a resistivity of 0.5-20 Ω-cm, if not defined otherwise. In some cases, a heavily doped wafer was used and its resistivity was 0.001-0.002 Ω-cm. All the experimental processes were done in the TRL (Technology Research Laboratory), which is a class 100 cleanroom. The wafer was treated with RCA cleaning, and went through the 10% diluted HF dipping for 20 to 30 seconds to remove native oxide from its surface. The HF solution used was a ULSI grade 49% aqueous hydrofluoric acid. Deionized water was added to prepare a 10: 1 solution by volume. Then the wafer was rinsed with deionized water for about three minutes. At the end of the water rinsing, the wafer was dried by blown nitrogen or spin-dried. The spin/dry sequence was comprised of a 160 second DI water spin-rinse at 1000 rpm (revolution per minute) and a 240 second spin-dry in nitrogen at 2000 rpm. An RCA-cleaned Teflon tweezer was used in handling the wafer.

An *ex-situ* cleaned wafer was loaded into the Load Lock Chamber which was then pumped down to about 1x 10^{-7} Torr. After the wafer was loaded onto the heater stage, the base pressure was measure to be around 1-2 x 10^{-8} Torr. The wafer was then heated up to 600°C or 660°C in hydrogen flow with a pressure of 1mTorr and a flow rate of 20 sccm. It took about 7 minutes to heat the wafer from 25°C to 600°C and took another minute to heat it from 600°C to 660°C. In some cases, *in-situ* predeposition cleaning was done by using an ECR hydrogen plasma and depositions were done by flowing SiH_4, immediately after the plasma was extinguished. In other cases, silane gas, without carrier gases, was introduced with a pressure of 1 mTorr and a flow rate of 10 sccm. The standard (Chapter 4) *in-situ* cleaning was applied, to maintain consistency.

The evaluations of the *ex-situ /in-situ* cleaning processes were done by depositing epitaxial films on the substrate surface and performing material characterizations ; XTEM (Cross-sectional Transmission Electron Microscopy) and SIMS (Secondary Ion Mass Spectroscopy). Cross-sectional transmission electron microscopy (XTEM) was used to observe the epitaxial layer and the epilayer/ substrate interface. The SIMS measurement was done in Evans East, New Jersey and Cs^+ ion was used as the ion source for sputtering. The detected elements included carbon, oxygen and nitrogen.

6.3 Results

Samples 6.A and 6.B were RCA cleaned and dipped into 10: 1 DI water: HF solutions. Sample 6.A was rinsed in deionized water and dried by blowing nitrogen, while Sample 6.B was dried by blowing nitrogen without water rinsing. Both wafers were directly loaded into the Load Lock Chamber of our CVD system. Deposition was performed at 600°C.

Fig.4.1(c) shows the XTEM micrographs of Sample 6.A. Stacking faults and dislocations were nucleated in the epilayer/substrate interfaces and the thickness of the interface was measured to be 100 to 150Å. The SIMS analysis was done for Sample 6.A and its data are in Table 6.1. The interfacial oxygen concentration was 1.0 x10^{15} atoms/cm^2. The oxygen peak was wide : FWHM (Full

Width at Half Maximum) was about 200Å and the FWHM of the oxygen peak was consistent with the thickness of the epilayer/substrate interface. The carbon peak was lower in height and narrower in FWHM, and the interfacial carbon concentration was 1.1 $x10^{14}$ atoms/cm^2. There was no ion bombardment, no chance of substrate mechanical damage and the stacking faults seemed to be oxygen-induced. The growth of the silicon film around the patches of oxide occurred as a result of the generation of stacking faults at the oxide-silicon boundary. In some cases, the oxidation of silicon substrate may have generated the stacking faults [112] and these defects may have extended to the epitaxial layer. In Fig.4.1(c), the angle between the defects and the {100} substrate is about 60 degrees. Similar defects were observed in the high resolution cross sectional TEM lattice images of epitaxial silicon films grown at 550°C on {100} substrate [25]. Stacking faults may have been generated from the tetrahedron-shaped defects and these faults were extended throughout the epitaxial layers.

Fig.6.1 shows the XTEM micrographs of Sample 6.B. The epitaxial layer on the substrate was almost defect-free and the thickness of the epilayer/substrate interface was measured to be 50Å. The structural quality of the epilayer/substrate interface in Sample B was higher than that of Sample 6.A. In Sample 6.A, additional water rinsing seems to have assisted the growth of surface natural oxide on the silicon surface, and the oxide could not be removed during heating to 600°C prior to epitaxial growth.

An*in-situ* cleaning process inside the chamber followed the *ex-situ* wafer cleaning step mentioned above. The optimized standard *in-situ* cleaning process at 600°C was used. Samples 6.C and 6.D were dipped into 10: 1 DI water: HF solutions. Sample 6.C was rinsed in DI water for about 3 minutes, while Sample 6.D did not receive the water rinsing. Sample 6.C and 6.D were then dried by blowing nitrogen on them and were loaded into the reactor. After being loaded into the Load Lock Chamber, the wafer was heated up to 600°C, which is the deposition temperature. The standard *in-situ* cleaning was applied for 5 minutes.

Figs.4.1(a) and (b) show the XTEM micrographs of Sample 6.C. It was observed that a defect-free epitaxial layer was deposited and the epilayer/substrate interface under HRXTEM was almost invisible. The

thickness was measured to be about 10Å. The surface of the epitaxial layer was smooth and flat (not shown here). From the SIMS data (Table 6.2), the oxygen concentration inside the film was about $1x10^{18}$ atoms/cc and was comparable to that of the substrate. The interfacial oxygen concentration was measured to be 4.3 $x10^{13}$ atoms/cm^2 and the FWHM of the oxygen peak was about 30Å. Additionally, interfacial carbon contamination was measured to be 4.5 $x10^{14}$ atoms/cm^2. Fig.6.2 shows the XTEM micrographs of Sample 6.D. A defect-free epitaxial layer was deposited. The thickness of the epilayer/substrate interface was 20-30 Å. The surface of the epitaxial layer was not as smooth as that of Sample 6.C, where the water rinsing step was added. In SIMS analysis, the interfacial oxygen and carbon concentration in Sample 6.D was 6.1 x 10^{14} and 9.1 x 10^{13} atoms/cm^2, respectively. Rinsing should have added some oxygen species by helping surface oxide to grow, but the standard *in-situ* cleaning was effective in removing considerable amounts of oxygen species. The interfacial carbon concentration of Sample 6.D was smaller than that of Sample 6.C. Rinsing did not affect the interface thickness significantly, as long as *in-situ* cleaning was applied. However, the surface smoothness of the epitaxial film was degraded by employing the water rinsing.

Samples 6.L, 6.M, and 6.N received an HF dipping to remove the surface natural oxide. In Sample 6.L, the wafer was rinsed in DI water and spin-dried (rinse 160 min./dry 240 min.). In Sample 6.M, the wafer was then spin-dried and loaded into the Load Lock Chamber. In Sample 6.N, the wafer was dried by blowing nitrogen, without water rinsing. In Samples 6.L, 6.M, and 6.N, the wafer received a standard *in-situ* cleaning at 660°C. Deposition was done at 660°C.

Fig.6.3(a) shows the XTEM micrographs of Sample 6.L. A defect-free epitaxial layer was deposited and the interface was continuous. The thickness of the epilayer/substrate interface was about 80Å. The XTEM micrograph of Sample 6.M is shown in Fig.6.3(b) and its SIMS data are listed in Table 6.2. A defect-free epitaxial layer was deposited and the thickness of the epilayer/substrate interface was measured to be about 20-30Å. The interfacial oxygen concentration was 1.0 $x10^{14}$ atoms/cm^2 and the interfacial carbon concentration was 1.7 $x10^{14}$ atoms/cm^2.

6.1 XTEM micrograph of epitaxial film, without *in-situ* cleaning (blow dried).

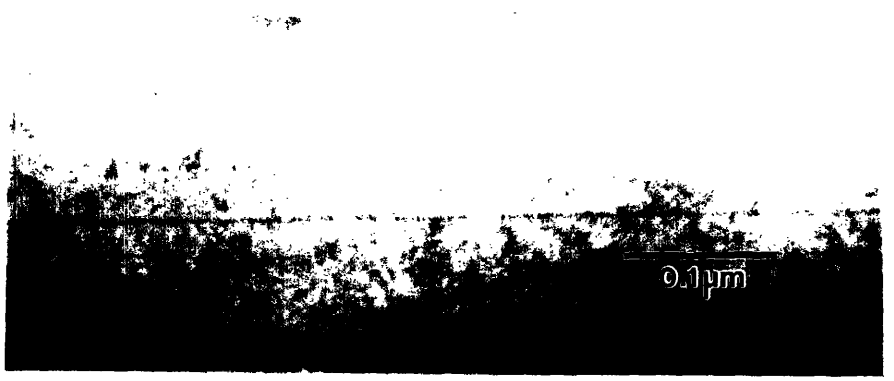

6.2 XTEM micrograph of epitaxial film, cleaned *in-situ* with standard condition at 600°C (blow dried without rinsing)

The XTEM micrograph of Sample 6.N is not shown here. The thickness of the epilayer/substrate interface is about 20Å, and was comparable to that of Sample 6.M. Sample 6.L, 6.M, and 6.N were compared and it can be assumed that the water rinsing added some interfacial oxygen species by assisting the growth of surface oxide. The following *in-situ* cleaning process did not completely remove the natural oxide. The effect of water rinsing on the interfacial carbon concentration was unclear. Rinsing seemed to improve the surface smoothness.

An alcohol/HF combination was reportedly more efficient in surface cleaning than the water/HF combination [99]. In Sample 6.E, a 10:1 methanol:HF solution was used to remove the surface natural oxide and the wafer was then dried by blowing nitrogen on it and the standard *in-situ* wafer cleaning process was applied at 600°C. Fig.6.4 shows the XTEM micrograph of Sample 6.E, where the thickness of the epilayer/substrate interface was about 15-20Å. Sample 6.E can be compared to Sample 6.D; the surface smoothness of the epilayer became higher, by replacing DI water with methanol. Rinsing in DI water has resulted in the planarization of the surface of the epitaxial layer. In Sample 6.D, by omitting the rinsing step, the surface of the epitaxial layer became roughened. We found that, however, a smooth surface was obtained by replacing water with methanol, without applying the water rinsing. Because the addition of alcohol is surmised to lower the surface energy of the HF solution [99], a droplet of the solution has a smaller contacting angle on the silicon surface. Therefore, the HF solution with methanol would have a higher ability to spread onto the wafer surface and, as a result, would attack the surface oxide evenly.

Yasaka et al. [113] found that in a p-type substrate, the substrate dopant concentration did not affect the natural oxide layer thickness on Si {100} substrate in pure water, especially up to 100 minutes. Only in a very heavily doped n-type substrate, was the growth of the natural oxide layer significant. In addition to Sample 6.D, the same experiment was done on the p-type heavily doped substrate. Fig.6.5 shows the XTEM micrographs of Sample 6.F. A defect-free epitaxial layer was deposited and the thickness of the epilayer/substrate interface of Sample 6.F was measured to be about 30-40Å. From Fig.6.2 the thickness of Sample 6.D was measured to be about 20-30Å. If it is assumed that

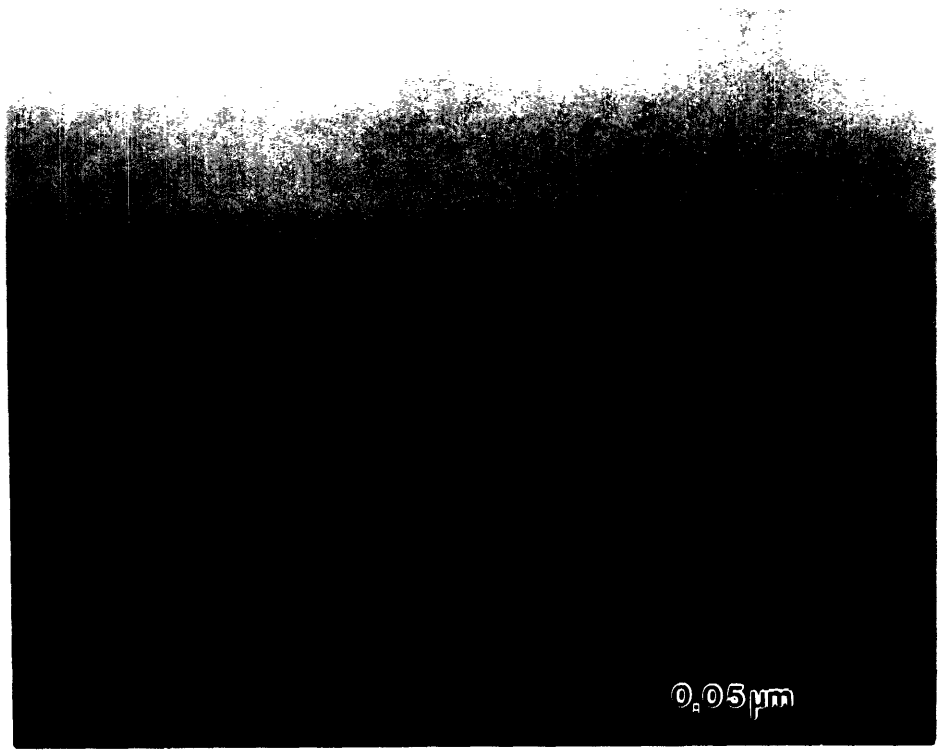

6.3 (a) XTEM micrograph of epitaxial film, cleaned *in-situ* with standard condition at 660°C (rinsed and spin-dried).

6.3 (b) XTEM micrograph of epitaxial film, cleaned *in-situ* with standard condition at 660°C (spin-dried).

this feature may differ slightly from one part of the wafer to the other, the structural qualities of Samples 6.D and 6.F can be regarded as equivalent.

Spin-drying was performed and investigated. Spin drying was accomplished by the physical removal of the water rather than by allowing it to evaporate. Samples 6.C, 6.G, 6.D and 6.H were dipped into aqueous HF solution. In Sample 6.C, the wafer was rinsed for 3 minutes and dried by blowing nitrogen on it. In Sample 6.G, the wafer was rinsed for 3 minutes and spin-dried (160 seconds rinse/240 seconds dry). In Sample 6.D, the wafer received a blow drying and in Sample 6.H, the wafer received a spin drying, immediately after an HF dipping. The standard *in-situ* cleaning process was applied at 600°C. Fig.6.6 shows the XTEM micrographs of Sample 6.G. The thickness of the epilayer/substrate interface was about 50 to 100Å. In the SIMS analysis, the interfacial oxygen and carbon concentration of Sample 6.G was 7.5 $x10^{14}$ atoms/cm^2 and 2.9 $x10^{14}$ atoms/cm^2, respectively. The carbon contamination was as much as that of Sample 6.C and the oxygen concentration was higher than that of Sample 6.C. The XTEM micrographs of Sample 6.H (not shown here) showed the broad and contaminated interface (50 to 100Å). In the SIMS analysis, the interfacial oxygen concentration was 1.5 x 10^{15} atoms/cc, respectively. By comparing Sample 6.H with Sample 6.D, the interfacial oxygen concentration of Sample 6.H was higher than that of Sample 6.D. For both cases, in comparing with blow-drying, spin drying did not reduce the surface contamination in our experiments and even degraded the quality of the epitaxial layer and its interface by providing more chances for oxygen adsorption. Hydrophobic surfaces after an HF dipping are susceptible to particle deposition [114]. Drying can be an important source of particle deposition. Verhaverbeke et al. found that particles and metallic contamination depended on drying techniques [115]. The spin dry-rinse technique was more detrimental than the blow-drying technique in terms of contamination, in our experiments.

Samples 6.I, 6.J, and 6.K were dipped into aqueous HF solution. Sample 6.I was then N_2 blow-dried without water rinsing, in Samples 6.J and 6.K, the wafer was delivered directly into the Load Lock Chamber without blow-drying or water rinsing. In Samples 6.I and 6.J, the wafers were directly loaded into the Load Lock Chamber of our CVD system, within 10 seconds. In Sample 6.K,

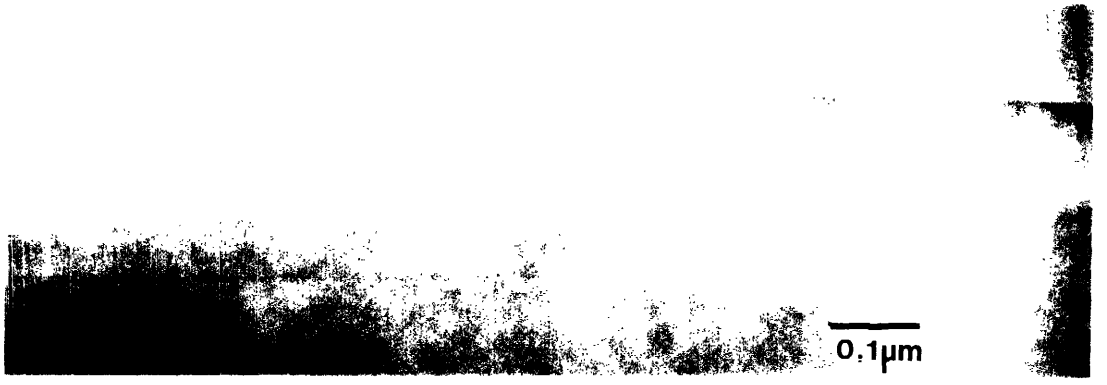

6.4 XTEM micrograph of epitaxial film, cleaned *in-situ* with standard condition at 600°C. (methanol/HF solution was used, blow-dried without rinsing)

6.5 XTEM micrograph of epitaxial film, cleaned *in-situ* with standard condition at 600°C (blow-dried without rinsing) on P^+ substrate.

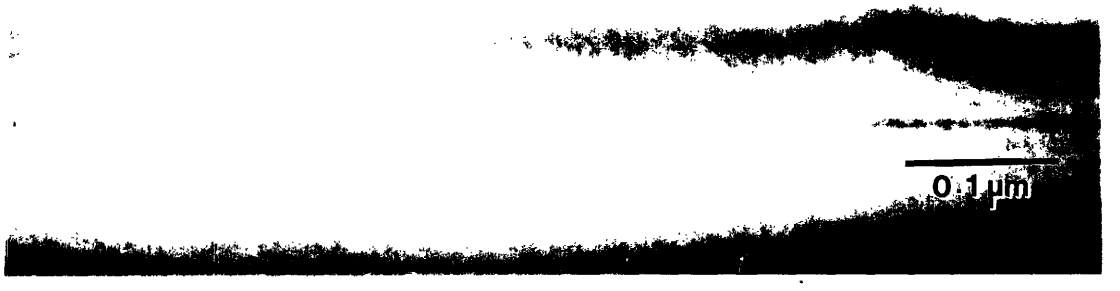

6.6 XTEM micrograph of epitaxial film, cleaned *in-situ* with standard condition at 600°C (rinsed and spin-dried)

the wafer had been kept for about 5 hours in a cleanroom atmosphere, before being loaded into the Load Lock Chamber. Samples 6.I, 6.J, and 6.K were heated up to 660°C. In Sample 6.I, hydrogen gas was flowed during heating.

Fig.6.7 shows the XTEM micrographs of Sample 6.I. The base pressure was around $1x10^{-8}$ Torr and 1mTorr and 20 sccm of hydrogen was kept flowing during heating. It took about 8 minutes to heat up to 660°C. At this temperature, the deposition was started. The XTEM micrograph showed a defect-free epitaxial layer with an almost invisible interface. SIMS data are listed in Table 6.2, the oxygen concentration of the epitaxial film was 1-2 $x10^{18}$ atoms/cc, which was comparable to that of czochralski-grown substrates. Interfacial oxygen concentration at highest point was about $9x10^{18}$ atoms/cc. The interfacial concentration was one order of magnitude higher than those of the substrate and the film. The integrated dose of oxygen at interface was 1.4 x 10^{13} atoms/cm^2. Thus it can be assumed that when no ion bombardment is applied, 1) exposure to atmosphere or 2) water rinsing significantly helps growing natural oxide and inhibits successful epitaxial growth.

Fig.6.8(a) shows the XTEM micrographs of Sample 6.J. Defect-free epitaxial layers were observed and the thickness of the epilayer/interface was measured to be about 80-90Å. The interfacial oxygen concentration of Sample 6.J was 5.2 $x10^{14}$ atoms/cm^2 and higher than that of Sample 6.I. Sample 6.J was exposed to the atmosphere for a shorter exposure compared to Sample 6.I. Some droplets of HF solution should have stayed on the silicon surface because the wafer was not subjected to nitrogen-blowing after the HF dipping treatment. In addition, the wafer did not receive an hydrogen-baking during heating. Therefore, if the effect of blow-drying on the disappearance of the solution droplets are not so significant, it is surmised that some kinds of reaction should occur on the wafer surface during heating, these reaction may play a major role in removing surface oxygen contaminants. Interfacial carbon concentration of Sample 6.J was a little bit higher than that of Sample 6.I. From the previous studies, a large amount of organic contaminants were on the surface after HF treatment because the purity of the aqueous HF solution was not sufficient [13].

The XTEM micrographs of Sample 6.K are shown in Fig.6.8(b) and a highly defective epitaxial layer was observed. SIMS data for Sample 6.K was shown in Table 6.2. Sample 6.K had a much higher oxygen level (1 order of magnitude higher) in the interfaces and the oxygen concentration in the film was also higher. The FWHM (Full width at half maximum) of the oxygen peak in the SIMS analysis was more than 100Å. It was shown from the XTEM micrographs that there are major differences in the structural quality of the epitaxial layer as a result of keeping it in the cleanroom environment for long period. Fig.6.8(b) represents the well-grown oxygen-induced stacking faults and this can be confirmed by the very high interfacial oxygen concentration of Sample 6.K. So natural oxide seems to be grown further in the cleanroom atmosphere and these oxygen species could not be desorbed easily under the vacuum condition ($1x10^{-8}$ Torr) inside the CVD chambers [24]. The growing and thicknesses of the native oxide in clean room air at room temperature is reported [116] and it was about 2Å up to 200 minutes and reached to 4Å in 5 hours.

This reasoning can be applied to Sample 6.A, and it can be surmised that in this case there was about a 5 minute interval before the wafer was loaded into the Load Lock chamber and the silicon surface had a chance to be oxidized. It is also reported that DI (deionized) water rinsing resulted in oxygen adsorption on the surface [21] and water rinsing for only 10 seconds resulted in an about 4 to 5 times increase in the interfacial oxygen concentration compared to the wafer which did not receive the water rinsing. Additional oxide could be grown during ultra-pure water rinsing and this process may add about 2Å of natural oxide [116]. Considerable amounts of oxygen on the interface of sample 6.A may have adsorbed during water rinsing. Sanganeria et al. reported that [21] the Si-OH bonds on the silicon substrate were responsible for the increased oxygen at the epilayer/substrate interface in a water rinsed substrate.

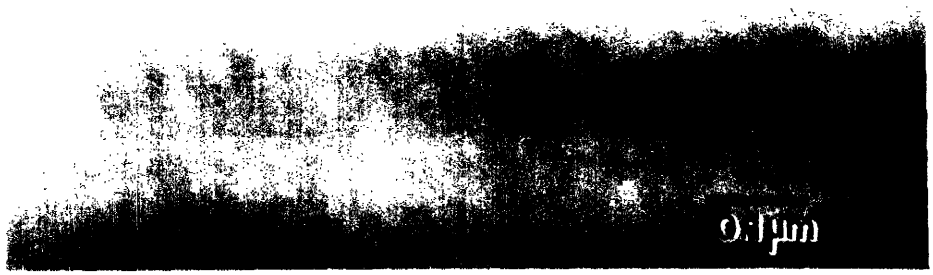

6.7 XTEM micrograph of epitaxial film, deposited at 660°C without *in-situ* cleaning (blow dried without rinsing).

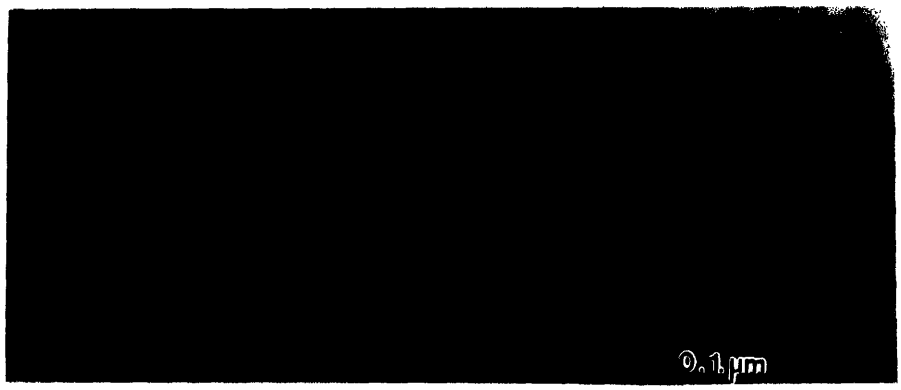

6.8 (a) XTEM micrograph of epitaxial film, deposited at 660°C without *in-situ* cleaning (without blow-drying and rinsing).

6.8 (b) XTEM micrograph of epitaxial film, deposited at 660°C without *in-situ* cleaning (without blow-drying and rinsing). It was kept for 5 hours in cleanroom.

Table 6.1. *Ex-situ* cleaning characteristics

	Rinse/dry	*In-situ* Cleaning	Deposition	Characteristic
Sample 6.A	rinse/blow	none	600°C	
Sample 6.B	/blow	none	600°C	
Sample 6.C	rinse/blow	done at 600°C	600°C	
Sample 6.D	/blow	done at 600°C	600°C	
Sample 6.E	/blow	done at 600°C	600°C	HF / methanol
Sample 6.F	/blow	done at 600°C	660°C	P^+ substrate
Sample 6.G	rinse/spin	done at 600°C	600°C	
Sample 6.H	/spin	done at 600°C	600°C	
Sample 6.I	/blow	none	660°C	
Sample 6.J		none	660°C	
Sample 6.K		none	660°C	exposure to air
Sample 6.L	rinse/spin	done at 660°C	660°C	
Sample 6.M	/spin	done at 660°C	660°C	
Sample 6.N	/blow	done at 660°C	660°C	

Table 6.2. SIMS data for deposited epitaxial layers

	oxygen(cm^{-2})	oxygen(cm^{-3})	carbon(cm^{-2})	carbon(cm^{-3})
Sample 6.A	$1.0x10^{15}$	$7x10^{20}$	$1.1x10^{14}$	$1x10^{20}$
Sample 6.C	$4.8x10^{13}$	$7x10^{19}$	$4.5x10^{14}$	$5x10^{20}$
Sample 6.D	$6.1x10^{14}$	$1x10^{20}$	$9.1x10^{13}$	$3x10^{19}$
Sample 6.G	$7.5x10^{14}$	$6x10^{20}$	$2.9x10^{14}$	$3x10^{20}$
Sample 6.H	$1.5x10^{15}$	$8x10^{20}$	$1.7x10^{13}$	$1x10^{19}$
Sample 6.I	$1.4x10^{13}$	$9x10^{18}$	$6.7x10^{13}$	$1x10^{19}$
Sample 6.J	$5.2x10^{14}$	$2x10^{20}$	$9.0x10^{13}$	$3x10^{19}$
Sample 6.K	$1.8x10^{15}$	$2x10^{21}$	$1.4x10^{13}$	$1x10^{19}$
Sample 6.L	$1.8x10^{14}$	$5x10^{19}$	$9.6x10^{14}$	$2.5x10^{20}$
Sample 6.M	$1.0x10^{14}$	$3x10^{19}$	$1.7x10^{14}$	$7x10^{19}$

6.4 Discussions

When no *in-situ* cleaning was applied at 600 C, the water rinsing step in the *ex-situ* wafer cleaning process increased the thickness of the resulting epilayer/substrate interface. This implies the increase of interfacial oxygen

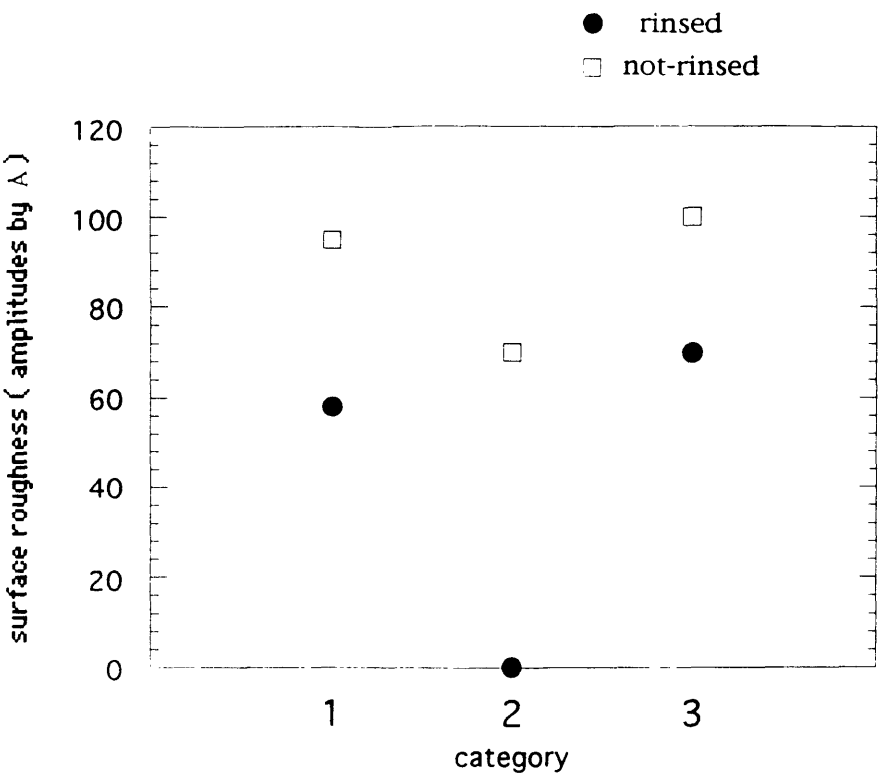

6.9 Effect of water rinse on surface roughness

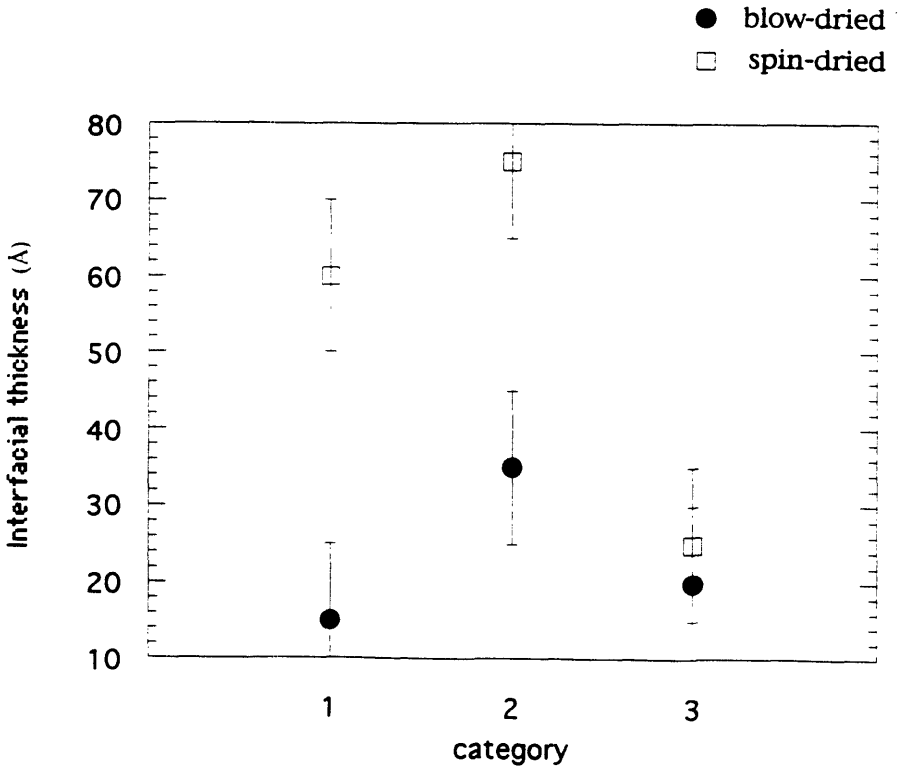

6.10 Effect of drying technique on interfacial thickness

concentration. This tendencies are supposed to decrease if the *in-situ* cleaning is applied. When the standard *in-situ* cleaning was applied at 660°C, the interfacial oxygen concentration increased with the water rinsing. The effect of the water rinsing on the interfacial carbon concentration was unclear. Excessive water rinsing resulted in a thick epilayer/substrate interface. In Sanganeria et al.'s studies [21], interfacial oxygen concentration increased with increasing DI water rinsing time. However, interfacial carbon concentration was not affected by the water rinse. These observations can be explained by the assumption that Si-OH bonds increase with the water rinse and these Si-OH bonds on the silicon surface are responsible for the increased interfacial oxygen concentration in water rinsed substrate.

The degree of surface smoothness of the epitaxial layer was observed to be improved by application of the water rinsing (Fig.6.9). Rinsing in DI water has resulted in the planarization of the surface of epitaxial layers. HF dipping removes the surface native oxide but the resulting silicon surface is prone to contamination. If the wafer is not rinsed after HF dipping, HF solutions may stay on the silicon surface, produces Si-H and Si-F species [117]. The solution can be locally present on the surface and HF acid etching begins on a fluorine terminated surface. These F-terminated surfaces are unstable and are subject to further HF attack [118]. Surface silicon atoms can be removed locally as a form of SiF_4 and minute surface irregularities will be generated. Therefore, subsequently grown epitaxial layer may have rough surface. However, DI water rising may result in the elimination of HF solutions from the silicon surface and local etching will not proceed.

Spin-drying technique was compared to the blow-drying technique. When the standard *in-situ* cleaning was applied at 600°C and 660°C, broad and contaminated interfaces were observed in samples which were spin-dried (Fig.6.10). A spin-drying step in the *ex-situ* cleaning process helped to increase the oxygen concentration at the epilayer/substrate interface (Fig.6.11(a)). Spin-drying process is comprised of spin-rinsing and spin-drying step. By applying spin-drying, 160 minutes' rinsing is added compared to blow-drying and rinsing water at high pressure will help to increase surface native oxide on the wafer surface. However, it was shown that interfacial carbon concentration was reduced by the additional spin-rinsing

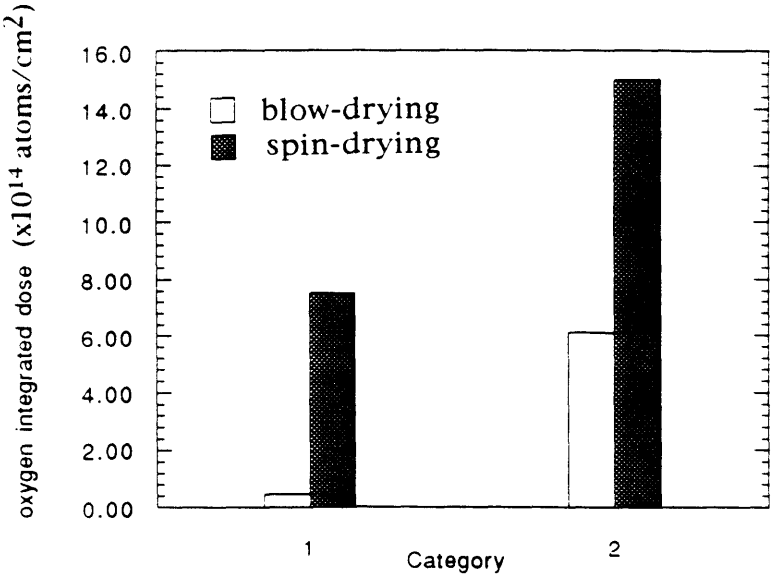

6.11 (a) Effect of drying technique on interfacial oxygen concentration

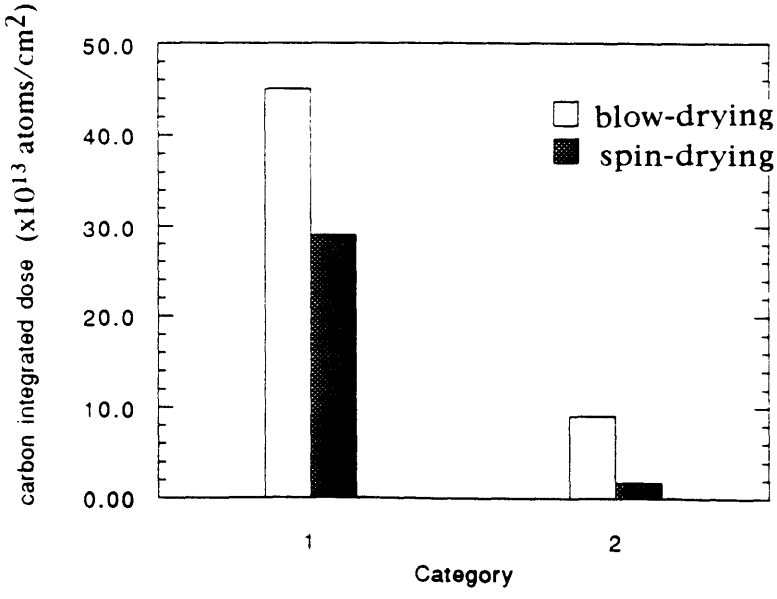

6.11 (b) Effect of drying technique on interfacial carbon concentration

(Fig.6.11(b)), spin-rinsing turned out to be efficient in removing hydrocarbons or organic species. Hydrocarbons on the water surface may be removed by physical force of rinsing water molecules or by dissolution in spin-rinsing step. Cleaning effects of running deionized water was reported on GaAs substrate in removing surface oxides [119].

When no standard *in-situ* cleaning was applied at 660°C, omitting both the blow-drying and water rinsing steps was not an effective cleaning technique for subsequent epitaxial growth. It means that blow-drying is one of the essential step in reducing surface contaminants after HF dipping. Usually, drying should be done after rinsing to physically remove the water on the wafer surface. In our case, wafers did not receive the water rinsing, however, HF aqueous solution already contains water and additional water can be generated by the reaction: $SiO_2 + 6HF \rightarrow H_2SiF_6 + H_2O$ as long as the etching continues. From SIMS data (Table 6.2), the wafer surface which did not receive the blow-drying contained higher carbon contaminants, although the difference is small compared to oxygen contaminants. When no standard *in-situ* cleaning was applied at 660°C, blow-drying (by nitrogen) without a water rinsing step turned out to be an effective process in reducing the interfacial oxygen concentration and getting a discrete epilayer/substrate interface (Fig.6.7). It is surmised that flowing hydrogen is necessary to maintain a reducing environment.

Chapter 7

Surface Contamination : Oxygen and Carbon

The focus of the research was on the removal of the wafer surface contaminants, especially oxygen and carbon prior to epitaxial deposition, by *ex-situ* cleaning with HF dipping and *in-situ* ECR plasma cleaning techniques. *In-situ* cleaning, especially when it was optimized, was effective in removing the natural oxide on the wafer surface. Room temperature *in-situ* cleaning was effective in removing carbon species from the wafer surface. High temperature processing was needed to minimize the interfacial oxygen concentration and at this high temperature, omitting the *in-situ* cleaning step resulted in reduction of the interfacial carbon concentration. The possible reaction mechanisms of oxygen and carbon removal were discussed. In this study, thermal equilibrium of reactants and products was discussed.

7.1 Introduction

Only carbon and oxygen can be taken into account as contaminants, since other contaminants such as metals can be suppressed to negligible levels through careful wafer handling [128]. Atomically clean surfaces can be generated by thermal treatment of silicon surfaces at high temperature (~1250°C). At high temperatures the surface oxides are reduced by the underlying silicon to produce a volatile silicon monoxide. Oxygen is removed after annealing at 830°C. Carbon is much more tenacious [121] and stable on the silicon surface. Temperatures over 1100°C are required to remove carbon from the surface [107]. Also during heating of the substrate, the hydrocarbons decompose and carbon reacts with the silicon to form silicon carbide, which may form in its crystalline from, β-SiC [122]. This form was quite stable and was difficult to remove. Hydrogen plasma was used to clean semiconductor surfaces and the usage of microwave electron cyclotron resonance (ECR) sources were reported in the literature [123] [93]. Removal of carbon from the surface proved to be easier than removal of oxygen; primarily due to the relatively fast etch rate of hydrocarbons by atomic hydrogen. The carbon removal in low temperature *in-situ* cleaning was surmised to occur by

volatilization through hydrogenation. Volatilization of the hydrocarbons appeared to proceed via slow oxidation of the long carbon chain at every carbon atom; in the final stage of this process the carbon desorbs as CO_2 [124]. Low temperature (room temperature) *in-situ* cleaning was performed in our experiments to reduce the interfacial carbon concentration.

The vacuum system, the process itself (*in-situ* cleaning process/ the process gases) and the substrate (maybe from *ex-situ* cleaning) can be possible sources of gas impurities. The potential sources of gases and vapors in a vacuum system can be found in the literature [124]: real and internal leaks, vaporization, diffusion, desorption, permeation through the chamber materials, backstreaming from the pumps. Oxygen may be originated from the natural oxide on the silicon surface, which may grow during the exposure to air or water rinsing process. Water vapor may enter into the chamber when the wafer is loaded. Internal surfaces of the main chamber should be evenly coated with layers of water molecules and will become a predominant residual gas [125]. Therefore, during heating, some water molecules desorb and may adsorb onto the wafer surface. To reduce this phenomenon, the Load Lock Chamber was installed in our CVD system. The bake-out treatment was performed to remove some of water molecules. Carbon can be originated from the organic contaminants on the oxide layer, from the HF solution, and from DI water [126]. Vacuum pumps can be a source of hydrocarbons. If the turbomolecular pump is operated in an improper manner, there will be danger of oil backstreaming into the process chamber. Hydrocarbons can also be originated from the mechanical pump which is oil-sealed. The source of carbon and oxygen needs to be investigated in more detail.

7.2 Experimental

Substrates were 4 inch, czochralski-grown, p-type <100> Silicon with 0.5-20 Ω-cm resistivity. The wafers were RCA cleaned and HF dipped for 20-30 seconds in 10:1 aqueous solutions and rinsed in DI (deionized) water and then dried by blowing nitrogen on them. All the processes were done inside the class 100 cleanroom and it took only 10 seconds to load the wafer into the Load Lock Chamber of the CVD reactor after the wafer was blow-dried. The Load Lock Chamber had its own turbomolecular pump (80 l/s) and backing mechanical

pump. After the Load Lock Chamber was pumped down to about 1x 10^{-7} Torr the wafer could be transferred to the main chamber by opening the gate valve. The hydrogen was kept flowing through the main chambers when the gate valve was opened to avoid cross contamination. After the wafers were transferred and loaded onto the heater stage, the main chamber was pumped down and ultimately 1-2x10^{-8} Torr could be attained. The main pumping unit consisted of a chemical resistive 1500l/s turbomolecular pump (Leybold Turbovac 1500) and a backing mechanical pump.

In-situ predeposition wafer cleaning was done by using ECR hydrogen plasma. The ECR chamber was at the side of the CVD chamber. ECR was operated at the 2.45 GHz S-band microwave frequency. Depositions were done by flowing 10 sccm SiH_4 without carrier gases, immediately after the plasma was extinguished. Pure silane and house hydrogen were used and these gases passed through the Nanochem purifiers, which were known to be effective in reducing trace impurities.

Thermal heating (bakeout) was performed by using heating tapes outside the chambers. They were coiled around the CVD Chamber, the Analysis chamber and the main turbomolecular pump. The QMS scan was done during bakeout to check the appearance of water vapor. After bakeout treatment, a hydrogen plasma exposure was performed to provide an energy to help remove the contaminants inside the chamber. Silane gas was introduced and kept flowing at 600°C for 20 minutes, mainly to pre-coat the wafer heating elements. The QMS (Quadrupole Mass Spectroscopy) was mounted on the CVD chamber [72] and it used a Micromass PC (VG Quadruples). The unit was differentially pumped with an independent pumping system consisting of a 450 l/s turbomolecular pump (Alcatel CFF450) backed by a mechanical pump. Gases were extracted from the wafer edge and then were transported through the capillary to the analyzer and real time information on gas concentration could be obtained.

Cross-sectional transmission electron microscopy (XTEM) was used to observe the epitaxial layer and the epitaxy/substrate interface. The SIMS measurement was done in Evans East, New Jersey and a Perkin Elmer 6600 secondary ion mass spectrometer was used. Cs^+ ion is used as the ion source for

sputtering and primary ion energy was 5 keV and beam current was 200nA. The detected elements included carbon, oxygen and nitrogen.

7.3 Results

The wafers were dipped in 10:1 aqueous HF solution. They were rinsed in DI water for 3 minutes and dried by blowing nitrogen. Sample 7.A did not receive an *in-situ* plasma cleaning, and Sample 7.B received a standard *in-situ* plasma cleaning. Samples 7.C, 7.D and 7.E received the same *in-situ* cleaning as Sample 7.B, except that in Sample 7.C, the DC bias was set at 0V and in Sample 7.D, the hydrogen pressure was set at 8mTorr and in Sample 7.E, the cleaning time was set at 20 minutes (Table 7.1).

Fig.4.1(b) is the HRXTEM (High Resolution Cross-sectional Transmission Electron Microscopy) micrograph of Sample 7.B, and shows an almost discrete feature of the interface. RBS channeling experiments confirmed that the epitaxial film had an almost perfect crystallinity. The χ_{min} was measured to be in the 3-4% range. Fig.7.1 shows the SIMS data of Sample 7.B, where the oxygen concentration inside the film was about 1-2x10^{18} atoms/cc and almost the same level as the substrate concentration (1x10^{18} atoms/cc). Interfacial oxygen concentration was 4.8 x10^{13} atoms/cm^2. This value was the lowest among the samples, which were cleaned *in-situ* and grown at 600°C. Interfacial carbon concentration was 4.5 x10^{14} atoms/cm^2.

The SIMS data of Samples 7.A, 7.B, C, 7.D, and 7.E were investigated. The oxygen and carbon concentrations at the epilayer/substrate interface were listed in Table.7.2. Table.7.2 shows the interfacial oxygen concentration of Sample 7.B was less than 5 x10^{13} atoms/cm^2, and those of Samples 7.A, 7.C, 7.D, and 7.E were more than 5 x10^{13} atoms/cm^2. It is notable that the interfacial carbon concentration of Sample 7.B was higher than any of Samples 7.A, 7.C, 7.D and 7.E. The structural qualities of the epitaxial layer and the epilayer/substrate interface were closely related to the interfacial oxygen concentration. It is possible that an effective *in-situ* cleaning process (in Sample 7.B) generated some carbon species. *In-situ* plasma cleaning at 600°C reduced the interfacial carbon concentration below the level of Sample 7.A, if the DC bias became more negative (Sample 7.C), or if the hydrogen pressure

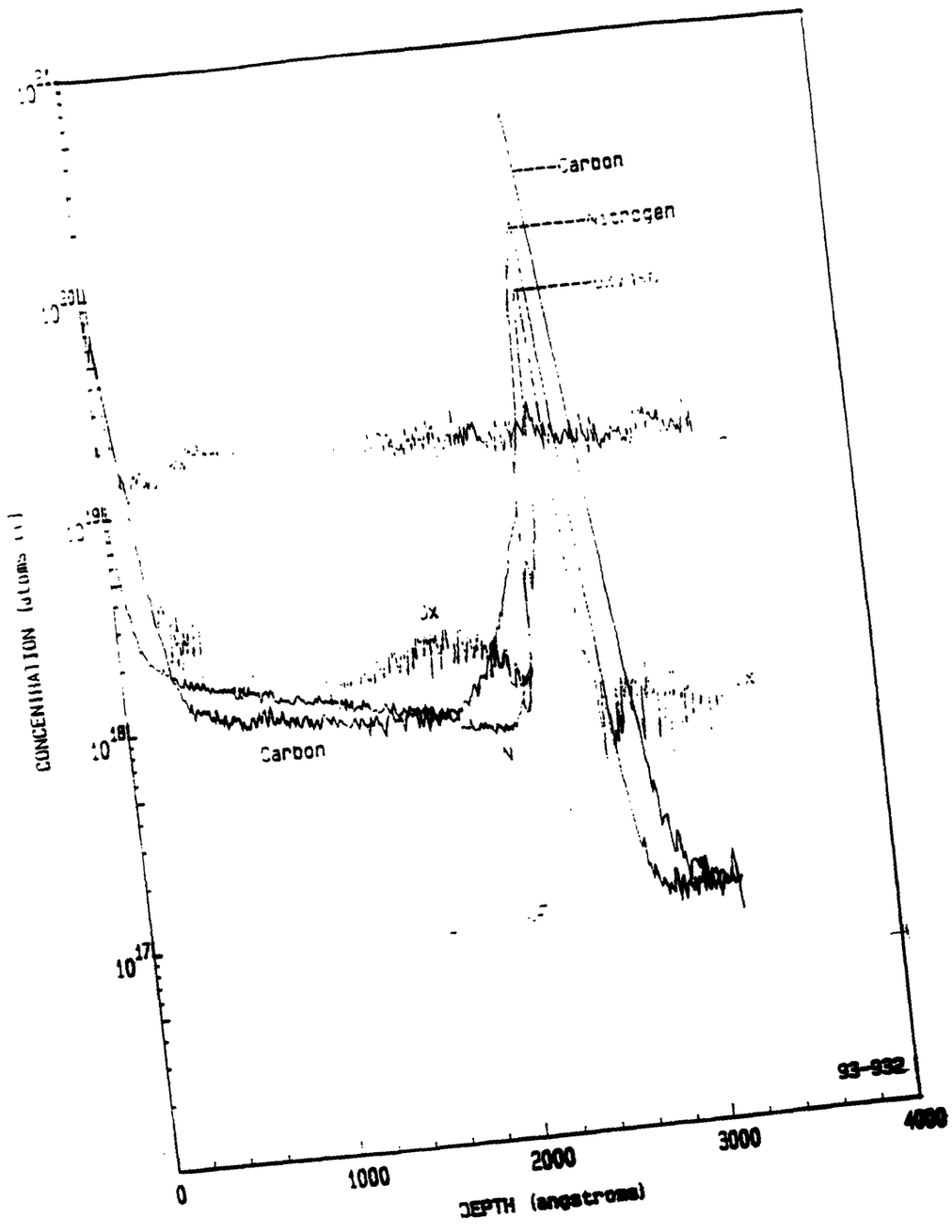

7.1 SIMS depth profiles of epitaxial film, cleaned *in-situ* with standard condition at 600°C (rinsed and blow-dried)

became higher (Sample 7.D), or if the cleaning time became longer (Sample 7.E), compared to Sample 7.A. It means that higher density and higher total numbers of hydrogen atoms or ions, with a higher energy were efficient in removing carbon from the wafer surface. However, it was shown in Chapter 5 that interfacial carbon concentration was not affected by substrate DC bias significantly.

Samples 7.F, 7.G and 7.H were room temperature *in-situ* cleaned. Their SIMS data showed high (more than 3 $x10^{14}$ atom/cm^2) interfacial oxygen concentrations. Their interfacial carbon concentration were low, with 1.4 $x10^{13}$, 6.9 $x10^{12}$ and 8.0 $x10^{12}$ atoms/cm^2, respectively (Table 7.2). In Samples 7.F and 7.G, defect-free epitaxial layers were deposited and in Sample 7.H, a polycrystalline film was deposited. The structural qualities of the deposited film and the epilayer/substrate interface were not degraded by the presence of carbon. Very low temperature (room temperature) *in-situ* cleaning resulted in less interfacial carbon concentration than high temperature (more than 600°C) *in-situ* cleaning. The hydrogen gas we used in our reactor passed through the Nanochem purifier (Simigas systems, inc. Model 3000). The purifier reduced the levels of complex hydrocarbons to less than 1 ppb. From Chapter 4, it was shown that standard *in-situ* cleaning at 600°C generated carbons, compared to the sample which did not receive the *in-situ* cleaning.

Fig.7.2(a) shows the dependence of interfacial oxygen and carbon concentration on the temperature of *in-situ* cleaning and deposition. The wafers were spin-dried after being dipped into HF aqueous solution. Processing at 660°C (Sample 7.J) was more efficient in removing oxygen than processing at 600°C (Sample 7.I). It showed the reverse tendency for carbon. Oxygen was greatly reduced by raising processing temperatures by 60°C. However this effect should be a sum of the hydrogen pre-bake effect and *in-situ* plasma cleaning effect. It means that Sample 7.J not only received a higher temperature (660°C) *in-situ* cleaning, but also heated up to higher temperature in hydrogen ambient. Fig.7.2(b) shows the dependence of interfacial oxygen concentrations on the standard *in-situ* cleaning process. The *in-situ* cleaning temperature was set at 25°C (Sample 7.F) and 600°C (Sample 7.B) and deposition was performed at 600°C. The wafers received an HF dipping, rinsed in DI water and blow-dried. First sample (Sample 7.A) did not

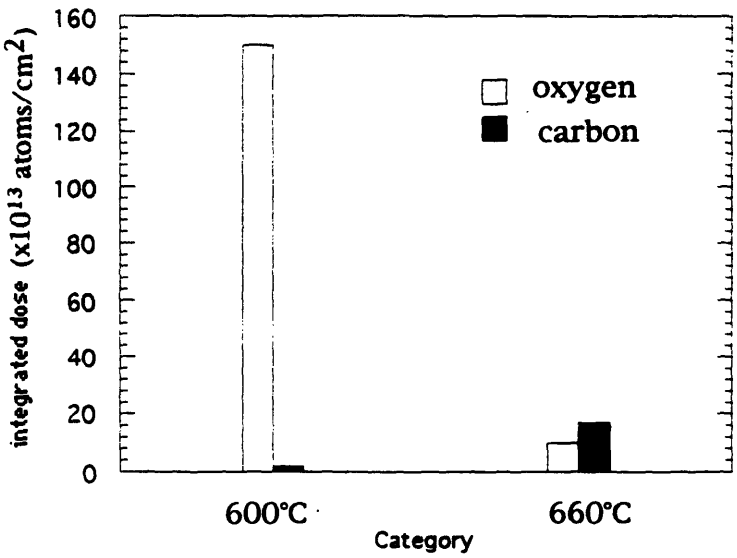

7.2 (a) Effect of *in-situ* cleaning and deposition temperature (600°C, 660°C) on interfacial oxygen and carbon concentration

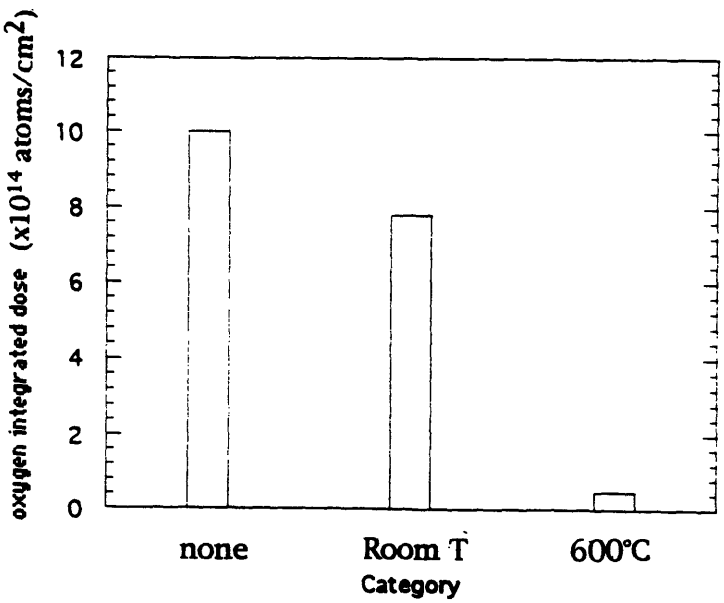

7.2 (b) Effect of *in-situ* cleaning temperature (none, 25°C, 600°C) on interfacial oxygen concentration

receive the *in-situ* plasma cleaning. The oxygen concentration decreased with increasing the cleaning temperature. Even room temperature *in-situ* cleaning, if it is optimized, reduced the interfacial oxygen concentration.

Fig.6.7 shows the XTEM micrographs of Sample 7.K, in which case an almost invisible interface was observed. In Sample 7.K, the wafer received an HF dipping, and blow-dried with nitrogen without DI water rinsing, and was then loaded into the Load Lock Chamber. It was heated up to 660°C in the hydrogen environment, and deposition was done at 660°C. Fig.7.3 shows the SIMS data for Sample 7.K. Interfacial oxygen concentration was 1.4 $x10^{13}$ atoms/cm^2 and the interfacial carbon concentration was 6.7 $x10^{13}$ atoms/cm^2. Oxygen contents inside the film were almost the same as the oxygen level in the substrate. Sample 7.K was compared to Sample 7.L, where the deposition was performed at 600°C. Interfacial oxygen concentration was reduced by high temperature hydrogen-baking, which can be inferred by the observation of the epilayer/substrate interface.

To investigate the origin of the surface contaminates, in Sample 7.M, a total of three layers were deposited. The wafer was dipped into HF aqueous solution and blow dried by nitrogen, before being loaded into the Load Lock Chamber. Standard *in-situ* cleaning was done at 600°C, followed by deposition at the same temperature, for 60 minutes. The standard *in-situ* cleaning and deposition was repeated for the second layer. Then hydrogen was kept flowing for 5 minutes, without ECR plasma and the third layer was deposited. In SIMS analysis, volumetric concentration at the highest point was used, because the widths of peaks were higher than the resolution depth of SIMS measurement.

Fig.7.4 and Table 7.3 show the SIMS data for Sample 7.M. The oxygen concentration of the first and second interface were $1.5x10^{20}$ atoms/cc and $4x10^{19}$ atoms/cc, respectively. The significant difference in the oxygen concentrations between the two interfaces means that there was surface natural oxide from the beginning and this oxide could not be removed completely by *in-situ* wafer cleaning. In the third interface, the hydrogen kept flowing at 600°C for 5 minutes and oxygen accumulated on the surface (9 $x10^{19}$ atoms/cc). The house hydrogen gas was used, and it was passed through

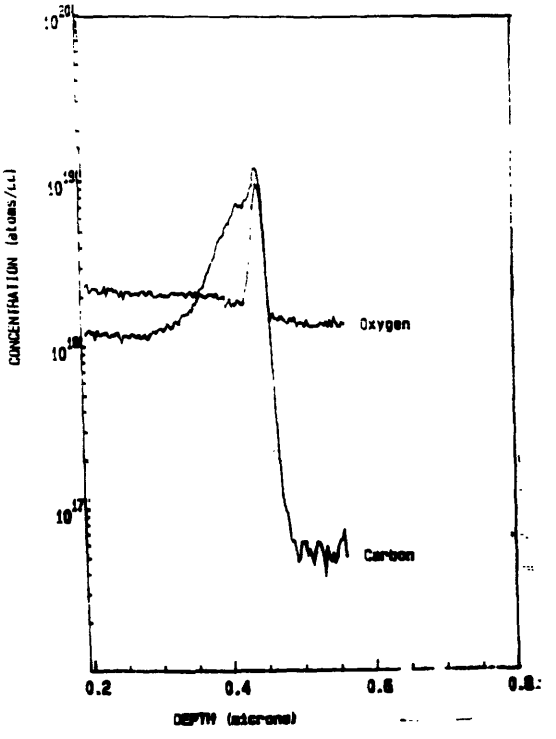

7.3. SIMS depth profiles of epitaxial film, deposited at 660°C without *in-situ* cleaning (blow-dried without rinsing)

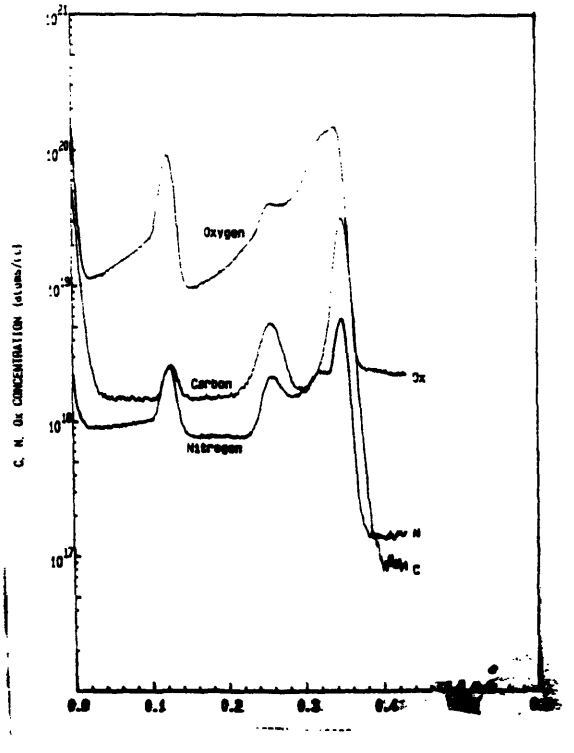

7.4 SIMS depth profiles of epitaxial film, cleaned *in-situ* with standard condition at 600°C (blow-dried without rinsing). For second layer, *in-situ* with standard condition at 600°C and for third layer, with hydrogen kept flowing for 5 minutes.

the Nanochem purifier before being introduced into the chamber. This purifier reduces the level of water, oxygen to less than 1 ppb level. This means that less than $2x2.7x10^{13}$ atoms of oxygen were introduced within 5 minutes. But the oxygen peak indicates that, by calculation of its areal density, $2.5x10^{14}$ oxygen atoms accumulated at the epilayer/substrate interface per square centimeter. Therefore, most of the oxygen may have originated from within the chamber. Oxygen was originated from the *ex-situ* cleaning and from within the chamber and *in-situ* plasma cleaning played a role in removing the oxygen species from the wafer surface. This analysis can be applied to carbon, as well. By comparing the first and second interface, it is evident that considerable amounts of carbon were adsorbed onto the surface after the *ex-situ* cleaning. By comparing the second and third interfaces, it seems that the ECR plasma cleaning generated carbon in addition to carbon atoms which came from the hydrogen gas or from inside the reactor.

Residual gas analysis was performed using a quadruple mass spectrometer in our CVD system. During the plasma excitation at room temperature, a small increase of the N_2 + CO (mass=28) level and a drastic increase of the SiO (mass=44) level was observed. Therefore, it is surmised that the ECR hydrogen plasma cleaning process generated volatile SiO(g) in our system. It is also possible that CO_2 (g) was generated, carbon species may have originated from the plasma etching of silicon substrate surfaces or from the etching-enhanced outgassing of the chamber walls and surfaces of other equipment. $N_2 + CO$ (mass=28) level was noticeably increased after plasma excitation.

From the current literature, vacuum materials (especially inside the chamber) are a potential source of contaminants [127]. Thermal desorption is the heat-simulated release of gases or vapors, which may have been adsorbed on the chamber surface while it was exposed to the atmospheric environment. The thermal energy (bakeout) was effective in desorbing water and stainless steel components, and 250 to 300°C was commonly used, but in our system, we were careful to avoid temperature above 150°C, so as not to damage other critical components. Thermal heating (bakeout) was performed by using heating tapes outside the chambers. They were coiled around the CVD chamber, the analysis chamber and the main turbomolecular pump. The temperature was kept at 120°C throughout the heating process. The QMS scan

was done during bakeout and showed a gradual increase and saturation of nitrogen. A small amount of water vapor has appeared after three hours' bake-out. However, the later overnight bakeout did not show any appearance of water vapor in this measurement. In Sample 7.N, the standard *in-situ* cleaning was applied at 600°C, after the bake-out treatment. Sample 7.N was compared to sample 7.O. By admitting that the error of the SIMS profile is in the 15-20% range, the interfacial oxygen and carbon concentration did not change significantly by bake-out treatment at 120°C.

Table 7.1 *In-situ* cleaning conditions

	Power	DC bias	Temp.	Time	Pressure
Sample 7.B	300W	10V	600°C	5 min	1mTorr
Sample 7.C	300W	0V	600°C	5 min	1mTorr
Sample 7.D	300W	10V	600°C	5 min	8mTorr
Sample 7.E	300W	10V	600°C	20 min	1mTorr
Sample 7.F	300W	10V	room T	5 min	1mTorr
Sample 7.G	750W	10V	room T	5 min	1mTorr
Sample 7.H	300W	0V	room T	5 min	1mTorr
Sample 7.I	300W	10V	600°C	5 min	1mTorr
Sample 7.J	300W	10V	660°C	5 min	1mTorr
Sample 7.L	300W	10V	660°C	5 min	1mTorr
Sample 7.N	300W	10V	600°C	5 min	1mTorr
Sample 7.O	300W	10V	600°C	5 min	1mTorr

Table 7.2 SIMS data at the epilayer/substrate interface

	oxygen(cm^{-2})	oxygen(cm^{-3})	carbon(cm^{-2})	carbon(cm^{-3})
Sample 7.A	1.0×10^{15}	7×10^{20}	1.1×10^{14}	1×10^{20}
Sample 7.B	4.8×10^{13}	8×10^{19}	4.5×10^{14}	5×10^{20}
Sample 7.C	8.1×10^{14}	3.5×10^{20}	3.8×10^{13}	3×10^{19}
Sample 7.D	1.0×10^{15}	8×10^{20}	6.3×10^{14}	7×10^{19}
Sample 7.E	5.9×10^{14}	6×10^{20}	2.1×10^{13}	2×10^{19}
Sample 7.F	7.8×10^{14}	7×10^{20}	1.4×10^{13}	1×10^{19}
Sample 7.G	3.0×10^{14}	3×10^{20}	6.9×10^{12}	6×10^{18}
Sample 7.H	8.5×10^{14}	1×10^{21}	8.0×10^{12}	7×10^{18}
Sample 7.I	1.5×10^{15}	8×10^{20}	1.7×10^{13}	1×10^{19}
Sample 7.J	1.0×10^{14}	3×10^{19}	1.7×10^{14}	7×10^{19}
Sample 7.K	1.4×10^{13}	9×10^{18}	6.7×10^{13}	1.5×10^{19}
Sample 7.N	6.2×10^{14}	4×10^{20}	4.1×10^{14}	2.5×10^{20}
Sample 7.O	7.6×10^{14}	6×10^{20}	2.9×10^{14}	2.5×10^{20}

Table 7.3 SIMS data for Sample 7.M

	oxygen(cm^{-2})	oxygen(cm^{-3})	carbon(cm^{-2})	carbon(cm^{-3})
Interface 1	6.1×10^{14}	1.5×10^{20}	7.1×10^{13}	3×10^{19}
Interface 2		4×10^{19}	2.7×10^{13}	5×10^{18}
Interface 3	2.5×10^{14}	9×10^{19}	1.1×10^{13}	2.5×10^{18}

7.4 Discussions

7.4.1 Carbon Removal

The mechanism of carbon removal at low temperature (≤ 700°C) is not clear, Thomas et al. suggested that removal of surface carbon occur by volatilization through hydrogenation in hydrogen plasma cleaning process. To study the carbon removal mechanism, it is necessary to be informed on the form and behavior of carbon species on the silicon surface. Carbon may be present as elemental carbon bonded to silicon atom or hydrocarbons chemically or physically bonded to silicon atoms. Licciardello et al. suggested that after HF dipping, organic compounds are chemically bonded to the silicon surface and this organic layer will not be affected by the growth of surface oxide layer [128]. Kinoski et al. found that removal of carbon at 400°C was less efficient than at 250°C in their hydrogen plasma cleaning experiments. It is thought that the carbon removal mechanism was related to the removal of methyl group from the surface by H(g) [99]. Cheng et al also observed that the carbon removal rate decreased with increasing temperature at temperatures above 177°C in their experiments on the interaction of atomic hydrogen with surface methyl group on Si(100) [97]. Surface carbon present as CH_3 (ad) was removed by the chemical reaction, producing volatile methylsilane, CH_3SiH_3 (g).

Colaianni et al. investigated the behavior of Si-CH_3 at low temperatures (≤ 577°C). At above 427°C, -CH_3 has begun to decompose to CH_2 (ad) and/or CH(ad) species and at above 577°C, only the presence of adsorbed carbon on the surface was verified [129]. Therefore, at temperatures below 327°C, surface

carbon will be present as CH_3 (ad) and this can be removed easily by reactions $Si\text{-}CH_3 + 3H(g) \rightarrow CH_3SiH_3$ (g). In this situation, CH_3 (ad) + H(g) $\rightarrow$ CH_4 (g) will be another possible reaction, however, this reaction was not dominant because of its low reaction cross section [97]. By theoretical studies of the thermochemistry of molecules in the Si-C-H system done by Allendorf et al., among the molecules in the series of $H_mSi(CH_3)_n$ and H_mSiCH_n, $H_mSi(CH_3)_n$ (m+n=4) had the lowest free energies of formation [130] and CH_3SiH_3 is known to have lower boiling point (-57°C) than that of $(CH_3)_2SiH_2$ and $(CH_3)_3SiH$. In carbon removal process, etchant are formed and these etchant will be adsorbed on the substrate for subsequent reaction. And product should be desorbed, for etching to be continued. The following reactions are considered and their free energy changes are calculated at room temperature, 600°C and 660°C (Table 7.4).

In ECR hydrogen plasma, hydrogen gas (H_2(g)) will be converted into more reactive H(g), at low temperatures (< 600°C) Reaction 1 will occur and volatile CH_3SiH_3 (g) will be produced. It was shown in Fig.6.11(b) that a low temperature is favored for carbon removal. Therefore, desorption of reaction products will not be a rate-determining step in carbon removal processes. The number of molecule of a gas at rest that strike is given by [132]:

$$v = 3.513 \times 10^{22} \frac{P_{mm}}{\sqrt{MT}} \text{ cm}^{-2} \text{ sec}^{-1}$$

and for hydrogen at 300°K and at a pressure of 1mTorr ($\equiv 10^{-3}$ mmHg), v = 1.43×10^{18} cm^{-2} sec^{-1}. The number of hydrogen molecules adsorbed on the wafer surface per second is v x p x a x s where p is the gas pressure in mmHg, a is the area of the wafer in cm^{-2} and s is the sticking probability ($\equiv 10^{-5}$). Therefore hydrogen flux = $1.43 \times 10^{18} \times 10^{-3} \times 10^{-5}$ cm^{-2} sec^{-1} = 1.43×10^{10} cm^{-2} sec^{-1}. If ionization efficiency of 10^{-1} is assumed, adsorption flux of H(g) can be approximately 2.06×10^{9} cm^{-2} sec^{-1}. In the hydrogen flow of 10 sccm, 1.6×10^{22} molecules will be introduced into the chamber in every second, adsorption/reaction can be a rate-determining step.

From Table 7.4, since Reaction 1 can occur with a high driving force, in room temperature *in-situ* cleaning, this reaction will be a dominant reaction.

It is notable that even without plasma, reaction 2 will occur. In 5 minutes during *in-situ* cleaning, $300 \times 1.43 \times 10^{10} \cong 4 \times 10^{12}$ hydrogen species will adsorb on the surface, and this order matches with our SIMS measurement. Therefore, at low temperature (room temperature), Reaction 1 and 2 occur and adsorption of hydrogen molecules and ions seem to play an important role. Reaction 2 may consist of the dissociation of $H_2(g)$ to H(g) and Reacion 1. In this case, Dissociation on the surface can be a rate-determining step. From the observation that room temperature *in-situ* cleaning was particularly efficient than by flowing hydrogen, Reaction 1 dominates the carbon removal process. It is evident that reactive H(g) played a major role, even C=C bonds in organic layer on the silicon surface can be reduced to CH-(ad), CH_2-(ad) and up to CH_3 (ad) and thus can be easily removed.

At high temperature (> 600°C), although carbon should be in SiC form in equilibrium, most carbon will be in silicon lattice in their metastable state. Reaction 3 can occur considering thermal equilibrium, it means that carbon in metastable state can react more easily to from $CH_4(g)$. If we accept the observation that 600°C was more favored temperature than 660°C, atomic diffusion through silicon or desorption of CH_4 gas should not be a rate-determining step. In Reaction 4, $\Delta G_{600°C}$ = 72,020 J at equilibrium and $P_{CH4} \cong 8.7 \times 10^{-17}$ (0.1 MPa) = 6.5×10^{-14} Torr at 1mTorr of hydrogen pressure. Reaction 4 does not occur and thus at high temperatures, carbon cannot be removed by just hydrogen pre-bake. It should be noted that standard state in our thermodynamic data is defined as 0.1MPa, which is 750 Torr.

Unexpected carbon can be generated during *in-situ* cleaning because of SiC-coated filament. Reaction 3 may occur and increase the level of gaseous CH_4 in the atmosphere. These species may directly adsorb on the silicon surface, however, this action does not seem to occur significantly, because Reaction 2 is favored at lower temperature, however the room temperature *in-situ* cleaning was efficient in our experiments. It is probable that carbon was generated during high temperature *in-situ* cleaning, because the sample which receive a standard *in-situ* cleaning at 600°C turned out to have higher interfacial carbon concentration than the sample which did not receive the *in-situ* cleaning (Chapter 4).

Table 7.4 Free energy changes for carbon removal reactions (J/mole) [130] [131]

Reactions	27°C	600°C	600°C
1. $SiCH_3 + 3H(g) \rightarrow CH_3SiH_3(g)$	-895,325	-713,361	-669,859
2. $SiCH_3 + 3/2H_2(g) \rightarrow CH_3SiH_3(g)$	-285,767	-195,444	-162,055
3. $SiC(\beta) + 4H(g) \rightarrow Si(s) + CH_4(g)$	-792,527	-618,536	-602,362
4. $SiC(\beta) + 2H_2(g) \rightarrow Si(s) + CH_4(g)$	20,217	72,020	74,710

7.4.2 Oxygen Removal

Surface native oxide has been known to be removed by hydrogen pre-bake at high temperatures. Kobayashi [133] studied on thermal cleaning at 760°C and 900°C without hydrogen flowing, the reaction product was identified as SiO. Racanelli et al. revealed that hydrogen bake aided the removal of surface oxygen and that higher temperature bake (795°C) was more efficient [134] in their UHVCVD system. Meyerson also used high temperature bakes to remove surface native oxide in an hydrogen ambient [23]. They all suggested that a dominant etching reaction should be: $Si(s) + SiO_2 \rightarrow 2SiO(g)$. It can be assumed that other reduction reactions by hydrogen may occur and in addition to that, hydrogen was necessary for the first reaction to proceed. Because silicon can be actually etched in the presence of oxidizing species as in the following reactions:

$$Si(s) + H_2O \rightarrow SiO(g) + H_2(g) \; ; \quad 2Si(s) + O_2 \rightarrow 2SiO(g).$$

The possible thermal etching reactions in hydrogen ambient at relatively low temperatures (≤ 660°C) in our system were listed in Table 7.5 and their free energies of reactions are presented.

In Table 7.5, Reaction 4: $SiO_2(s) + 3/2H_2 \rightarrow SiH_3(g) + O_2(g)$ and Reaction 9: $SiO_2(s) + 7/2H_2 \rightarrow SiH_3(g) + 2H_2O(g)$ and some reactions which generates SiH(g) were excluded because in Si_mH_n, the species with odd n are known to be thermodynamically unstable [137]. In considering free energy changes,

Reactions 1,3,6, and 7 cannot occur. In Reaction 10, $\Delta G_{660°C}$ = 406,212J. At equilibrium, P_{SiH4} = 1.0 x 10^{-23} Torr (if P_{H2O} = 10^{-8} Torr) and Reaction 10 will not proceed. In Reaction 8, $\Delta G_{660°C}$ = 346,296J. At equilibrium, $P_{SiH2}\,P_{H2O}^2 \cong 4.09 \times 10^{-29}$ $Torr^3$. In our system, base pressure is about 1 x 10^{-8} Torr and P_{H2O} will be more than 10^{-9} Torr [138] and $P_{SiH2(eq)}$ will be less than 4.09 x 10^{-11} Torr, and therefore Reaction 8 will not occur in our system. In Reaction 5, $\Delta G_{660°C}$ = 290,685J and at equilibrium, $P_{H2O} \cong 7 \times 10^{-9}\,P_{H2} \cong 7 \times 10^{-12}$ Torr, and thus Reaction 5 will not proceed.

In Reaction 11, $\Delta G_{660°C}$ = 319,433J and $P_{SiO(eq)} \cong 10^{-6}$ Torr. In Reaction 2, $\Delta G_{660°C}$ = 305,059J and if it is assumed that P_{H2} = 1mTorr and P_{H2O} = 10^{-8} Torr, $P_{SiO(eq)} \cong 6.3 \times 10^{-10}$ Torr and this reaction may occur slightly, however, Reaction 11 occur in the same system and thus Reaction 2 can be neglected. (Note: standard state p_0 in out thermodynamic data is 0.1MPa, which is 750Torr). It was shown that in out system, Reaction 11 is a dominant etching reaction and by comparing Sample 7.K with Sample 7.L, interfacial oxygen concentration was reduced by heating from 600°C to 660°C in hydrogen ambient (1mTorr). Reaction 11 occurred and SiO(g) was generated and desorbed at 660°C. Thomas et al. found that SiO(g) was desorbed at 700°C [28]. Ishizaka et al. [139] suggested that the thermal etching process will be conducted in two steps, the reaction and the migration of SiO through the oxide film. They found that the migration of SiO though the oxide film was not a rate-determining step when the oxide film was very thin. Kobayashi [133] added the SiO desorption step, however, SiO(g) is known as a very volatile material.

Samples 7.K received an HF dipping and blow-dried. Morita et al. reported on the growth of native oxide on silicon surface, instantaneous thickness of 2Å was observed at room temperature [140]. Considering the density of SiO_2 at room temperature [141], 1Å of native oxide corresponds to 2.27 x 10^{14} molecules/cm^2, 4.54 x 10^{14} oxygen atoms/cm^2. If it is assumed that the initial native oxide thickness was 2Å, it corresponds to 9.1 x 10^{14} oxygen atoms/cm^2. By SIMS data in Table.7.2, interfacial oxygen concentration of Sample 7.K is 1.4 x10^{13} atoms/cm^2. In Sample 7.K, by heating up to 660°C in hydrogen ambient, 9.1 x 10^{14} - 1.4 x10^{13} = 9.0 x10^{14} oxygen atoms/cm^2 has been removed.

Table 7.5 Free energy changes for oxygen removal reactions without plasma excitement (J/mole) [130] [135] [136]

Possible reactions	25°C	600°C	660°C
1. $SiO_2(s) + 1/2H_2 \rightarrow SiH(g) + O_2(g)$	1,137,808	973,292	956,524
2. $SiO_2(s) + H_2 \rightarrow SiO(g) + H_2O(g)$	439,213	317,173	305,059
3. $SiO_2(s) + H_2 \rightarrow SiH_2(g) + O_2(g)$	999,024	764,364	738,836
5. $SiO_2(s) + 2H_2 \rightarrow Si(s) + 2H_2O(g)$	337,936	294,545	290,685
6. $SiO_2(s) + 2H_2 \rightarrow SiH_4(g) + O_2(g)$	851,927	803,232	798,752
7. $SiO_2(s) + 5/2H_2 \rightarrow SiH(g) + 2H_2O(g)$	680,644	574,202	563,984
8. $SiO_2(s) + 3H_2 \rightarrow SiH_2(g) + 2H_2O(g)$	541,920	365,284	346,296
10. $SiO_2(s) + 4H_2 \rightarrow SiH_4(g) + 2H_2O(g)$	394,763	404,152	406,212
11. $SiO_2(s) + Si(s) \rightarrow 2SiO(g)$	540,940	339,801	319,433

In ECR hydrogen plasma, dissociation, direct ionization and dissociative ionization of $H_2(g)$ will occur in the plasma chamber [104]. Dissociation reaction can be written as: $H_2(g) + e^- \rightarrow 2H(g) + e^-$. Burke et al. found that in his ECR hydrogen cleaning experiments, atomic hydrogen produced in the plasma was the dominant agent during the cleaning process, in reducing the native oxide and the carbonated compounds [142]. In our system, it was assume that $SiO_2 + nH(g)$ (n= 1, 2, ...) occurred and their free energy changes are listed in Table 7.6. Reaction 15 and 20 were omitted for the same reason as in subsection 7.4.2. Reaction 16, 17, 18, 19, and 21 cannot be dominant reactions because these reactions are thermodynamically more favorable at lower temperature.

Sample 7.A was rinsed and blow-dried, then heated up to 600°C for subsequent epitaxial growth. Its interfacial oxygen concentration was measured to be 1.0×10^{15} atoms/cm^2. By comparing Samples 7.B and 7.F, the standard *in-situ* plasma cleaning at 600°C and at room temperature may be compared directly. Their SIMS data are shown in Table 7.2. Both samples were rinsed and blow-dried and heated up to 600°C for 7 minutes. By calculation, the room temperature *in-situ* cleaning reduced $1.0 \times 10^{15} - 7.8 \times 10^{14} = 2.2 \times 10^{14}$ oxygen atoms/cm^2. The standard *in-situ* cleaning at 600°C reduced $1.0 \times 10^{15} - 4.8 \times 10^{13} = 9.5 \times 10^{14}$ oxygen atoms/cm^2. Therefore, *in-situ* plasma cleaning was

more efficient at higher temperature in removing oxygen contaminants in our system.

In Reaction 14, $\Delta G_{600°C}$ = 419,086J and at equilibrium, $P_{SiH2} P_{O2} = 8.4 \times 10^{-34}$ Torr^2 and this reaction cannot occur (it was assumed here that P_H = 0.1mTorr, by considering ionization efficiency of 0.1). In Reaction 12, $\Delta G_{600°C}$ = 800,653J and at equilibrium, $P_{SiH} P_{O2} = 9.3 \times 10^{-50}$ Torr^2. Reaction 12 will not occur in our system.

Therefore, Reaction 13: $SiO_2(s) + 2H(g) \rightarrow SiO(g) + H_2O(g)$ will be a dominant reaction. Since $\Delta G_{600°C}$ = -28,105J and at equilibrium, $P_{SiO}P_{H2O} \cong 2.7 \times 10^{-7}$ Torr^2. If $P_{H2O} = 10^{-8}$ Torr, $P_{SiO(eq)}$ = 27 Torr by calculation, this reaction has a high driving force to proceed. Also, $\Delta G_{25°C}$ = 32,657J and at equilibrium, $P_{SiO}P_{H2O} \cong 1.9 \times 10^{-14}$ Torr^2 and If $P_{SiO} = P_{H2O}$, $P_{SiO} = P_{H2O} \cong 1.4 \times 10^{-7}$ Torr and the reaction will proceed even at room temperature. The oxygen removal process with hydrogen plasma excitation will be reaction controlled or desorption controlled. By Reaction 13, SiO(g) and H_2O(g) are desorbed. The boiling point of SiO(g) is known to be lower than that of H_2O(g), SiO(g) is a volatile products. So it is possible that the removal process is dominated by desorption of water vapor.

From the above arguments, room temperature *in-situ* cleaning removed 2.2 x 10^{14} oxygen atoms/cm^2 and *in-situ* cleaning at 600°C removed 9.5 x 10^{14} oxygen atoms/cm^2. Since the *in-situ* cleaning was performed for 300 seconds, oxygen removal rates were 6.7 x 10^{11} atoms/cm^2 sec at room temperature and 3.2 x 10^{12} atoms/cm^2 sec at 600°C. Kinetic expression can be written as : rate = A exp (-E/RT) and if it is assumed that E is not a function of temperature,

$$\ln \frac{\text{rate at } T_2}{\text{rate at } T_1} = \frac{E}{R} \left(\frac{1}{T_1} - \frac{1}{T_2} \right).$$

By substituting T_1 = 298°K and T_2 = 873°K and R= 8.314 J/deg mole, E = 5,500 J/mole. Heat of evaporation of water is 41,090J/mole at 100°C [143]. If it is assumed that the activation energy of desorption process is equal to the heat of evaporation of water vapor, oxygen removal process with plasma excitation is shown to be reaction-controlled.

Table 7.6 Free energy changes for oxygen removal reactions with plasma excitement (J/mole) [130] [135] [136]

Possible reactions	25°C	600°C	660°C
12. $SiO_2(s) + H(g) \rightarrow SiH(g) + O_2(g)$	934,530	800,653	787,256
13. $SiO_2(s) + 2H(g) \rightarrow SiO(g) + H_2O(g)$	32,657	-28,105	-33.477
14. $SiO_2(s) + 2H(g) \rightarrow SiH_2(g) + O_2(g)$	592,468	419,086	400,300
16. $SiO_2(s) + 4H(g) \rightarrow Si(s) + 2H_2O(g)$	-475,176	-396,011	-358,744
17. $SiO_2(s) + 4H(g) \rightarrow SiH_4(g) + O_2(g)$	38,815	112,676	121,680
18. $SiO_2(s) + 5H(g) \rightarrow SiH(g) + 2H_2O(g)$	-335,746	-288,993	-282,356
19. $SiO_2(s) + 6H(g) \rightarrow SiH_2(g) + 2H_2O(g)$	-677,748	-670,550	-669,312
21. $SiO_2(s) + 8H(g) \rightarrow SiH_4(g) + 2H_2O(g)$	-1,231,461	-976,960	-947,932

Chapter 8

Conclusion and Recommendations

8-1. Conclusion

The objective of this thesis was to investigate the *in-situ* cleaning processes by the ECR hydrogen plasma technique and the *ex-situ* cleaning process by the HF dipping method. The applicability of these cleaning processes to the wafer surface treatment was investigated for silicon homoepitaxial deposition. The epitaxial deposition was performed in the Ultra-high vacuum chemical vapor deposition reactor, where the load lock chamber had been attached. Both structural and chemical qualities of the epilayer/substrate interface were studied. The interfacial oxygen concentration degraded the structural qualities of the epitaxial layer and the epilayer/substrate interface, while the interfacial carbon concentration did not affect it.

The standard condition with *in-situ* hydrogen plasma cleaning at 600°C was optimized, and process variables such as DC bias, cleaning time, microwave power, hydrogen gas pressure were varied and studied. *In-situ* cleaning time was optimized to be 5 minutes, and longer cleaning did not improve its efficiency. A substrate DC bias proved to play a major role in obtaining a damage-free, chemically clean interface. Low hydrogen gas pressure (~1mT) was required to obtain a damage-free interface.

The ECR hydrogen plasma cleaning was similar to an ion-assisted or physical sputtering process, because hydrogen ions turned out to play a crucial role in the *in-situ* cleaning process. By assuming the collision-cascade model, the threshold energy for physical sputtering was calculated. Ion-assisted etching proved to be the dominant process, rather than physical sputtering, in wafer surface cleaning by the ECR hydrogen plasma technique.

A defect-free epitaxial layer was successfully deposited by applying the room temperature *in-situ* ECR hydrogen plasma cleaning. *In-situ* FTIR results were suitable for an accurate measurement of the incubation time for film deposition. Hydrogen ion energy was required to be reduced by applying a positive DC bias; otherwise, the substrate and the interface was badly damaged. The interfacial oxygen concentration decreased (thus the structural quality of the epilayer/substrate interface improved) with the increase of the *in-situ* cleaning temperature from 25°C to 600°C. In our experiments, defect-free epitaxial layers were deposited by the *in-situ* wafer cleaning at temperatures between 25°C and 480°C, and deposition was performed at 600°C, eventually. Oxygen species are supposed to be desorbed at high temperatures. Thermal heating played a major role in removing the oxygen species.

While the removal of the oxygen species was an ion-etching process, the removal of carbon was a hydrogen chemical etching process. In particular, the room temperature *in-situ* cleaning was effective in reducing the interfacial carbon concentration. It was notable that the high temperature (600°C and above) *in-situ* cleaning increased the interfacial carbon concentration.

The origin of oxygen species was investigated. In the high temperature (600°C) process, oxygen species are surmised to be desorbed from the inner walls of the chambers. Additionally, considerable amounts of oxygen (natural oxide) are supposed to be present on the wafer surface after the *ex-situ* cleaning process. In addition to the surface natural oxide, the entrance of water vapor into the load lock chamber during loading is inevitable to some extent. Higher temperature (660°C) *in-situ* cleaning and deposition was effective in reducing the interfacial oxygen concentration further. Heating up and deposition at 660°C without *in-situ* cleaning turned out to be effective in reducing the interfacial oxygen concentration significantly, while keeping the interfacial carbon concentration to low values.

To reduce the interfacial oxygen concentration, it was necessary to have as little oxygen as possible on the wafer surface before loading into the chamber. The *ex-situ* cleaning process affected the interfacial oxygen concentration and the resulting structural quality of the epitaxial layer and the interface.

and the resulting structural quality of the epitaxial layer and the interface. The DI water rinsing step in the *ex-situ* cleaning process increased the interfacial oxygen concentration when no *in-situ* cleaning was applied. Even when the (optimized) standard *in-situ* cleaning was applied at 660°C, the interfacial oxygen concentration of the resulting film was proportional to the water rinsing time. However, the water rinsing turned out to help smooth the surface of the epitaxial layer.

The reaction mechanisms of oxygen and carbon removal process were studied. By thermodynamic calculation and our observation, carbon is surmised to be removed by the reaction which forms a volatile $CH_3SiH_3(g)$. This reaction is thermodynamically favorable at low temperatures, especially at room temperature in our experiments. Adsorption of hydrogen molecule or ions is suspected to be a rate-limiting step in our system. Oxygen was removed by heating in vacuum in hydrogen ambient and SiO(g) may be desorbed from the reactions. With plasma excitation, H_2 will change to more reactive H(g). *In-situ* hydrogen plasma cleaning in our experiments was more efficient at higher temperature, and by thermodynamic consideration, $SiO_2(s) + 2H(g) \rightarrow SiO(g) + H_2O(g)$ turned out to be a dominant reaction in this case. By kinetic consideration, the oxygen removal process with plasma excitation seems to be reaction controlled, rather than water vapor-desorption controlled.

8-2. Recommendations

The epilayer/substrate interface need to be observed by (Ultra-High Resolution TEM) technique. The interfacial carbon concentration did not affect the resulting structural qualities of the epilayer/substrate interface and the epitaxial film in our experiments. If the β-SiC was formed, it may not have generated many defects during initial growth. Since deposition and *in-situ* cleaning was performed at 600°C or 660°C, it is suspected that the β-SiC has formed at the epilayer/substrate interface. The exact temperature for *in-situ* cleaning, which provides the maximum carbon removal rate should be investigated, between 25°C and 600°C.

For more effective removal of water molecules from the vacuum material inside the chamber, UV (Ultra-Violet) energy should be used to provide the

out process at 120°C for up to 10 hours was not effective in removing the water vapor in our system. It is not allowed to heat the system up to more than 120°C for its protection. The Phototron source emits wavelengths of UV energy that are selectively absorbed by water vapor.

To minimize the interfacial oxygen and carbon concentration in the resulting epitaxial film, systematic studies should be done by adjusting the spinning and rinsing time. Initial thickness and morphology of native oxide are surmised to affect the kinetics of oxygen removal process. This kinetics can be related to the *ex-situ* cleaning conditions.

To further lower the levels of oxygen and carbon contamination at the epilayer/substrate interface, ethanol/HF and methanol/HF dipping should be tried and the resulting films should be studied. An aqueous HF dipping was used as one of the *ex-situ* cleaning step. However, alcohol/HF solution resulted in the lower levels of oxygen and carbon contamination at the epilayer/substrate interface. Addition of alcohol may lower the surface energy of the HF solution, could make the solution work more effectively.

Bibliography

[1] B.Anthony, L.Breaux, T.Hsu, S.Banerjee, and A.Tasch, *J.Vac.Sci.Technol.* B 7(4), Jul/Aug (1989) 621

[2] T.Y.Hsieh, K.H.Jung, and D.L.Kwong, K.S.Lee., *J. Electorchem. Soc.*, Vol.138, No.4, April (1991) 1188

[3] S.M.Jang, PhD thesis (1993)

[4] K.V.Ravi, Imperfection and Impurities in Semiconductor Silicon, (1981) 169

[5] R.H. Finch, H.J. Queisser, *J. of Appl. Phys.*, 34, 406 (1963)

[6] W.L. Bond and W. Kaiser, *J. Phys. Chem. Solids*, 16, 44 (1960)

[7] D. Helmreich and E. Sirtl, in Semiconductor Silicon 1977, ed. H. R. Huff and E.Sirtl, (1977) 626

[8] John F.O'Hanlon, A User's Guide to Vacuum Technology, John Wiley & Sons (1989) 57

[9] Application Manual Phototron, U.S.Patent No. 4660297

[10] T.Takahagi, I. Nagai, A. Ishitani, and H.Kuroda, Y. Nagasawa, *J. Appl. Phys.* 64 (7), 1 October (1988) 3516

[11] W.Kern and D.Puotinen, *RCA review*, June 1970, Vol 31, No.2, 187

[12] M.Liehr, *Mat.Res.Soc.Symp.Proc.* Vol. 259. (1992) 3

[13] T.Takahagi, I.Nagai, A.Ishitani, and H.Kuroda, *J.Appl.Phys.*, 64, 3516 (1988)

[14] K.V.Ravi, Imperfection and Impurities in Semiconductor Silicon, (1981) 46

[15] J.S.Judge, *J. Electrochem. Soc.*, 118, 1772 (1971)

[16] W.Kern, *J. Electrochem. Soc.*, Vol. 137, No. 6, June (1990) 1890

[17] W.Kern, *Semicond. Int.*, 7 (4),(1984) 94

[18] S.Watanabe, N.Nakayama and T.Ito, *Appl. Phys. Lett.* 59, 1458 (1991)

[19] H.M'saad, J.Michel, A.Reddy, and L.C.Kimerling, to be published in the Journal of Electrochemical Society

[20] A.Miyauchi, Y.Inoue, M.Ohue, N.Momma, and T.Suzuki, JES 89-12-074

[21] M.K.Sanganeria, K.E.Violette, M.C.Ozturk, G.Harris, C.A.Lee and D.M.Maher, MRS Fall meeting (1993)

[22] B.S.Meyerson, *Appl. Phys. Lett.* 48 (12), 24 March (1986) 799

[23] B.S.Meyerson, *Proceedings of the IEEE*, Vol. 80, No. 10, October (1992) 1606

[24] D.W.Greve, M.Racanelli, *J. Vac. Sci. Technol.* B 3 (3), May/June (1990) 511

[25] Z.Ye, Y.Liu, Z.Zhou and R.Reif, *J. Electron. Mater.*, Vol.22, No.2, (1993) 247

[26] W.G.Townsend and M.E.Uddin, *Solid State Electronics*, 16 (1973) 39

[27] S.Veprek and F.A. Sarott, *Plasma Chem. and Plasma Processing*, 2, (1982) 233

[28] R.E.Thomas, M.J.Mantini, R.A.Rudder, D.P.Malta, S.V.Hattangady, and R.J.Markunas, *J. Vac. Sci. Technol.* A 10 (4), Jul/Aug (1992) 817

[29] M.Delfino, S.Salimian, D.Hodul, A.Ellingboe, and W.Tsai, *J. Appl. Phys.* 71(2), 15 january (1992) 1001

[30] *Semiconductor International*, July 1991, 46

[31] L.Bourget, a research scientist at AsTex company

[32] *Semiconductor International*, May 1992, 71

[33] *Semiconductor International*, July 1992, 56

[34] P. Burggraaf, *Semicond. Int.* 5, 69 (1986)

[35] K.E.Bean, W.R. Runyan, and R.C.Murray, *Semicond. Int.* 5, 136 (1985)

[36] G.R.Srinivasan, in Silicon Processing, ASTM STP 804, ASTM, Philadelphia, PA, 151 (1983)

[37] G.R.Srinivasan, Silicon Processing, ASTM STP 804 IEDM Technical Digest, 398

[38] Y.Taur, W.H.Chang, and R.H.Dennard, 1984 *IEDM Technical Digest*, 398

[39] T.Deacon, *Microelectronic Mnufacturing and Testing*, 89, Sept. (1984)

[40] T.C.Mele, J.Hayden, F.Walczyk, M.Lien, Y.C.See, D.Denning, S.Cosentino, and A.H.Perera, *IEDM Technical Digest.* (1990) 18.4.1

[41] *Semiconductor International*, June (1990) 69

[42] W.B. Ard, M.C.Becker,R.A. Dandl, H.O. Eason, A.C. England, and J.R.Kerr, *Phys. Rev. Lett.* 10, 89 (1963).

[43] D.B.Miller and G.W.Bethke, AIAA J.4, 835 (1966).

[44] G.Loncar, Musil and L.Bardos, *Czech. J.Phys.* B30, 688 (1980).

[45] K.Suzuki, S.Okudairo, N.Sadudo and I.Kanoma, *Jpn. J. Appl. Phys.* 161979 (1977).

[46] S.Kanai, K. Nojiri, M. Nawata: *Semiconductor International* , May 1992 (1992) 71.

[47] Omar, Introduction to Solid State Physics (1975) 160.

[48] B.Chapman, Glow Discharge Processes, 17 (1980)

[49] J.Asmussen, *J.Vac.Sci.Technol.*A, Vol.7, No.3, May/June (1989) 883

[50] D.M.Manos,D.L.Flamm, Plasma etching, 30 (1989)

[51] B.Chapman, Glow Discharge Processes, 56 (1980)

[52] K.Shirai, S.Gonda, *J. Appl.Phys.* 68 (8),15 October (1990) 4258

[53] I.Langmuir, *Gen.Elect.Rev.* 26, 731(1923)
[54] D.M.Manos,D.L.Flamm, Plasma etching,31(1989)
[55] S.M.Rossnagel, S.J.Whitehair, R.C.Guarnieri, D.N.Ruzic, J.J.Cuomo, *J. Vac. Sci. Technol.* A, 9 (3), May/June (1991) 702
[56] J.B.CaughmanII, W.M.Holber, *J. Vac. Sci. Technol.* A9 (6), Nov/Dec (1991) 3113
[57] O.Popov, *J. Vac. Sci. Technol.* A, 9 (3), May/June (1991) 711
[58] S.Samukawa, S.Mori, M.Sasaki, *J. Vac. Sci. Technol*, Vol.9, No.1, Jan/Feb (1991) 85
[59] C.A.Outten, J.C.Barbour, W.R.Wampler, *J. Vac. Sci. Technol.* A (3), May/June (1991) 717
[60] M.Delfino, S.Salimian, D.Hodul, A.Ellingboe, W.Tsai, *J. Appl. Phys.* 71 (2), 15 January (1992) 1001
[61] ECR plasma source user manual, Applied Science and Technology, Inc, June (1991) 3-11
[62] Y.H.Lee, J.E.HeidenreichIII, G.Fortuno, *J. Vac. Sci. Technol.* A7 (3), May/Jun (1989) 903
[63] N.Sadeghi, T.Nakano, D.Trevor, R.Gottscho, *J. Appl. Phys.* 70 (5), 1 September (1991) 2552
[64] J.H.Comfort, Ph.D Thesis, June (1988)
[65] S.Salimian, C.B.Cooper III, A.Ellingboe, *Appl. Phys. Lett.* 56 (14), 2 April (1990) 1311
[66] D.M.Manos, D.L.Flamm, Plasma etching, 39 (1989)
[67] R.Glang, in "Handbook of Thin Film Technology," L.I. Maissel and R.Glang, eds., 1-27, 1-26, McGraw Hill, New York (1970)
[68] K. Denbigh in "The Principles of Chemical Equilibrium," 2nd ed., 197-200 Cambridge University Press, Cambridge (1968)
[69] D.M.Manos, D.L.Flamm, Plasma etching, 41(1989)
[70] A.S. Bergendahl, et.al., *Semiconductor International*, Sept.(1990) 94
[71] Industry News, *Semiconductor International*, Dec. (1989) 22
[72] Z.H.Zhou, SM Thesis (1989)
[73] F.F.Chen, in Plasma Diagnostic Techniques, edited by R.H. Huddlestone and S.L.Leonard, (1965)
[74] T.O.Sedgwick, *Appl. Phys. Lett.*, 56 (25), (1989) 2689
[75] Z.H.Zhou, F.Z.Yu, and R.Reif, *J.Vac.Sci.Tech.*, B.9 (2),(1991) 374
[76] H.Tae, S.Hwang, S.Park, E.Yoon, and K.Hwang, AVS conference, (1993)

[77] Keizo Suzuki, Ken Ninomiya and Nishimatsu, *Vacuum*, vol.34, No.10/11, (1984) 953

[78] D.M.Manos, D.L.Flamm, Plasma etching: an introduction, (1988) 35

[79] Z.Zhou, E.Aydil, R.Gottscho, Y.Chabel, R.Reif, *J.Electrochem.Soc.*, Vol.140, No.11, November (1993) 3316

[80] J.Ramm, E.Beck, and A.Zuger, *Mat.Res.Soc.Symp.Proc.*220, (1991) 15

[81] T.D.Mantei and S.Dhole, *J.Vac.Sci.Technol.*B 9, (1991) 26

[82] J.Bohdansky, J.Roth and H. L.Bay, *J.Appl.Phys.* 51(5), May (1980) 2863

[83] Y.H.Lee and Z.H.Zhou, submitted to *Appl.Phys.Lett.*

[84] C.A.Outten, J.C.Barbour and W.R.Wampler,*J.Vac.Sci.Technol.*A9(3), May/Jun (1991) 717

[85] R.Reif, *J. Vac. Sci. Technol.*, A2, (1984) 429

[86] T.R.Yew, R.Reif, *J. Appl. Phys.* 68 (9), November (1990) 4681

[87] I.Suemune, Y.Kunitsugu, Y.Tanaka, Y.Kan.and M.Yamanishi, *Appl. Phys. Lett.* , 53, (1988) 2173

[88] H.W.Kim, Z.H.Zhou, to be submitted (1994)

[89] M.Delfino, S.Salimian, D.Hodul, A.Ellingboe, and W.Tsai, *J. Appl. Phys.* 71 (2), 15 January (1992) 1007

[90] B.S.Meyerson, *Proceedings of the IEEE*, Vol. 80, No.10, October (1992) 1594

[91] E.Yablonovitch, D.L. Allara, C.C.Chang, T.Gmitter, and T.B. Bright, *Phys. Rev. Lett.* 57, 249 (1986)

[92] V.A.Burrows, Y.J. Chabal, G.S. Higashi, K. Raghavachari, and S.B.Christman, *Appl.Phys.Lett.*53,998 (1988)

[93] A.Kishimoto, I.Suemune, K.Kamaoka, T.Koui, Y.Honda and M.Yamanishi, *Jpn.Journal of Appl.Phys*, vol.29, no.10, october, (1990) 2273

[94] Z.H.Zhou, H.Kim, and R.Reif, 1993 fall MRS proceedings

[95] S.S.Iyer, M.Arienzo, and E.de Fresart, *Appl.Phys.Lett.* 57 (9) 27 August (1990) 895

[96] S.H.Wolff, S.Wagner, J.C. Bean, R.Hull, and J.M.Gibson, *Appl. Phys. Lett.* 55 (19), 6 November (1989) 2017

[97] C.C.Cheng, S.R.Lucas, H.Gutleben, W.J.Choyke and J.T.Yates,Jr., *Surface Science Letters* 273 (1992) L441-L448

[98] S.S.Iyer, M.Arienzo, and E.de Fresart, *Appl.Phys.Lett.* 57 (9),27 August (1990) 893

[99] D.Kinoski, R.Qian, A.Lahajan, S.Thomas, P.Munguia, J.Fretwell, S.Banerjee, and A.Tasch, *Mat.Res.Soc. Symp. Proc.* Vol.315, (1993) 223

[100] K.Kim, P.Maillot, A.E.Morgan, A.Kermani and Y.H.Ku, *J.Appl.Phys.* 67 (4), 15 February (1990) 2176

[101] T.Nozaki, Y.Yatsurugi, and N.Akiyama, *J. Electrochem. Soc.*, 117(12), December (1970)1566

[102] R.C.Henderson, R.B.Marcus, and W.J. Polito, *J. Appl. Phys.*, 42, 1208 (1971)

[103] M.J.Bozack, P.A.Taylor, W.J. Choyke, and J.T.Yates, Jr., *Surf.Sci.*177 (1986) L933

[104] H.Yamada, *J. Appl. Phys.* 65 (2), 15 January (1989) 776

[105] J.R.Engstrom, D.J.Bonser, M.M.Nelson, and T.Engel, *Surf. Sci.* 256, 317 (1991)

[106] T.Isagawa, L.Kogure, T.Imaoka and T.Ohmi, *Extended Abstracts of the 1992 International Conference on Solid State Devices and Materialss*,Tsukuba, 1992, pp193

[107] A.Ishizaki and Y.Shiraki, *I. Electrochemical Soc.*, 133, 666 (1986)

[108] P.I.Grunthaner et al., *Thin Solid Films*, 183, 197 (1990)

[109] B.S.Meyerson, E.I. Himpsel, J.I.Uram, *Appl. Phys. Lett.*, 57, 1034 (1990)

[110] Y.I.Chabal, F.S.Higashi, J.Raghavachari, and V.A.Burrows, *I. Vac. Sci. Technol.* A 7, 2104 (1989)

[111] B.S.Meyerson, *Proceedings of the IEEE*, vol.80, No.10, October (1992) 1592

[112] J.V.Ravi and C.I.Varker, *Journal of Applied Physics*, Vol 45, No.1, January (1974) 263

[113] T.Yasaka, S.Uenaga, G.Yasutake, L.Takakura, S.Miyazaki and L.Hirose, *Mat. Res. Soc. Symp. Proc.* Vol.259., (1992) 387

[114] V.B.Menon, R.P.Donovan, Proc. 1st Int. Symposium on Cleaning Technology, 1989, Vol 90-9, 167-181

[115] S.Verhaverbeke, I.Alay, P.Mertens, L.Heyns, W.Vandervorst, L.Murrell and C.Sofield, *Mat. Res. Soc. Symp. Proc.* Vol. 259. (1992) 394

[116] L.Morita, T.Ohmi, D.Hasegawa, L.Kawakami, and L.Ohwada, *I.Appl.Phys.* 68 (3), 1 August (1990) 1272

[117] T.Takahagi, I.Nagai, A,Ishitani, and H.Kuroda, *J.Appl.Phys.* 64(7), 1 October (1988) 3516

[118] G.W.Trucks, K.Raghavachari, G.S.Highashi, and Y.J.Chabel, *Phys.Rev.Lett,* 65(4) 23 July (1990) 504

[119] Y.Hirota, K.Sugii, and Y.Homma, *J.Electrochem.Soc.*, Vol.138 (3), March (1991) 799

[120] M.Tabe, *Appl. Phys. Lett.* 45 (10), 15 November (1984) 1073

[121] W.R.Burger, PhD thesis, (1987) 37
[122] B.J. Baliga, Epitaxial Silicon Technology, (1986) 106
[123] K. Nakashima, M. Ishii, I. Tajima, and M. Yamamoto, *Appl. Phys. Lett.* 58, 2664 (1991)
[124] S.R.Kasi, M.Liehr, *Appl. Phys. Lett.* 57 (20). 12 November (1990) 2095
[125] T.Takahagi, I. Nagai, A. Ishitani, and H.Kuroda, Y. Nagasawa, *J. Appl. Phys.* 64 (7), 1 October (1988) 3516
[126] Application Manual Phototron, U.S.Patent No. 4660297
[127] John F.O'Hanlon, A User's Guide to VacuumTorrechnology (1989) 57
[128] A. Licciardello, O. Puglisi, and S. Pignataro, *Appl. Phys. Lett.* 48 (1), 6 January (1986) 42
[129] M.L.Colaianni, P.J.Chen, H.Gutleben, and J.T. Yates Jr., *Chem. Phys. Lett.* 191 (6) 17 April (1992) 561
[130] M.D.Allendorf and C.F.Melius, *J.Phys.Chem.* 96 (1) (1992) 428
[131] JANAF Thermochemical Tables
[132] J.T.Law and E.E.Francois, "The adsorption of gases on a silicon surface", March (1956) 353
[133] Y.Kobayashi, Y.Shinoda, and K.Sugii, *Jpn. J. Appl. Phys.* 29(6), June (1990) 1004
[134] M.Racanelli and D.W.Greve, "Effect of Surface Cleaning on Quality of GeSi Epitaxail layers Grown by UHVCVD"
[135] Samsonov, "The Oxide Handbook"
[136] L.Fredin, R.H.Hauge, Z.H.Kafari, and J.L.Margrave, *J.Chem.Phys.*82(8), 15 April (1985) 3544
[137] H.K.Moffat and K.F.Jensen, *J.Electrochem.Soc.*,135(2) February (1988) 459
[138] J.G.Lee, PhD Thesis (1991)
[139] A.Ishizaka and Y.Shiraki, *J. Eectrochem. Soc.* 133(4) April (1986) 666
[140] M.Morita, T.Ohmi, E.Hasegawa, M.Kawakami, and M.Ohwada, *J. Appl. Phys.* 68(3), 1 August (1990) 1272
[141] J.W.Mayer, S.S.Lau, "Electronic Materials Science: For Integrated Circuits in Si and GaAs",(1990)
[142] R.Burke, J.Pelletier, C.Pomot, and L.Vallier, *J. Vac. Sci. Technol.* A 8(3), May/June (1990) 2931
[143] D.R.Gaskel, "Introduction to Metallurgical Thermodynamics",(1981)